STRUCTURE STUDY OF EXOTIC NUCLEI USING CLUSTER MODELS

Thesis submitted to the University of Calicut
in partial fulfillment of the requirements
for the award of the degree of

DOCTOR OF PHILOSOPHY
in
PHYSICS

by

DEEPTHY MARIA JOSEPH

Under the guidance of

Prof. (Dr.) ANTONY JOSEPH

DEPARTMENT OF PHYSICS
UNIVERSITY OF CALICUT
KERALA, INDIA 673 635
OCTOBER 2017

UNIVERSITY OF CALICUT

Dr. ANTONY JOSEPH
Professor & Former Head
Department of Physics
University of Calicut

Calicut University P.O
Kerala India 673 635
Tel: 0494-2407416(O)
+919446164109(M)
email: aj@uoc.ac.in

CERTIFICATE

This is to certify that this thesis entitled **'Structure study of exotic nuclei using cluster models'** is a bonafide record of research work carried out by **Ms. Deepthy Maria Joseph** under my supervision for the award of the Ph.D degree of University of Calicut and that no part of this thesis has been presented elsewhere for the award of any degree, diploma or other similar title.

Calicut University
20 October 2017

Antony Joseph

DECLARATION

I hereby declare that this thesis entitled **'Structure study of exotic nuclei using cluster models'** is a bonafide record of research work done by me and that no part of this thesis has been presented before for the award of any degree or diploma.

Calicut University
20 October 2017

Deepthy Maria Joseph

ACKNOWLEDGEMENT

First and foremost, I would like to thank God Almighty for giving me the strength, knowledge, ability and opportunity to undertake this research study and to persevere and complete it successfully. Without His blessings, this achievement would not have been possible.

I wish to express my heart-felt gratitude to my supervisor, Prof. (Dr.) Antony Joseph for guiding me through the different stages of the research. I am extremely indebted to him for imparting his knowledge and expertise in this study. He has been a great source of inspiration and information, illuminating the path all through the conduct of the research, through which this thesis has acquired its present shape. I hereby record my indebtedness to him with a heart overwhelmed with thankfulness.

I wish to express my sincere gratitude to Prof. George Varghese, Prof. Antony Joseph and Prof. M. M. Musthafa, former heads of the Department of Physics and Prof. P. P. Pradyumnan, the present head of the Department of Physics, University of Calicut, for providing me the necessary facilities to carry out my research work.

I am grateful to all the faculty members of the Department of Physics, University of Calicut, for their co-operation and suggestions which helped me to complete my work successfully.

I am grateful to the office staff in the Department of Physics, University of Calicut, for their help and co-operation throughout my work.

I wish to express my gratitude to all other Research scholars in the Department for their co-operation and support throughout my work.

I would like to acknowledge with gratitude, the financial support from University Grants Commission, Govt. of India, for carrying out my research work.

I am deeply indebted to my family for their constant support, encouragement and prayers throughout my research career.

I express my sincere thanks to all my relatives, friends and well-wishers whose prayers and blessings are with me.

Deepthy Maria Joseph

Dedicated to

My beloved parents

LIST OF PUBLICATIONS/PROCEEDINGS

1. "A systematic study of proton, alpha and cluster decays in Rhenium isotopes using the effective liquid drop model", Deepthy Maria Joseph, Nithu Ashok and Antony Joseph, *Modern Physics Letters A*, Vol. 31, No. 5, 1650031, 2016.

2. "Cluster decay in Osmium isotopes using Hartree-Fock-Bogoliubov theory", Nithu Ashok, Deepthy Maria Joseph and Antony Joseph, *Modern Physics Letters A*, Vol. 31, No. 7, 1650045, 2016.

3. "Theoretical study of cluster radioactivity in Re isotopes", Deepthy Maria Joseph, Antony Joseph and Nithu Ashok, *Proceedings of the International conference on 75-years of nuclear fission*, 83, 2014.

4. "Investigation of probable decays in Rhenium isotopes", Deepthy Maria Joseph, Antony Joseph and Nithu Ashok, *Proceedings of the DAE – BRNS Symposium on Nuclear Physics 60,* 284-285, 2015.

5. "Probable exotic decays in Tungsten isotopes", Deepthy Maria Joseph, Antony Joseph and Nithu Ashok, *Proceedings of the DAE – BRNS Symposium on Nuclear Physics 62,* 2017 (Accepted).

6. "A theoretical study of cluster radioactivity in Platinum isotopes", Deepthy Maria Joseph, Nithu Ashok and Antony Joseph (Communicated).

LIST OF CONFERENCE PRESENTATIONS

1. "Theoretical studies of proton, alpha and cluster emissions from Re isotopes", National seminar on isotope and nuclear techniques– applications to basic and applied sciences, March 11-12, 2014, MAMO College, Mukkam, Calicut, Kerala.

2. "Theoretical study of cluster radioactivity in Re isotopes", International conference on 75 years of nuclear fission, May 8-10, 2014, Bhabha Atomic Research Centre, Mumbai.

3. "Nuclear structure calculations with the cluster-phonon model", National Seminar on Nuclear, Astro and High Energy Physics, October 29-30, 2015, Kuriakose Elias College, Mannanam, Kerala.

4. "Investigation of probable decays in Rhenium isotopes", DAE – BRNS symposium, December 7-11, 2015, SSSIHL, Prasanthi Nilayam, Puttaparthi.

CONTENTS

LIST OF FIGURES

LIST OF TABLES

Abstract

A nucleus is said to be stable when the N/Z ratio (neutron number to proton number ratio) becomes that of the nuclei which are in the beta stability line of the Segre chart. Highly unstable nuclei which lie above or below the valley of stability near the proton drip line or neutron drip line are called exotic nuclei. These unstable nuclei attain stability by emitting radiations. They undergo decay processes such as α decay, β decay, γ decay, nuclear fission, exotic or cluster decay and particle emission. The present study is an investigation of exotic nuclear decay in Tungsten (W), Rhenium (Re), Iridium (Ir) and Platinum (Pt) isotopes. Exotic decay or cluster radioactivity is the emanation of a cluster of nucleons with mass number heavier than that of an alpha particle and lighter than that of the lightest fission fragment. This phenomenon is a radioactive decay process intermediate between alpha decay and spontaneous fission. The model employed in this study is the effective liquid drop model (ELDM), in which the interacting potential is the sum of Coulomb, surface and centrifugal potentials. All possible combinations of parent and cluster have been considered for which the Q value is positive. The half-lives are evaluated for the probable exotic decay modes in W, Re, Ir and Pt isotopes in the mass range $150 < A < 200$. The predicted values are compared with another theoretical model and with the available experimental data. The effect of shapes of parent and daughter nuclei on exotic decays are analysed. The decay characteristics of the probable exotic decay modes are investigated. The role of neutron magicity in exotic decay is studied. Finally, we have derived a general equation for half-life governing the probable exotic decay modes in these nuclei.

CHAPTER 1
INTRODUCTION

1.1 Radioactive decay in nuclei

At the beginning of the twentieth century, the first informations about the atomic nucleus were obtained by studying radioactivity. This led to the fields of particle physics, nuclear physics, radiochemistry as well as to many applications in medicine, biology, industry and agriculture. While trying to see a connection between Wilhelm Conrad Roentgen's X-rays with fluorescence phenomena, Antoine Henri Becquerel discovered a "mysterious" radiation from uranium salt in 1895. Pierre and Marie Curie found that thorium also emits this radiation and they discovered the new elements radium and polonium, which were the strong emitters. From scattering experiments, Ernest Rutherford deduced that atomic particles consisted primarily of empty space surrounding a well-defined central core called nucleus. He transmuted one element into another artificially and elucidated the concepts of the half-life and decay constant. Rutherford demonstrated the production of oxygen by bombarding nitrogen with alpha particles. The atomic nucleus was discovered around 1911.

Geiger and Nuttall, in 1911 gave a semi-empirical relationship of the alpha decay half-life versus the range of alpha particles in the air. Gamow [1] explained this by tunneling the alpha particle through the barrier which was the first application of quantum theory to nuclei. John William Strutt and Lord Rayleigh introduced the liquid drop model (LDM), in a series of papers, treating liquid droplets charged with electricity and the capillarity instability of an infinite jet of fluid [2].

In 1930, Gamow attempted to calculate the nuclear binding energy using the LDM, which was finally accomplished by Von Weizsacker in 1935. Otto Hahn and Fritz Strassman, in 1939, discovered the induced fission, which was explained by Lise Meitner and Otto Frisch by using the LDM. The name fission was borrowed by Otto Frisch from biology of cell division. Many properties of the fission process were explained by Bohr and Wheeler [3] and they stated that fission was more likely to occur with ^{235}U than ^{238}U.

Only three kinds of nuclear decay modes (α, β and γ) have been known for a long period of time. They explain three of the fundamental interactions in nature : strong, weak and electromagnetic. Spontaneous fission, which was discovered in 1940 by Petrzhak and Flerov, had both military and peaceful applications of the neutron-induced fission.

Other kinds of decay modes like proton radioactivity were predicted in 1960 by Goldansky. Karnaukhov et al. [4] and Hofmann et al. [5,6] observed the proton radioactivity from the ground state. The α and ^{10}Be accompanied cold fission decays were discovered in 1998 [7]. Using the macroscopic-microscopic approach [8], the mass asymmetry of fission fragments and the shape isomers could be explained.

1.2 Cluster radioactivity

The emanation of a cluster of nucleons with mass heavier than that of an alpha particle and lighter than that of the lightest fission fragment was first predicted by Sandulescu et al. [9] in 1980. This phenomenon, identified as cluster radioactivity or exotic decay, is a radioactive decay process intermediate between alpha decay and spontaneous fission. Experimentally, cluster decay was first observed by Rose and Jones [10] in the year 1984, in the radioactive decay of ^{223}Ra by the emission of ^{14}C cluster, with ^{209}Pb as daughter. Many such emissions were discovered later [11]. This rare decay is

experimentally found in the mass region A > 220 with daughter around ^{208}Pb and is also predicted around ^{100}Sn and ^{132}Sn daughters [10,12,13], based on the quantum mechanical fragmentation theory (QMFT) [14,15].

Usually, the emitted clusters in this process are the isotopes of C, O, Ne, Mg, Si, etc. In earlier years, the phenomenon called cluster radioactivity was found mostly in actinide nuclei like uranium, radium, etc. Recently, it has been noticed that such decays occur in lower mass region near ^{114}Ba. The exciting experimental discovery of ^{12}C cluster emission from ^{114}Ba resulting in ^{102}Sn [16,17,18], attracts a lot of attention and therefore broadens the scope of cluster radioactivity.

Researchers tried to find other radioactive decay modes in which heavy nuclei break up by emission of fragments of intermediate mass. Theoretically, the interest in these decays is found in the evaluation of lifetimes, branching ratios and decay constants and hence deduce various properties of the nuclei involved in these decays. Over last three decades, with the help of various models, the lifetimes for the emitted cluster fragments from radioactive nuclei have been assessed and compared with the experimental data.

There are various theoretical models to investigate the phenomenon of cluster radioactivity. Generally these models fall under two categories : 1) the unified fission model (UFM) and 2) the preformed cluster model (PCM). The physics of both the models is entirely different. In the UFM, cluster decay is simply considered as a barrier penetration phenomenon without worrying about the preformation of cluster in the parent nucleus. In the PCM, some cluster of nucleons is assumed to be preformed in a parent nucleus, before penetrating the nuclear potential barrier. The basic presumption of the UFM is that clusters have equal probability of being preformed, but in PCM, clusters with different sizes have different probabilities of being preformed in the

parent nucleus. The idea of the two approaches is seemingly different, though there are some similarities between them [19].

The cluster radioactivity is based on the fragmentation theory [14,15], where the cold fission or fusion reaction valleys are seen [20-23] in the estimated fragmentation potentials. In accordance with the earlier calculations in the case of transactinides, cold reaction valleys are formed by the shell effects of one or both the partners of the reaction. For the radioactive nuclei, the significance of cold reaction valleys, which correspond to the observed cluster emissions was later illustrated explicitly by Gupta et al. [24].

As mentioned earlier, experimentally, cluster radioactivity was established as a new decay process for the first time in the spontaneous decay of ^{14}C emission from ^{223}Ra nuclear system. However, in literature there was an old fission data of ^{24}Ne decay of ^{232}U, observed by Jaffey and Hirsch [25]. This implies that cluster decay was already found as early as 1951 and the authors could not distinguish it from the process of spontaneous fission. Few years back, Bonetti et al. [26] have ascertained that the ^{24}Ne emission from ^{232}U, observed in 1951, is not due to spontaneous fission, since the presently measured upper limit of spontaneous fission decay constant is smaller than the then observed decay constant. Only three nuclei are observed to decay emitting two heavy clusters other than alpha particle. They are ^{231}Pa, ^{234}U and ^{238}Pu, but no nuclei are found to decay with the emission of more than two heavy clusters. Also, it is now possible to measure the spontaneous fission probability and cluster decay probability simultaneously in the same experiment [26]. Since the spontaneous fission half-lives are smaller than the cluster decay half-lives, cluster decay differs from the spontaneous fission in radioactive nuclei.

A fine structure, equivalent to that observed for alpha decay by Rosenblum [27] was also experimentally observed [28,29] for ^{14}C decays of

^{222,223}Ra nuclei. Over the years, various measurements of branching ratios of alpha decay versus those of cluster decay to the excited states of daughter nucleus were carried out. So far, this has been possible only for the branching ratios of ^{14}C emission to the 1st excited state of ^{208}Pb and to the 1st and 2nd excited states of ^{209}Pb. In the case of ^{209}Pb, some events corresponding to a transition to the 3rd excited state of ^{209}Pb were also seen in ^{14}C emission from ^{223}Ra nucleus. Here the calculations of Greiner and Scheid [30] were done before the experiments [28]. They showed that if decay to excited states is taken into account in addition to the decay to the ground state of daughter nucleus, the decay constant corresponding to cluster decay can go up by a factor of 5. In these cases, it has been observed that the decay to excited states is far more increased than that to the ground state of daughter nucleus.

So far, the heaviest cluster observed is ^{34}Si, which is far from the lightest fission fragment measured until now. The limiting value of the mass asymmetry for the normal fission or the cluster decay is not established yet. There is also a possibility for the two processes to overlap for some range of asymmetry. Recently, some attempts were performed [31] to find out the very light cold fission products with maximum kinetic energy, having the size of the exotic clusters. This would lead to many new possibilities and questions, some of which are studied in recent times.

In cluster decays, the observed daughter nuclei are always a proton or neutron (or both) closed shell, or almost near to the closed shell spherical nucleus. This led to the prediction of new cluster radioactivity based on earlier calculations. In the earlier calculations, the minimum value in the evaluated fragmentation potential energy surface pointed to at least a spherical closed shell nucleus. This implies that cluster decay is not an isolated process in nature. It must be related to other processes like the cold fission and cold fusion in which similar closed shell effects play an important

role. This problem was analysed by Gupta et al. [32]. Furthermore, the topic of either the spherical or both the deformed and spherical closed shell effects becomes significant due to the observation of the existence of stable deformed closed shell effects in nuclei [33,34]. At present, there exists no experimental data of cluster decay referring to deformed daughters.

Theoretically, the question comes up whether alpha decay, cluster decay and the spontaneous fission are simply the three types of a unified fission process with super-asymmetric, asymmetric and nearly-symmetric fission fragments or both alpha and cluster decays are indistinguishable and stick to the Gamow theory of alpha decay but differ from the spontaneous fission. Both the possibilities have been studied extensively by various groups [35,36].

Apparently, the fission theories are used to understand the cluster decay phenomenon. In the saddle point fission model (SPF), the charge and mass distributions of the fragments are determined at the saddle point, after the penetration of the decaying system through the barrier. This supposition is on the basis of an earlier computation in which an explicit time-dependent Schrodinger equation, in the charge and the mass-asymmetry co-ordinates and the relative co-ordinate, was solved. Here both the assault frequencies and barrier penetrabilities are independent of the size of the fragment and they are difficult to calculate. In one of the SPF models, the decaying nucleus is assumed to arrive at the touching configuration, and then penetrates the interaction barrier. Up to the touching configuration, the SPF model uses the idea of an incessantly deforming shape of a nucleus undergoing fission and then uses the potential barrier of the already detached fragments, since in such potentials, the touching configuration lies before the barrier height. In another SPF like fission model [37,38], the neck degree of freedom is taken into account and minimizing the action integral, solution of a second order

differential equation in multidimensional deformation space is found out. There are other theories of cluster decay which convey many new exotic concepts but are not studied in detail yet.

Considering that cluster decay competes with the alpha decay and distinguishes itself from spontaneous fission, a new definition was suggested for radioactive nuclei : a radioactive nucleus is one which spontaneously disintegrate to other stable nuclei either by fission or by the emission of a cluster, the alpha particle, the beta particle and the gamma ray or a combination of these. The branching usually occurs between the alpha particle and the cluster or between the fission fragments and the cluster. If we establish the use of clusters in radiation studies, this definition would be more appropriate.

Theoretical studies of cluster decay exhibited by different nuclei involves evaluations of parameters like spectroscopic factor or preformation probability, barrier penetrability, assault frequency, decay constant, etc. Based on these calculations, half-lives of various cluster decay modes are usually predicted for different parent nuclei. These investigations are done either by using various theoretical models by assuming different kinds of potentials as interacting potential or by employing model-independent or model-dependent semi-empirical formulae. These studies have been widely done around doubly magic nuclei, in support of the predictions by nuclear shell model. This is because of the fact that the most experimentally feasible cluster decay modes are those resulting in the production of doubly magic daughters like ^{100}Sn, ^{132}Sn and ^{208}Pb.

In the early years, cluster radioactivity displayed by heavy parent nuclei, resulting in the production of doubly magic daughter nucleus, ^{208}Pb or in the neighbourhood of it were studied both theoretically and experimentally. This type of radioactivity was named as Pb radioactivity or trans-lead cluster

radioactivity. Subsequently, there began investigations of cluster decay near other doubly magic nuclei. As a result, another island of cluster radioactivity was predicted near doubly magic ^{100}Sn and ^{132}Sn isotopes. This was termed as Sn radioactivity or trans-tin cluster radioactivity. Cluster physics is, in general, a common topic in physics, especially in material science.

1.3 Objectives of the present work

A nucleus is said to be stable when the N/Z ratio (neutron number to proton number ratio) becomes that of the nuclei which are in the beta-stability line of the Segre chart (see Fig. 1.1). Highly unstable nuclei, which lie above or below the valley of stability near the proton drip line or neutron drip line are called exotic nuclei. These unstable nuclei attain stability by emitting radiations. They undergo decay processes such as α decay, β decay, γ decay, nuclear fission, exotic or cluster decay and particle emission. The present thesis is an investigation of exotic nuclear decay in tungsten (W), rhenium (Re), iridium (Ir) and platinum (Pt) isotopes using the effective liquid drop model.

Nuclei in the mass range $150 < A < 190$ are predicted to exhibit cluster radioactivity [39]. Therefore W, Re, Ir and Pt nuclei are chosen hoping they provide a good platform for the study of exotic decay. Also, exotic decay of these nuclei is not studied theoretically or experimentally yet. Both cold nuclear fusion and fission involving either singly magic or doubly magic component are considered as feasible paths for the synthesis of heavy and superheavy nuclei. We also explore, whether the exotic decay will be possible around singly magic daughter nuclei.

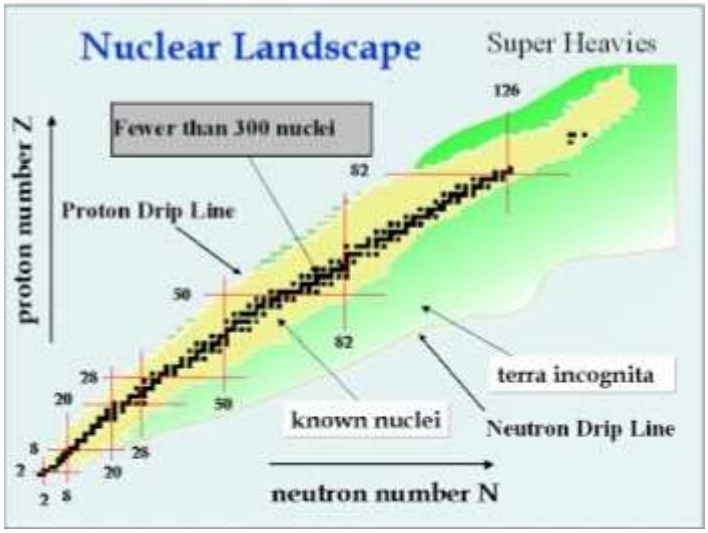

Fig. 1.1. Segre chart

The main objectives of the present work are

1. To evaluate the half-lives of probable exotic decay modes in W, Re, Ir and Pt isotopes in the mass range 150 < A < 200 using the effective liquid drop model (ELDM).

2. To compare the half-life values predicted by ELDM with other theoretical model and with the available experimental data.

3. To study the shapes of parent and daughter nuclei involved in exotic decays.

4. To study the decay characteristics of the probable exotic decay modes in these nuclei.

5. To investigate the role of neutron magicity in exotic decays.

6. To derive a general equation for half-life, governing the probable exotic decay modes in W, Re, Ir and Pt isotopes.

1.4 Organisation of the thesis

The thesis comprises of eight chapters. The second chapter introduces various theoretical approaches which are in use for the study of exotic decay process. The effective liquid drop model which is employed to carry out the present work, is also discussed in this chapter. Chapter 3 gives a review of earlier works on the theoretical and experimental studies of exotic decay or cluster radioactivity.

In chapter 4, exotic decay in W isotopes is studied using the effective liquid drop model. The half-lives are evaluated for the probable exotic decay modes in W isotopes in the mass range $150 < A < 200$. The predicted values are compared with another theoretical model and with the available experimental data. The role of neutron magicity in cluster radioactivity is studied. Geiger-Nuttall plots are drawn for the probable decay modes in W isotopes and we have derived a general equation for half-life governing the probable exotic decay modes in W isotopes. Similar studies are carried out for Re, Ir and Pt isotopes in chapters 5, 6 and 7 respectively.

Chapter 8 gives the summary of the present studies. All our predictions and findings are summarised here.

References

1. G. Gamow, *Z. Phys.* **51**, 204 (1928).
2. J. W. S. Rayleigh Lord, *Proc. Lond. Math. Soc.* **10**, 4 (1879).
3. N. Bohr and J. Wheeler, *Phys. Rev.* **56**, 426 (1939).
4. V. A. Karnaukhov, G. M. Ter-Akopyan, L. A. Petrov and V. G. Subbotin, *JETF* **45**, 1280 (1963).
5. S. Hofmann, in *Nuclear Decay Modes*, Chap. 3 (IOP, Bristol, 1996), p. 143.
6. S. Hofmann, W. Reisdorf, G. Munzenberg, F. P. HeBberger, J. R. H. Schneider and P. Armbruster, *Z. Phys. A* **305**, 111 (1982).
7. A. V. Ramayya, J. K. Hwang, J. H. Hamilton, A. Sandulescu, A. Florescu, G. M. Ter-Akopian, A. V. Daniel, Y. T. Oganessian, G. S. Popeko, W. Greiner and J. D. Cole, *Phys. Rev. Lett.* **81**, 947 (1998).
8. V. M. Strutinsky, *Nucl. Phys. A* **95**, 420 (1967).
9. A. Sandulescu, D. N. Poenaru and W. Greiner, *Sov. J. Part. Nuclei* **11**, 528 (1980).
10. H. J. Rose and G. A. Jones, *Nature (London)*, **307**, 245 (1984).
11. D. N. Poenaru and W. Greiner, in *Handbook of Nuclear Properties*, edited by D. N. Poenaru et al. (Oxford Univ. Press, 2008), p. 131.
12. D. N. Poenaru, W. Greiner and R. Gherghescu, *Phys. Rev. C* **47**, 2030 (1993).
13. S. Kumar, *J. Phys. : Conf. Ser.* **282**, 012015 (2011).
14. W. Greiner, H. J. Fink, J. A. Maruhn and W. Scheid, *Z. Phys.* **268**, 321 (1974).
15. J. A. Maruhn, W. Greiner and W. Scheid, in *Theory of Fragmentation in Heavy Ion Collisions*, edited by R. Bock, Vol. 2 (North Holland, 1980), p. 399.
16. Yu. Ts. Oganessian, Yu. A. Lazarev, V. L. Mikheev, Yu. A. Muzychka, I. V. Shirokovsky, S. P. Tretyakova and V. K. Utyonkov, *Z. Phys. A* **349**, 341 (1994).

17. A. Guglielmetti, R. Bonetti, G. Poli, P. B. Price, A. J. Westphal, Z. Janas, H. Keller, R. Kirchner, O. Klepper, A. Piechaczek, E. Roeckl, K. Schmidt, A. Plochocki, J. Szerypo and B. Blank, *Phys. Rev. C* **52**, 740 (1995).

18. A. Guglielmetti, B. Blank, R. Bonetti, Z. Janas, H. Keller, R. Kirchner, O. Klepper, A. Piechaczek, A. Plochocki, G. Poli, P. B. Price, E. Roeckl, K. Schmidt, J. Szerypo and A. J. Westphal, *Nucl. Phys. A* **583**, 867 (1995).

19. D. N. Poenaru, D. Schnabel, W. Greiner, D. Mazilu and R. Gherghescu, *At. Data Nucl. Data Tables*, **48**, 231 (1991).

20. A. Sandulescu, R. K. Gupta, W. Scheid and W. Greiner, *Phys. Lett. B* **60**, 225 (1976).

21. R. K. Gupta, A. Sandulescu and W. Greiner, *Phys. Lett. B* **67**, 257 (1977); *Z. Naturforsch.* **32a**, 704 (1977).

22. R. K. Gupta, C. Parvulescu, A. Sandulescu and W. Greiner, *Z. Phys. A* **283**, 217 (1977).

23. A. Sandulescu, H. J. Lustig, J. Hahn and W. Greiner, *J. Phys. G : Nucl. Phys.* **4**, L279 (1976).

24. R. K. Gupta, S. Gulati, S. S. Malik and R. Sultana, *J. Phys. G : Nucl. Phys.* **13**, L27 (1987).

25. A. H. Jaffey and A. Hirsch, unpublished data, quoted in : R. Vandenbosch and J. R. Huizenga, *Nuclear Fission* (Academic Press, New York, 1973).

26. R. Bonetti, E. Fioretto, C. Migliorino, A. Pasinetti, F, Barranco, E. Vigezzi and R. A. Broglia, *Phys. Lett. B* **241**, 179 (1990).

27. S. Rosenblum, *C. R. Acad. Sci. Paris* **188**, 1401 (1929).

28. L. Brillard, A. G. Elayi, E. Hourani, *C. R. Acad. Sci. Paris Ser.* II309, 1105 (1989).

29. M. Hussonnois, J. F. Ledu, L. Brillard, J. Dalmasso and G. Ardisson, *Phys. Rev. C* **43**, 2599 (1991).

30. M. Greiner and W. Scheid, *J. Phys. G : Nucl. Phys.* **12**, L229 (1986).

31. F. Gonnenwein, in *Frontier Topics in Nuclear Physics*, edited by W. Scheid and A. Sandulescu (Plenum Press, New York, 1994), p. 113.

32. R. K. Gupta, S. Singh, W. Scheid and W. Greiner, *J. Phys. G : Nucl. Part. Phys.* **18**, 1243 (1992).

33. R. K. Gupta, W. Scheid and W. Greiner, *J. Phys. G : Nucl. Part. Phys.* **17**, 1731 (1991).

34. R. K. Gupta, S. Singh, R. K. Puri and W. Scheid, *Phys. Rev. C* **47**, 561 (1993).

35. D. N. Poenaru, W. Greiner, M. Ivascu and A. Sandulescu, *Phys. Rev. C* **32**, 572 (1985); *J. Phys. G : Nucl. Phys.* **10**, L183 (1984).

36. D. N. Poenaru, W. Greiner and K. Depta, *At. Data Nucl. Data Tables* **34**, 423 (1986).

37. W. Greiner and A. Sandulescu, *J. Phys. G : Nucl. Part. Phys.* **17**, 3429 (1991).

38. D. N. Poenaru, M. Mirea, W. Greiner, I. Cata and Z. Mazilu, *Mod. Phys. Lett. A* **5**, 2101 (1990).

39. K. K. Girija and A. Joseph, *Turk. J. Phys.* **37**, 172 (2013).

CHAPTER 2
THEORETICAL MODELS

Different types of formalisms or models are usually employed for the theoretical study of exotic decay process. Some of them relevant to the present study are discussed here. In the present study, we have used the effective liquid drop model (ELDM).

2.1 The Quantum Mechanical Fragmentation Theory

The phenomena like cold fusion, cold fission and exotic decay can be described using quantum mechanical fragmentation theory (QMFT) [1,2,3,4,5]. Taking the mass asymmetry and the length of the nucleus as dynamical co-ordinates, the closed shell effects get exposed for one or both the reaction partners for fusion or that of the decay products for fission and exotic decay. The potential energy and dynamical mass are calculated using the asymmetric two center shell model (ATCSM).

The collective Hamiltonian is given by

$$H = T(R,\beta_1,\beta_2,\eta,\eta_z,\dot{R},\dot{\beta}_1,\dot{\beta}_2,\dot{\eta},\dot{\eta}_z) + V(R, \beta_1, \beta_2, \eta, \eta_z) \quad (2.1)$$

where R is the relative separation, β_1 and β_2 are quadrupole deformations. η and η_z are the dynamical collective co-ordinates of mass and charge asymmetries and are represented as

$$\eta = \frac{A_1 - A_2}{A} \quad \text{and} \quad \eta_z = \frac{Z_1 - Z_2}{Z} \quad (2.2)$$

where A and Z are mass and charge of the parent nucleus respectively. The collective potential V is calculated with the standard Strutinsky method [6,7] and is given by

$$V(R,\eta,\eta_z) = V_{LDM} + \delta U \tag{2.3}$$

where V_{LDM} is the liquid drop model potential and δU is the shell correction.

The stationary Schrodinger equation is obtained by assuming that the relative motion R is slow compared to the η and η_z motions and that the coupling between η and η_z is weak.

$$\left\{\frac{-\hbar^2}{2\sqrt{B_{\eta\eta}}}\frac{\partial}{\partial\eta}\frac{1}{\sqrt{B_{\eta\eta}}}\frac{\partial}{\partial\eta} + V(R,\eta)\right\}\Psi_R^{(\upsilon)}(\eta) = E_R^{(\upsilon)}\Psi_R^{(\upsilon)} \tag{2.4}$$

Here B_{ij} is the mass parameter defining the kinetic part T in H [8,9]. The vibrational states $\Psi_R^{(\upsilon)}$ are counted by the quantum numbers $\upsilon = 0,1,2,\ldots$ The probability $|\Psi_R^{(0)}(\eta)|^2$, which is obtained from the ground state ($\upsilon = 0$) solution of equation (2.4), is proportional to the percentage mass distribution yield,

$$Y(A_2) = |\Psi_R^{(0)}(\eta)|^2\sqrt{B_{\eta\eta}(\eta)}\,\frac{200}{A} \tag{2.5}$$

The effects of higher excited states ($\upsilon \neq 0$) can be taken into account through Boltzmann – like occupation function

$$|\Psi_R|^2 = \sum_{\upsilon=0}^{\infty}|\Psi_R^{(\upsilon)}|^2\exp(-E_R^{(\upsilon)}/\Theta) \tag{2.6}$$

where Θ is the nucleus temperature in MeV. The excitation energy [10] is calculated as

$$E^* = \frac{1}{9}A\Theta^2 - \Theta \tag{2.7}$$

The shell effect will be damped by the excitation energy in the form

$$V = V_{LDM} + \delta U\exp(-\frac{\Theta^2}{\Theta_0^2}) \tag{2.8}$$

The parameter Θ_0 = 1.5 MeV is chosen so that shell effect vanishes when $E^* \geq 60$ MeV.

2.2 Analytical Super Asymmetric Fission Model (ASAFM)

By extending three variants of liquid drop model [11], finite range of nuclear forces model [12] and Yukawa plus exponential model [13] to systems with charge asymmetry different from mass asymmetry, a numerical super asymmetric fission model (NSAFM) was developed by Poenaru et al. [14,15,16]. Since, within WKB approximation, half-lives computed are time consuming, an analytical relationship for half-life, that is, analytical super asymmetric fission model (ASAFM) [17] was developed to describe angular momentum and small excitation effects.

For a system, logarithm of the half-life time is given by

$$\log T = 0.43429(K_{0\upsilon} + K_s) - \log E_\upsilon - 20.8436 \tag{2.9}$$

where E_υ is the zero point vibration energy which is calculated as

$$E_\upsilon = Q[0.056 + 0.039\exp[(4 - A_2)/2.5]] \text{ for } A_2 \geq 4 \tag{2.10}$$

and $K_{0\upsilon}$ is the action integral corresponding to the overlap region and is given by the analytical expression,

$$K_{0\upsilon} = 0.2196(E_b^0 A_1 A_2/A)^{1/2}\left[(b^2 - a^2)^{1/2} - \frac{a^2}{b}\ln\left[\frac{b+(b^2-a^2)^{1/2}}{a}\right]\right] \tag{2.11}$$

Also K_s is the action integral corresponding to separated configuration and is expressed as

$$K_s = 0.4392\left[\frac{Q'A_1A_2}{A}\right]^{1/2} R_b\tau_{mc} \tag{2.12}$$

where $Q' = Q + E_\upsilon + E^*$, with E^* being the fraction of the excited energy concentrated in the collective mode leading to separation. The interaction energy at the top of the barrier is given by

$$E_i = E_c + E_l = \frac{1.44 Z_1 Z_2}{R_t} + \frac{20.735\, l(l+1) A}{R_t^2 A_1 A_2} \quad (2.13)$$

$R_i = R_0 - R_2$ is the initial separation distance, where R_0 is the radius of parent and R_2 is the radius of the daughter nucleus. $R_t = R_1 + R_2$ is the touching separation distance, where R_1 is the radius of the emitted cluster. R_b is the outer turning point of W.K.B penetrability and is given by

$$R_b = \frac{R_t E_c}{Q'}\left[\frac{1}{2} + \left[\frac{1}{4} + \frac{Q' E_l}{E_c^2}\right]^{1/2}\right] \quad (2.14)$$

$$a = b\left[\frac{Q'-Q}{E_b^0}\right]^{1/2};\ b = R_t - R_i \quad (2.15)$$

$$\tau_{mc} = (c + m - 1)^{1/2}[r(c - r) + m]^{1/2}$$
$$+ \frac{c}{2}\left[\arcsin\frac{c-2r}{(c^2+4m)^{1/2}} - \arcsin\frac{c-2}{(c^2+4m)^{1/2}}\right]$$
$$+ \sqrt{m}\ \ln\left[\frac{2\sqrt{m}[r(c-r)+m]^{1/2} + cr + 2m}{r[2\sqrt{m}(c+m-1)^{1/2} + c + 2m]}\right] \quad (2.16)$$

where $r = R_t/R_b$; $m = r^2 E_l/Q'$; $c = rE_c/Q'$ (2.17)

2.3 Proximity potential model by Shi and Swiatecki

In this model [18], the explicit formula for deformation energy is given by

$$V(L) = -Q + Z_1 Z_2 e^2/r + V_p(z) \qquad \text{for } L > L_c \quad (2.18)$$

$$V(L) = a(L - L_0)^{\upsilon} \qquad \text{for } L_0 < L < L_c \quad (2.19)$$

where L is the major axis of the configuration and L_0 is the diameter of the parent nucleus. L_c is the sum of fragment diameters and Q is the energy released. By applying the smooth continuity condition on potential at touching configuration, the parameters a and υ are determined. z is the

distance between the near surfaces of the fragments and r is the separation between fragment centres. The proximity potential V_p is given by

$$V_p(z) = K\varphi(z/b) \tag{2.20}$$

where $K = 4\pi\bar{R}\gamma b$ (2.21)

φ is the universal nuclear proximity function.

$$\varphi(\xi) \approx -4.41e^{-\xi/0.7176} \text{ for } \xi \geq 1.9475 \tag{2.22}$$

$$\varphi(\xi) \approx -1.7817 + 0.9270\xi + 0.01696\xi^2 - 0.05148\xi^3 \text{ for } 0 \leq \xi \leq 1.9475 \tag{2.23}$$

$\xi = z/b$, b is the width of nuclear surface ($b \approx 1$fm) and γ is the specific nuclear surface tension.

$$\gamma = 0.9517[1 - 1.7826(N - Z)^2/A^2] \text{ MeV/fm}^2 \tag{2.24}$$

The reduced radius, $\bar{R} = c_1c_2/(c_1 + c_2)$ (2.25)

where c_i (i = 1,2) is the central radii of the fragments.

$$c_i \approx R_i - b^2/R_i \tag{2.26}$$

The effective sharp radius,

$$R = 1.28A^{1/3} - 0.76 + 0.8A^{-1/3} \tag{2.27}$$

The Gamow penetrability factor is

$$G = \exp\left\{\frac{2}{\hbar}\int_{z_0}^{z_{exit}}\sqrt{2M_rV}\,dz\right\} \tag{2.28}$$

Here M_r is the effective mass and z_0 and z_{exit} are approximate zeros of the integrand. The absolute value of lifetime is calculated as

$$\tau = \tau_0 G \tag{2.29}$$

where τ_0 is the frequency factor and is taken as 10^{-22} s for even-A and 10^{-20} s for odd-A parent nuclei [19].

2.4 Cubic plus Yukawa plus exponential potential model (CYEM)

In this model [20], the potential for post scission region is given as

$$V(r) = Z_1Z_2e^2/r + V_n(r) - Q \tag{2.30}$$

where Q is the energy released and $V_n(r)$ is the nuclear interaction energy [13], given by

$$V_n(r) = -D\left[F + \frac{r-r_t}{a}\right]\frac{r_t}{r}\exp[(r_t - r)/a] \tag{2.31}$$

Here r_t is the sum of sharp radii of fragments. D is the depth constant given by

$$D = \frac{4a^3g_1g_2e^{r_t/a}[C_s(1)C_s(2)]^{1/2}}{r_0^2r_t} \tag{2.32}$$

The constant F is given as

$$F = 4 + \frac{r_t}{a} - \frac{f_1}{g_1} - \frac{f_2}{g_2} \tag{2.33}$$

where $g_j = (R_j/a)\cosh(R_j/a) - \sinh(R_j/a)$ (2.34)

$f_j = (R_j/a)^2\sinh(R_j/a)$ (2.35)

$C_s(j) = a_s(1 - K_sI_j^2)$ (2.36)

and $I_j = (N_j - Z_j)/A_j \quad ; \ (j = 1,2)$ (2.37)

Here $r_0 = 1.16$ fm, $a = 0.68$ fm, $a_s = 21.13$ MeV and $K_s = 2.3$.

The potential for the overlap region is approximated by a 3rd order polynomial [20] as

$$V(r) = -E_\upsilon + [V(r_t) + E_\upsilon]\left[s_1\left[\frac{r-r_i}{r_t-r_i}\right]^2 - s_2\left[\frac{r-r_i}{r_t-r_i}\right]^3\right] \tag{2.38}$$

E_υ is the zero point vibration energy which is given by [21]

$$E_\upsilon = \frac{\pi\hbar}{2}\frac{(2Q/\mu)^{1/2}}{(C_1+C_2)} \tag{2.39}$$

μ is the reduced mass. C_1 and C_2 are the central radii of fragments.

$$C_i = 1.18A_i^{1/3} - 0.48 \quad ; \quad (i = 1,2) \tag{2.40}$$

The half-life time of the system is given by [22]

$$T = \frac{1.4333 \times 10^{-21}}{E_\upsilon}[1 + \exp(K)] \tag{2.41}$$

$$\text{where } K = \frac{2}{\hbar}\int_{r_a}^{r_t}[2B_r(r)V(r)]^{1/2}dr + \frac{2}{\hbar}\int_{r_t}^{r_b}[2B_r(r)V(r)]^{1/2}dr \tag{2.42}$$

Here r_a and r_b are two approximate zeros of the integrand and $B_r(r)$ is the effective mass, which is deformation dependent [23].

2.5 Microscopic model by Blendowske et al.

In this formalism [24,25], the potential is calculated as

$$U(R) = V(R) + V_{coul}(R) + V_L(R) \tag{2.43}$$

where V(R) is the semi-empirical heavy ion potential, $V_{coul}(R)$ is the Coulomb potential and $V_L(R)$ is the centrifugal potential.

$$V_{coul}(R) = Z_1Z_2e^2/r \tag{2.44}$$

$$V_L(R) = \hbar^2L(L + 1)/2M \tag{2.45}$$

where M is the reduced mass and L is the angular momentum. The semi-empirical heavy ion potential [26] is calculated as

$$V(R) = -50 \text{ MeV/fm}\frac{R_1R_2}{R_1+R_2}\exp[-(R - R_1 - R_2)/a] \tag{2.46}$$

where a = 0.63 fm

$$R_j = 1.233A_j^{1/3} - 0.978A_j^{-1/3} \text{ fm} \;;\; j = 1,2 \quad (2.47)$$

Within WKB approximation, the decay constant is calculated as

$$\lambda_0 = (\nu/2R_i)P \quad (2.48)$$

$$\text{where } P = \exp\left\{-2\int_{R_i}^{R_0} dR[(2M/\hbar^2)(U(R) - Q)]^{1/2}\right\} \quad (2.49)$$

Q is the Q value for the reaction, R_i is the inner turning point and R_0 is the outer turning point.

Blendowske et al. [24] assumed a kinetic energy within the barrier of 10^2 MeV in the case of alpha particle and the scaled value $10^2(14/4)$ MeV in the case of ^{14}C cluster. In the microscopic model, decay constant is calculated as

$$\lambda = \lambda_0 S \quad (2.50)$$

where S is the spectroscopic factor, which is obtained from the overlap of proton/neutron states of the cluster with those in the parent nucleus [24].

2.6 Preformed cluster model (PCM)

The preformed cluster model [27] consists of two steps: 1) cluster formation and 2) tunneling of nuclear interaction barrier. The decay constant and half-life time are calculated as

$$\lambda = P_0 \nu P \quad (2.51)$$

$$T_{1/2} = (\ln 2)/\lambda \quad (2.52)$$

where P_0 is the probability of cluster formation, ν is the assault frequency and P is the probability of barrier penetration.

Dynamical collective co-ordinates for mass asymmetry and charge asymmetry are given by

$$\eta = \frac{A_1 - A_2}{A} \qquad \text{and} \qquad \eta_z = \frac{Z_1 - Z_2}{Z} \tag{2.53}$$

At a relative separation of R, the probability of finding fragments of masses A_1 and A_2 is obtained by solving the following Schrodinger equation,

$$\left[\frac{-\hbar^2}{2\sqrt{B_{\eta\eta}}}\frac{\partial}{\partial\eta}\frac{1}{\sqrt{B_{\eta\eta}}}\frac{\partial}{\partial\eta} + V(\eta, \eta_z, R)\right]\Psi(\eta) = E_{g.s}\Psi(\eta) \tag{2.54}$$

where $B_{\eta\eta}$ is the mass parameter and $V(\eta,\eta_z,R)$ is the potential energy of collective interaction.

Normalization of the equation (2.54) gives the probability of cluster formation in the ground state,

$$P_0(A_2) = |\Psi(\eta)|^2\sqrt{B_{\eta\eta}}\,\frac{2}{A} \tag{2.55}$$

The collective interaction energy is given by

$$V(\eta,\eta_z,R) = -\sum_{i=1}^{2} B_i(A_i, Z_i) + \frac{Z_1 Z_2 e^2}{r} + V_p \tag{2.56}$$

where the first term is the experimental binding energy, second term is the Coulomb potential and V_p is the nuclear proximity potential, which is given as

$$V_p = 4\pi\gamma b\frac{C_1 C_2}{C_1 + C_2}\varphi(z/b) \tag{2.57}$$

where γ is the coefficient of nuclear surface tension and z is the separation between the nearby surfaces.

$$\gamma = 0.9517[1 - 1.7826(N - Z)^2/A^2]\ \text{MeV/fm}^2 \tag{2.58}$$

φ is the universal proximity potential which is given by

$$\varphi(\zeta) = -(1/2)(\zeta - 2.54)^2 - 0.0852(\zeta - 2.54)^3 \text{ for } \zeta \leq 1.2511 \tag{2.59}$$

$$\varphi(\zeta) = -3.437\exp(-\zeta/0.75) \text{ for } \zeta \geq 1.2511 \tag{2.60}$$

where $\zeta = (C - C_1 - C_2)/b$ and b is the nuclear surface width ($b \approx 1$). C_i ($i = 1,2$) is the Sissmann central radius of fragments which is related to radius R_i as $C_i \approx R_i - (b^2/R_i)$. The semi-empirical formula for R_i is given as

$$R_i = 1.28A_i^{1/3} - 0.76 + 0.8A_i^{-1/3} \tag{2.61}$$

The assault frequency is expressed as $\nu = (2E_2/\mu)^{1/2}/R_0$, where μ is termed as the reduced mass, R_0 the nuclear radius of the parent and E_2 the kinetic energy for the emitted cluster. The tunneling probability is expressed as

$$P = P_i W_i P_b \tag{2.62}$$

where P_i is the penetrability from R_t to R_i, W_i the deexcitation probability and P_b the penetrability from R_i to R_b. The deexcitation probability changes exponentially with excitation energy E_i and is given as $W_i = \exp(-bE_i)$. In the case of clusters which are heavier than alpha particle, $b = 0$. The penetrabilities P_i and P_b are given as

$$P_i = \exp\left\{-\frac{2}{\hbar}\int_{R_t}^{R_i}[2\mu(V - V(R_i))]^{1/2}dR\right\} \tag{2.63}$$

$$P_b = \exp\left\{-\frac{2}{\hbar}\int_{R_i}^{R_b}[2\mu(V - Q)]^{1/2}dR\right\} \tag{2.64}$$

2.7 Cluster model by Buck et al.

In this model [28,29], the parent nucleus is assumed to have a daughter nucleus core of mass A_1 and a preformed cluster of mass A_2. The interaction between these fragments is described with a simple local potential, which is obtained by using a double folding integral, i.e.,

$$V_N(r) = \iint \rho_1(r_1)\rho_2(r_2)U(|r + r_2 - r_1|)d^3r_1 d^3r_2 \tag{2.65}$$

where $\rho_1(r_1)$ and $\rho_2(r_2)$ are the respective densities of the fragments and $U(|r_1 - r_2|)$ is the effective nucleon-nucleon potential. This equation can be approximately written in the form of a simple potential,

$$V_N(r) = \frac{-V_0[1+\cosh(R/a)]}{[\cosh(r/a)+ \cosh(R/a)]} \tag{2.66}$$

where V_0 is the depth of the potential barrier and a is the nonzero diffuseness. The radius R is expressed as

$$R = 1.04(A_1^{2/3} + A_2^{2/3})^{1/2} \tag{2.67}$$

The interaction potential between core and cluster is given by

$$V(r) = V_N(r) + V_c(r) + \frac{\hbar^2}{2\mu r^2}\left[L + \frac{1}{2}\right]^2 \tag{2.68}$$

Here μ represents the reduced mass, $V_c(r)$ the Coulomb potential and the third term is Langer modified centrifugal barrier. The classical turning points, r_1, r_2 and r_3 are obtained by numerically solving the equation $V(r) = Q$, in which Q is the Q value for the reaction. If L has a very small value, r_1 is approximately zero and if we neglect the nuclear term $V_N(r)$ in the asymptotic region, the resulting quadratic equation can be solved to find r_3. The decay width can be expressed as [30]

$$\Gamma = PF\frac{\hbar^2}{4\mu}\exp\left[-2\int_{r_2}^{r_3} K(r)dr\right] \tag{2.69}$$

Here P is called the preformation probability and K(r) is the semi-classical wave number which is given by

$$K(r) = \left[\frac{2\mu}{\hbar^2}|Q - V(r)|\right]^{1/2} \tag{2.70}$$

F is the normalization factor for semi-classical bound state, which is expressed as

$$F \int_{r_1}^{r_2} \frac{1}{K(r)} \cos^2 \left[\int_{r_1}^{r} K(r') dr' - \frac{\pi}{4} \right] dr = 1 \quad (2.71)$$

Then the half-life time can be computed using the relation,

$$T_{1/2} = \hbar \frac{\ln 2}{\Gamma} \quad (2.72)$$

2.8 Double folded Michigan-three-Yukawa (M3Y) potential model

In this model [31], the M3Y potential involves Coulomb plus nuclear interaction between the separated fragments and is expressed as

$$V_{M3Y}(R) = \int dr_1 dr_2 \rho_1(r_1) \rho_2(r_2) V(r_{12}) \quad (2.73)$$

with $V(r_{12})$ being the nucleon-nucleon interaction potential [32] and is given by

$$V(r_{12}) = V_{00}(r_{12}) + \bar{J}_{00} \delta(r_{12}) + V_{01}(r_{12}) \tau_1 . \tau_2 \quad (2.74)$$

$V_{00}(r)$ is the central component in M3Y force and is expressed as

$$V_{00}(r) = \left[7999 \frac{e^{-4r}}{4r} - 2134 \frac{e^{-2.5r}}{2.5r} \right] \text{ MeV} \quad (2.75)$$

$$V_{01}(r) = \left[-4885.5 \frac{e^{-4r}}{4r} + 1175.5 \frac{e^{-2.5r}}{2.5r} \right] \text{ MeV} \quad (2.76)$$

$\bar{J}_{00}$ is the zero pseudopotential which approximates the exchange effects of a single nucleon and is given by $\bar{J}_{00}$ = -262 MeVfm^3. The spin-spin component V_{10} and spin-isospin component V_{11} are neglected since their final contributions are small. The final nuclei are assumed as coaxial spheroids with nuclear density,

$$\rho(r) = \rho_0 \left\{ 1 + \exp \frac{1}{a} \left(r - \frac{R}{C} \left[1 + \beta_2 Y_2^0(\cos\theta) \right] \right) \right\}^{-1} \quad (2.77)$$

Here ρ_0 is a constant, which is fixed by normalizing the neutron and proton densities to neutron number N and proton number Z respectively. β_2

represents the quadrupole deformation whereas C represents the usual constant which obey the condition for volume conservation,

$$\int d^3r = \frac{4\pi}{3} R^3 \tag{2.78}$$

C can be expressed in terms of β_2 as

$$C(\beta_2) = \left[1 + \frac{3}{4\pi}\beta_2^2 + \frac{1}{14\pi}\sqrt{\frac{5}{4\pi}}\beta_2^3\right]^{1/3} \tag{2.79}$$

R and a are the two parameters for Fermi density. For light clusters, $R = 0.95A^{1/3}$ fm and a = 0.67 fm. For heavy daughter nuclei, $R = 1.19A^{1/3}$ fm and a = 0.63 fm.

In this model, the penetrability is calculated as

$$P = \exp\left\{-\frac{2}{\hbar}\int_{R_i}^{R_0}[2\mu(V(R) - Q)]^{1/2}dR\right\} \tag{2.80}$$

The distance between the separated fragment mass centres is represented by R and the reduced mass is represented by μ. R_i is the inner turning point and R_0 is the outer turning point and they are defined by

$$V(R_i) = V(R_0) = Q \tag{2.81}$$

where Q is the Q value for the reaction. The half-life time is calculated as

$$T_{1/2} = \frac{\ln 2}{\nu P_0 P} \tag{2.82}$$

where ν represents the collision frequency and P_0, the preformation factor.

2.9 Dynamical cluster model (DCM)

This model [33] is a reformulation of preformed cluster model (PCM) of Gupta and collaborators [27]. DCM is mainly used in the decay of hot, rotating compound nucleus. Here, the orientation and deformation effects are

considered in addition to the angular momentum and temperature effects. In DCM, calculations are done in terms of the collective co-ordinates of mass asymmetry and charge asymmetry ($\eta = (A_1 - A_2)/A$, $\eta_Z = (Z_1 - Z_2)/Z$) and the relative distance between the fragments (R). η and η_Z determines the division of nucleons between the fragments. R characterizes the kinetic energy transfer from the entrance channel to the exit channel. In the case of decay of a hot compound nucleus,

$$E^*_{CN} + Q_{out}(\theta) = TKE(\theta) + TXE(\theta) \quad (2.83)$$

E^*_{CN} represents the excitation energy for the compound nucleus which is expressed in terms of temperature θ as

$$E^*_{CN} = (1/9)A_{CN}\theta^2 - \theta \quad (2.84)$$

Q_{out} is the Q value for the exit channel. TKE(θ) is the total kinetic energy and TXE(θ) is the total excitation energy of the fragments. The decay cross section is expressed as

$$\sigma = \frac{\pi}{k^2}\sum_{l=0}^{l_{max}}(2l+1)P_0P \quad (2.85)$$

where $k = \sqrt{2\mu E_{cm}/\hbar^2}$, P_0 denotes the preformation factor corresponding to η motion and P is the penetrability corresponding to R motion. The reduced mass of the fragments is represented by μ and l_{max} represents the maximum angular momentum. P and P_0 are functions of l and θ. For $l = 0$,

$$\sigma_0 = \frac{\pi}{k^2}P_0P \quad (2.86)$$

which is similar to the equation for decay constant ($\lambda = \nu_0 P_0 P$) in PCM. P_0 is obtained from the solution of the Schrodinger equation,

$$\left[\frac{-\hbar^2}{2\sqrt{B_{\eta\eta}}}\frac{\partial}{\partial\eta}\frac{1}{\sqrt{B_{\eta\eta}}}\frac{\partial}{\partial\eta} + V(R,\eta,\theta)\right]\Psi^{(v)}(\eta) = E^{(v)}\Psi^{(v)}(\eta) \quad (2.87)$$

with ν = 1,2,3,… corresponding to the solutions in ground state and excited state. $B_{\eta\eta}$ represents the smooth hydrodynamical masses. The fragmentation potential is given by

$$V(R,\eta,\theta) = \sum_{i=1}^{2} V_{LDM}(A_i,Z_i,\theta) + \sum_{i=1}^{2} \delta u_i \exp(-\theta^2/\theta_0^2) + V_c(R,Z_i,\theta) + V_p(R,A_i,\theta) + V_l(R,A_i,\theta) \quad (2.88)$$

where V_{LDM} is the liquid drop potential, δu the shell correction, V_c the Coulomb potential, V_p the nuclear proximity potential and V_l is the centrifugal potential.

$$P_0(A_i) = \frac{2}{A}\sqrt{B_{\eta\eta}}\,|\Psi(\eta(A_i))|^2 \quad (2.89)$$

i = 1 or 2 represents cluster or daughter fragment. The solution $\Psi\Psi^{(\nu)}(\eta)$ is given by

$$\Psi\Psi\Psi^{(\nu)}(\eta) = \sum_{\nu=0}^{\infty} |\Psi\Psi^{(\nu)}|^2 \exp(-E^{(\nu)}/\theta) \quad (2.90)$$

The first turning point is given by

$$R_a = R_1(\theta) + R_2(\theta) + \Delta R(\theta) = R_t(\theta) + \Delta R(\theta) \quad (2.91)$$

Radii is expressed in terms of temperature θ as

$$R_i(\theta) = [1.28A_i^{1/3} - 0.76 + 0.8A_i^{-1/3}](1 + 0.0007\theta^2) \quad (2.92)$$

ΔR(θ) is the neck length parameter which accounts the nuclear deformation. Using WKB approximation, the penetrability is calculated as

$$P = \exp\left\{-\frac{2}{\hbar}\int_{R_a}^{R_b}[2\mu(V(R,\theta) - Q_{eff})]^{1/2}dR\right\} \quad (2.93)$$

with

$$V(R_a) = V(R_b) = Q_{eff} \quad (2.94)$$

where R_b denotes the second turning point.

The critical value of angular momentum where the fusion barrier of the entrance channel vanishes is given by

$$l_c = R_a[2\mu(E_{cm} - V(R_a,\eta,l = 0))]^{1/2}/\hbar \quad (2.95)$$

where μ = reduced mass and E_{cm} = bombarding energy

2.10 Generalised liquid drop model (GLDM)

This model [34,35] has been used to evaluate the half-lives of the unfavored and the favored alpha decay. GLDM can describe in a unified way, the phenomenon of shape evolution from the system of one body to that of two separated fragments. Within the GLDM, the macroscopic energy is determined as

$$E = E_v + E_s + E_c + E_{prox} + E_{cen}(r) \quad (2.96)$$

where E_v is the volume energy, E_s the surface energy, E_c the Coulomb energy, E_{prox} the proximity energy and $E_{cen}(r)$ the centrifugal potential energy. When the fragments are separated,

$$E_v = -15.494[(1 - 1.8I_1^2)A_1 + (1 - 1.8I_2^2)A_2] \quad \text{MeV} \quad (2.97)$$

$$E_s = 17.9439[(1 - 2.6I_1^2)A_1^{2/3} + (1 - 2.6I_2^2)A_2^{2/3}] \quad \text{MeV} \quad (2.98)$$

$$E_c = 0.6e^2Z_1^2/R_1 + 0.6e^2Z_2^2/R_2 + e^2Z_1Z_2/r \quad (2.99)$$

where A_i are the mass numbers, Z_i the charge numbers, R_i the radii and I_i the relative neutron excesses for the two nuclei. R_i are given by

$$R_i = (1.28A_i^{1/3} - 0.76 + 0.8A_i^{-1/3}) \ \text{fm} \quad (2.100)$$

For one-body shapes,

$$E_v = -15.494(1 - 1.8I^2)A \quad MeV \tag{2.101}$$

$$E_s = 17.9439(1 - 2.6I^2)A^{2/3}(S/4\pi R_0^2) \quad MeV \tag{2.102}$$

$$E_c = 0.6e^2(Z^2/R_0) \times 0.5\int (V(\theta)/V_0)\,(R(\theta)/R_0)^3 \sin\theta d\theta \tag{2.103}$$

S is the surface area for one-body deformed nucleus, $V(\theta)$ the electrostatic potential present at the surface and V_0 represents the surface potential of the sphere. When nucleons are present in the neck or the gap between the separated fragments, proximity energy must be taken into account to incorporate the effects of nuclear forces present between the close surfaces. The proximity energy is expressed as

$$E_{prox}(r) = 2\gamma \int_{h_{min}}^{h_{max}} \Phi\,[D(r,h)/b]2\pi h dh \tag{2.104}$$

Here h is the distance that varies from zero or the neck radius to the height of the neck border. D is the separation between the surfaces under consideration and b is the surface width, which is given as b = 0.99 fm. Φ represents the proximity function of Feldmeier [36]. γ is the surface parameter, which is given by the geometric mean taken between the surface parameters for the two fragments.

The centrifugal potential energy is given by

$$E_{cen}(r) = \frac{\hbar^2}{2\bar{\mu}} \frac{l(l+1)}{r^2} \tag{2.105}$$

where r denotes the separation between the two fragments.

The penetration probability is expressed as

$$P = \exp\left\{-\frac{2}{\hbar}\int_{R_{in}}^{R_{out}} [2B(r)(E(r) - E_{sph})]^{1/2} dr\right\} \tag{2.106}$$

The deformation energy with respect to the sphere is small up to the point of rupture between the fragments. R_{in} is the inner turning point and R_{out} is the

outer turning point of the WKB action integral. The approximation, B(r) = $\bar{\mu}$ may be used. The decay half-life is expressed as

$$T_{1/2} = \frac{\ln 2}{\nu P} \tag{2.107}$$

where ν is the assault frequency and is taken as 1.0×10^{20} s^{-1}.

2.11 Universal decay law (UDL)

Universal decay law was put forward by Qi et al. [37,38] for the study of alpha and cluster decays. This is a linear relation derived from the microscopic mechanism of radioactive decay and the α-like R-matrix theory. This model provides the relation between the logarithm of decay half-life and two variables, χ' and ρ', which depend on the charges and masses of the nuclei which are involved in the decay and also on the Q values of outgoing clusters. In this model, the expression for half-life is given by

$$\log_{10}T_{1/2} = aZ_cZ_d\sqrt{\frac{A}{Q}} + b\sqrt{AZ_cZ_d(A_d^{1/3} + A_c^{1/3})} + c \tag{2.108}$$

$$= a\chi' + b\rho' + c \tag{2.109}$$

$$\text{where } A = \frac{A_dA_c}{A_d + A_c} \tag{2.110}$$

A_d and A_c are the mass numbers of daughter and cluster respectively. Z_d and Z_c are the atomic numbers of daughter and cluster respectively and Q is the Q value of the decay. a, b and c are constants [39] given by a = 0.4314, b = -0.4087 and c = -25.7725. These are obtained by fitting to experiments of alpha and cluster decays. Clustering effects are incorporated in the term bρ' + c. This relation for half-life, which is a generalization of Geiger-Nuttall law [40], holds for all known cluster decays and therefore it is known as universal decay law.

2.12 The present model : Effective liquid drop model (ELDM)

This model [41,42] can explain alpha decay, cluster radioactivity and cold fission considering different inertial coefficients. The nuclear system can assume either fission-like or cluster-like shape on the basis of shape parameterization chosen in this model.

In the case of cluster-like approach, the preformation of cluster within the parent nucleus is assumed and the inner turning point in the Gamow penetrability factor is evaluated. The radius and shape of the cluster remain unaltered throughout the dynamical evolution of the decaying nuclear system. For fission-like approach, inner turning point can't be determined and for all the systems, it is taken as 1×10^{-8}. For both approaches, the half-life and decay constant are evaluated.

Assuming the geometrical constraint that is necessary to preserve the shape of the nuclear system with a fixed volume during the whole process, the multidimensional evolution of the nuclear system is simplified to a one-dimensional one and Gamow penetrability factor is evaluated. In this model, the shell effects on the surface potential are taken into account.

The geometrical configuration of the decaying nuclear system is approximately assumed as two intersecting spheres of different radii. Disregarding the position of centre of mass of the nuclear system, four independent co-ordinates are considered for the complete specification. Fig. 2.1 shows the shape parameterization of the decaying nuclear system. R_1 and R_2 are the radii of cluster and daughter respectively. ξ is the distance between the plane of intersection and geometrical centre of the daughter nucleus.

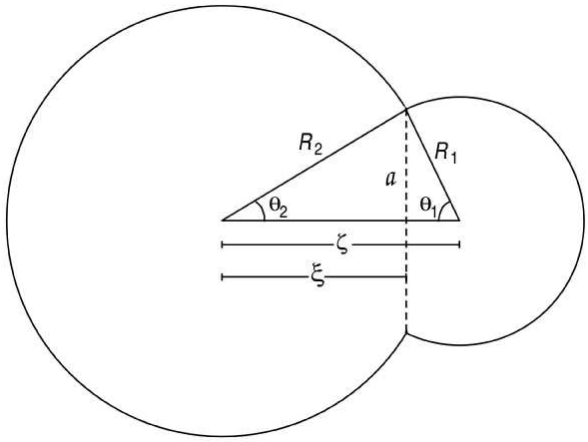

Fig 2.1. Shape parameterization of decaying system [41]

ζ represents the separation between the two geometrical centres. At the touching configuration referring to the end point of the pre-scission phase, the nuclear system attains a limiting configuration with two spherical fragments of radii $\overline{R}_1$ and $\overline{R}_2$ for cluster and daughter respectively. The intersection of spherical fragments is a circumference of radius a. The geometrical constraint is given by

$$a^2 = R_2^2 - \xi^2 = R_1^2 - (\zeta - \xi)^2 \tag{2.111}$$

The volume of the nuclear system in terms of the chosen co-ordinates is expressed as

$$2(R_1^3 + R_2^3) + 3[R_1^2(\zeta - \xi) + R_2^2\,\xi\,] - [(\zeta - \xi)^3 + \xi^3] = 4R_P^3 \tag{2.112}$$

R_P is the radius of parent nucleus. The third constraint provides two different descriptions in the case of mass transfer through the window that connects the two spheroids. VMAS (varying mass asymmetry shape) description is characterized by regarding the radius of lighter fragment as constant, i.e.,

$$R_1 - \overline{R}_1 = 0 \tag{2.113}$$

$\bar{R}_1$ denotes the final radius of the cluster. In CMAS (constant mass asymmetry shape) description, where mass of the fragments remains constant during the molecular phase, the volume of each spherical fragment is constant and the volume conservation in terms of R_1 is given by

$$2R_1^3 + 3R_1^2(\zeta - \xi) - (\zeta - \xi)^3 - 4\bar{R}_1^3 = 0 \tag{2.114}$$

In this model, Coulomb and surface energy contribute to the total potential barrier. Gaudin's expression [43] is used to calculate the Coulomb potential V_c.

$$V_c = \frac{8}{9}\pi a^5 \varepsilon(x_1,x_2)\rho_c \tag{2.115}$$

Here ρ_c denotes the initial charge density, ε is a function of angular variables, $x_1 = \pi - \theta_1$ and $x_2 = \theta_2 - \pi$ and a is the sharp neck radius. The expression for $\varepsilon(x_1,x_2)$ is given by

$$\varepsilon(x_1,x_2) = \left[\frac{1}{\sin^2 x_2} - \frac{1}{\sin^2 x_1}\right]\left[\frac{f(x_2)}{\sin^2 x_2} - \frac{f(x_1)}{\sin^2 x_1}\right] - (\cot x_2 + \cot x_1)\left[\frac{f'(x_2)+\frac{\pi}{4}}{\sin^2 x_2} - \frac{f'(x_1)+\frac{\pi}{4}}{\sin^2 x_1}\right]$$

$$+ \frac{1}{\sin^2 x_1 \sin^2 x_2}[f(x_1 + x_2) + \frac{1}{3}\sin^2(x_1 + x_2)] + \frac{\pi}{8}[g(x_1) + g(x_2)] \tag{2.116}$$

where f' represents the derivative of f. f, f' and g are the auxiliary functions which are expressed as

$$f(x) = 1 - x\cot x - \frac{\pi}{2}\tan\frac{x}{2} \tag{2.117}$$

$$f'(x) + \frac{\pi}{4} = \frac{2x - \sin(2x)}{2\sin^2 x} - \tan^2\frac{x}{2} \tag{2.118}$$

$$g(x) = [1.5 + \tan^2\frac{x}{2} + 0.3\tan^4\frac{x}{2}]\tan\frac{x}{2} + \frac{2}{\sin^3 x} \tag{2.119}$$

To calculate the surface potential energy, the effective surface tension σ_{eff} is introduced to the deformed system. By assuming that the difference in initial and final energy of the system is equivalent to the energy released in the decay, the Q value, we can define σ_{eff} through the equation,

$$\frac{3}{5}e^2\left[\frac{Z_P^2}{R_P} - \frac{Z_1^2}{R_1} - \frac{Z_2^2}{R_2}\right] + 4\pi\sigma_{eff}(R_P^2 - \bar{R}_1^2 - \bar{R}_2^2) \equiv Q \tag{2.120}$$

where Z_ie (i = P, 1, 2) denote the nuclear charges of the parent, cluster and daughter nuclei respectively. $Q = M - M_1 - M_2$. M, M_1 and M_2 represent the masses of parent, cluster and daughter respectively. The mass values have been obtained from the Nuclear mass data table [44]. Then the surface potential energy is given by

$$V_s = \sigma_{eff}(S_1 + S_2) \tag{2.121}$$

where

$$S_i = \pi R_i(R_i + \delta_i) \tag{2.122}$$

in which

$$\delta_i = \begin{cases} \zeta - \xi, & i = 1 \\ \xi, & i = 2 \end{cases} \tag{2.123}$$

After the scission point, the centrifugal potential energy is given by

$$V_l = \frac{\hbar^2}{2\bar{\mu}}\frac{l(l+1)}{\zeta^2} \tag{2.124}$$

The reduced mass $\bar{\mu} = M_1M_2/(M_1 + M_2)$. The total potential is expressed as

$$V = V_c + V_s + V_l \tag{2.125}$$

The final radii of the spherical fragments are given by

$$\bar{R}_i = \left[\frac{Z_i}{Z_P}\right]^{1/3} R_P, \quad i = 1, 2 \tag{2.126}$$

The radius of parent nucleus, R_P is given by

$$R_P = r_0 A_P^{1/3} \tag{2.127}$$

where $r_0 = 1.37$ fm. The barrier penetrability factor is given by

$$P = \exp\left\{-\frac{2}{\hbar}\int_{\zeta_0}^{\zeta_c}[2\mu(V(\zeta) - Q)]^{1/2}d\zeta\right\} \tag{2.128}$$

where μ is the inertia coefficient. ζ_0 is the inner turning point which is given by

$$\zeta_0 = R_P - \bar{R}_1 \tag{2.129}$$

ζ_c is the outer turning point and for $l = 0$,

$$\zeta_c = Z_1 Z_2 e^2/Q \tag{2.130}$$

The decay constant is

$$\lambda = \lambda_0 P \tag{2.131}$$

where λ_0 is the assault frequency and is taken as 10^{22} s^{-1}. The half-life is expressed as

$$T_{1/2} = \frac{\ln 2}{\lambda} \tag{2.132}$$

To define the inertia coefficient μ, Werner-Wheeler's approximation [45] for the velocity field of the nuclear flow is used. Werner-Wheeler's inertia coefficient μ_{ww} is expressed as

$$\frac{1}{2}\int \rho\vec{v}^2 dr = \frac{1}{2}\mu_{ww}\dot{\zeta}^2 \tag{2.133}$$

where ρ denotes the mass density of the system, $\dot{\zeta}$ represents the relative velocity for the geometric centres of the fragments and $\vec{v}$ is the velocity field obtained by solving the continuity equation using the irrotationality and incompressibility of the nuclear flow.

References

1. K. P. Santhosh, *Ph.D Thesis*, University of Calicut, Kerala (2002).

2. J. A. Maruhn and W. Greiner, *Phys. Rev. Lett.* **32**, 548 (1974).

3. K. H. Ziegenhain, H. J. Lustig, J. A. Maruhn, W. Greiner and W. Scheid, *Fizika* **9** (Suppl 4), 559 (1977).

4. J. A. Maruhn, W. Greiner and W. Scheid in *Heavy ion collisions* edited by R. Bock (North Holland, Amsterdam, 1980), p. 397.

5. H. J. Fink, W. Greiner, R. K. Gupta, S. Liran, J. A. Maruhn, W. Scheid and O. Zohni, *Pro. Int. Conf. on Reaction between Complex nuclei,* Nashville, TN, USA (North Holland, Amsterdam, 1974), Vol. 2, p. 21.

6. V. M. Strutinsky, *Nucl. Phys. A* **95**, 420 (1967).

7. V. M. Strutinsky, *Nucl. Phys. A* **122**, 1 (1968).

8. D. R. Inglis, *Phys. Rev.* **96**, 1059 (1954).

9. S. T. Balyaev, *K. Dan. vidensk. selsk. Mat. Fys. Medd.* **31**, 11 (1959).

10. K. J. Le Couteur and D. W. Lang, *Nucl. Phys.* **13**, 32 (1959).

11. W. D. Myers and W. J. Swiatecki, *Nucl. Phys.* **81**, 1 (1966); *Ark. Fys.* **36**, 343 (1967).

12. H. J. Krappe and J. R. Nix in *Proceedings of the Symposium on Physics and Chemistry of Fission* (IAEA, Vienna, 1974), Vol. I, p. 159.

13. H. J. Krappe, J. R. Nix and A. J. Sierk, *Phys. Rev. C* **20**, 992 (1979).

14. D. N. Poenaru, D. Mazilu and M. Ivascu, *J. Phys. G* **5**, 1093 (1979).

15. D. N. Poenaru, M. Ivascu and D. Mazilu, *Comput. Phys. Commun.* **19**, 205 (1980).

16. D. N. Poenaru, M. Ivascu, D. Mazilu and A. Sandulescu, *Rev. Roum. Phys.* **25**, 55 (1980).

17. D. N. Poenaru, M. Ivascu, A. Sandulescu and W. Greiner, *Phys. Rev. C* **32**, 572 (1985).

18. Y. J. Shi and W. J. Swiatecki, *Nucl. Phys. A* **438**, 450 (1985).

19. Y. J. Shi and W. J. Swiatecki, *Nucl. Phys. A* **464**, 205 (1987).

20. G. Shanmugam and B. Kamalaharan, *Phys. Rev. C* **38**, 1377 (1988).

21. H. G. de Carvalho, J. B. Martins and O. A. P. Tavares, *Phys. Rev. C* **34**, 2261 (1986).

22. D. N. Poenaru and M. Ivascu, *J. Phys. (Paris)* **45**, 1099 (1984).

23. P. Moller, J. R. Nix and W. J. Swiatecki, *Nucl. Phys. A* **469**, 1 (1987).

24. R. Blendowske, T. Fliessbach and H. Walliser, *Nucl. Phys. A* **464**, 75 (1987).

25. R. Blendowske and H. Walliser, *Phys. Rev. Lett.* **66**, 1930 (1988).

26. P. R. Christensen and A. Winther, *Phys. Lett.* **65B**, 19 (1976).

27. S. S. Malik and R. K. Gupta, *Phys. Rev. C* **39**, 1992 (1989).

28. B. Buck and A. C. Merchant, *Phys. Rev. C* **39**, 2097 (1989).

29. B. Buck, A. C. Merchant and S. M. Perez, *Nucl. Phys. A* **512**, 483 (1990).

30. S. A. Gurvitz and G. Kalbermann, *Phys. Rev. Lett.* **59**, 262 (1987).

31. G. R. Satchler and W. G. Love, *Phys. Rep.* **55**, 183 (1979).

32. G. Bertsch, J. Borysowicz, H. Mc Manus and W. G. Love, *Nucl. Phys. A* **284**, 399 (1977).

33. Raj K. Gupta, M. Balasubramaniam, Rajesh Kumar, Dalip Singh, C. Beck and W. Greiner, *Phys. Rev. C* **71**, 014601 (2005).

34. G. Royer, *J. Phys. G : Nucl. Part. Phys*. **26**, 1149 (2000).

35. R. Moustabchir and G. Royer, *Nucl. Phys. A* **683**, 266 (2001).

36. H. Feldmeier, *12th Summer School on Nuclear Physics,* Mikolajki, Poland, 1979.

37. C. Qi, F. R. Xu, R. J. Liotta and R. Wyss, *Phys. Rev. Lett.* **103**, 072501 (2009).

38. C. Qi, F. R. Xu, R. J. Liotta, R. Wyss, M. Y. Zhang, C. Asawatangtrakuldee and D. Hu, *Phys. Rev. C* **80**, 044326 (2009).

39. K. P. Santhosh and B. Priyanka, *Nucl. Phys. A* **929**, 20 (2014).

40. H. Geiger and J. M. Nuttall, *Philos. Mag.* **22**, 613 (1911).

41. S. B. Duarte, O. A. P. Tavares, F. Guzman and A. Dimarco, *At. Data Nucl. Data Tables* **80**, 235 (2002).

42. M. Goncalves, S. B. Duarte, F. Garcia and O. Rodriguez, *Comput. Phys. Commun.* **107**, 246 (1997).

43. M. Gaudin, *J. Phys. (France)* **35**, 885 (1974).

44. G. Audi, M. Wang, A. H. Wapstra, F. G. Kondev, M. MacCormick, X. Xu and B. Pfeiffer, *Chin. Phys. C* **36**, 1603 (2012).

45. D. N. Poenaru, J. A. Maruhn, W. Greiner, M. Ivascu, D. Mazilu and I. Ivascu, *Z. Phys. A* **333**, 291 (1989).

CHAPTER 3
REVIEW OF LITERATURE

3.1 Review of experimental work on cluster radioactivity

Cluster radioactivity is a rather young member in the family of nuclear radioactivity. Here we attempted to present the experimental works which confirmed the prediction of this phenomena and other subsequent investigations in a chronological order.

Through a systematic study of the characteristics of nuclei which are heavier than lead nucleus, Rose and Jones [1] could detect radioactive decay (cluster radioactivity) accompanied by the emission of particles which are heavier than alpha particle. They have identified such decay mode for ^{223}Ra parent with ^{14}C cluster emission with the help of a counter telescope. They have stated that the branching ratio for the emission of ^{14}C with respect to the emission of alpha particle from ^{223}Ra parent is $(8.5 \pm 2.5) \times 10^{-10}$, corresponding to a preformation probability which is smaller by a factor of approximately 10^5 to 10^6.

Aleksandrov et al. [2] have also observed spontaneous emission of ^{14}C from ^{223}Ra isotope. They have reported that their results agree well with the experimental data obtained by Rose and Jones [1]. They had used ΔE - E telescope method, with ^{227}Ac source, where there was a radioactive equilibrium between ^{223}Ra isotope and actinium decay products.

Price et al. [3] have produced sources of ^{221}Fr and $^{221\text{-}224}$Ra isotopes using ISOLDE on-line isotope separator at CERN. They have used polycarbonate track-recording films which are sensitive to carbon nuclei but insensitive to alpha particles and have discovered ^{14}C cluster emission from

^{222}Ra and ^{224}Ra isotopes. They had also measured the branching ratios (B) for cluster emission with respect to alpha decay for ^{221}Fr and ^{221}Ra.

Barwick et al. [4] have detected the cluster emission of ^{24}Ne from ^{232}U isotope with the help of polyethylene terephthalate track-recording films, sensitive to particles with Z > 6. They have mentioned that the branching ratio for the emission of ^{24}Ne cluster with respect to alpha particle emission for ^{232}U is $(2.0 \pm 0.5) \times 10^{-12}$.

Kutschera et al. [5] experimentally studied the spontaneous decay of ^{14}C from ^{223}Ra isotope with a ^{227}Th source that contained 9.2 mCi of ^{223}Ra nucleus. They have identified the mass of the emitted cluster unambiguously. They have used Enge split-pole magnetic spectrograph with which alpha radiations were suppressed to identify ^{14}C cluster. They have calibrated the spectrograph with tandem-accelerated beams of ^{12}C, ^{13}C and ^{14}C clusters. They have observed 24 ^{14}C cluster emission events in 6 decays with a branching ratio, $B = (4.7 \pm 1.3) \times 10^{-10}$ for ^{14}C cluster emission from ^{223}Ra parent. They have reported that their measured values agree well with the corresponding values obtained by Rose and Jones [1].

Barwick et al. [6] have investigated the systematics of spontaneous emission of fragments of intermediate mass from heavy nuclei. They have used polycarbonate track-recording films to confirm ^{14}C cluster decay from ^{226}Ra isotope. They have fixed stringent upper limits on the decay rates of ^{14}C cluster from ^{221}Ra, ^{221}Fr and ^{225}Ac isotopes. They have noticed that the decay of ^{14}C cluster exhibits a pronounced odd-even effect and have found that the hindrance factor for odd-even parents with respect to even-even parents is 10 times greater for ^{14}C emission than for alpha particle emission from Ra isotopes.

Moody et al. [7] have investigated the emission of heavy ions from ^{242}Am isotopes using phosphate glass detectors, which have the ability to withstand a background dose of approximately 10^{14} α particles per cm^2. They have measured the branching ratio of ^{34}Si cluster emission with respect to alpha particle emission from ^{241}Am parent, which varies from 4×10^{-13} to 4×10^{-16}. They have mentioned that they couldn't find any clusters with $12 \leq Z \leq 16$, using ^{241}Am source. Price [8] has discovered 12 various radioactive decay modes including the emission of monoenergetic clusters such as carbon, neon, magnesium and silicon nuclei. He has measured the partial half-lives which range from 10^{11} to 10^{28}s and also the branching ratios with respect to alpha decay ranging from 10^{-16} to 10^{-9}. The author has stated that both super asymmetric fission models and cluster models fit well with the corresponding experimental data.

Ogloblin et al. [9] have experimentally investigated the radioactive decay of ^{236}Pu. They could detect two cases of emission of ^{28}Mg cluster from ^{236}Pu isotope with the help of solid-state track registration detectors. They have reported the partial half-life for ^{28}Mg cluster emission as 1.5×10^{14} yr. They have also measured the relative probability of ^{28}Mg cluster decay with respect to alpha particle emission and is given as 2×10^{-14}.

Tretyakova [10] has studied the emission of nuclear clusters during the spontaneous fission in heavy nuclei. He could detect the emission of Ne and Mg clusters from heavy nuclei with proton number (Z) > 90. To conduct the experiment, he had used dielectric detectors with a permitted resolution of $\Delta Z = \pm 0.15$.

Bonetti et al. [11] have experimentally investigated neon cluster emission from uranium isotopes. They have measured the spontaneous decay rates for the emission of monoenergetic Ne from ^{232}U parent. They have

stated that their results point to the revision of rate of decay which were reported earlier for the emission of Ne clusters from $^{232-235}$U isotopes.

Moody et al. [12] have experimentally studied the cluster radioactivity in ^{237}Np isotope. They have found that ^{30}Mg and ^{32}Si-cluster emissions are the most probable modes of decay from ^{237}Np parent. They have measured the branching ratio relative to alpha particle emission as $B < 1.8 \times 10^{-14}$. From the experiments, they have fixed the upper limit of branching ratio for the emission of clusters with atomic number, $10 \leq Z \leq 14$ from ^{237}Np isotope as 1.5×10^{-14}.

Price et al. [13] have experimentally studied the cluster radioactivity in ^{231}Pa isotope. They have detected ^{23}F and ^{24}Ne-cluster emissions from ^{231}Pa parent. They were able to collect approximately 2100 tracks of monoenergetic clusters which were emitted from ^{231}Pa with the help of track-recording phosphate glass detector. They have measured the branching ratio for the emission of ^{24}Ne cluster with respect to alpha particle emission and is given as $B = (13.4 \pm 1.70) \times 10^{-12}$ and for ^{231}Pa, the half-life is 3.28×10^{4} yrs. They have predicted that the emission of ^{23}F cluster is the decay mode which has second highest branching ratio in the case of emission from ^{231}Pa isotope.

Bonetti et al. [14] have observed 27 events of ^{20}O cluster emission from ^{228}Th isotope. They have used solid-state nuclear track detectors which were arranged in 2π geometry to conduct the experiment. They have reported the branching ratio with respect to alpha decay as $(1.13 \pm 0.22) \times 10^{-13}$ and the partial half-life as $(5.29 \pm 1.01) \times 10^{20}$ s. They have reported that they are the first to observe the emission of oxygen clusters.

In another study, Bonetti et al. [15], in 1993, have investigated nuclear structure effects in the cluster radioactivity of ^{225}Ac parent. They have used track-recording glass detectors with ^{225}Ac source generated at ISOLDE, the

electromagnetic separator and have collected 305 events of ^{14}C cluster emissions from ^{225}Ac isotope. Their measured branching ratio of ^{14}C cluster emission relative to alpha particle emission was $B = (6.0 \pm 1.3) \times 10^{-12}$. They have stated that their result indicates that such an emission from nucleus of odd-Z is dominated by a transition to the ground state or the first excited level of daughter nucleus.

In the following year, Bonetti et al. [16] have studied carbon radioactivity in ^{221}Fr and ^{221}Ra isotopes and have investigated the hindered decay of odd-A emitters of exotic type. They have used ^{221}Fr and ^{221}Ra sources which were produced at ISOLDE, the on-line mass separator. They have measured branching ratios for ^{221}Fr and ^{221}Ra parents and are given by $B = (8.79 \pm 1.14) \times 10^{-13}$ and $B = (1.15 \pm 0.91) \times 10^{-12}$ respectively. They have mentioned that their results exhibit a hindrance of one-order-of-magnitude relative to even-even parent nuclei with the same penetrability for the emission of ^{14}C cluster.

Tretyakova et al. [17] have experimentally investigated the cluster radioactivity of ^{236}U parent. They could detect six tracks of magnesium cluster emission with solid-state track detectors. They have reported that in the case of ^{236}U isotope, the probability for this decay is approximately 2×10^{-13} of the probability of alpha decay. They have measured partial decay half-life for magnesium cluster emission and is given as 1.2×10^{20} yr.

Attempts to explore the possibility of trans-tin radioactivity from barium isotopes had been initiated by Oganessian [18] in 1994. They have produced ^{114}Ba isotope in the reaction, $^{58}Ni(^{58}Ni,2n)^{114}Ba$. They have used polycarbonate track detectors to detect the emission of ^{12}C cluster from ^{114}Ba isotope. They have assumed the total half-life for ^{114}Ba isotope as 0.1 s and have obtained the lower limit of partial half-life for ^{12}C cluster emission as $T_c \geq 10^3$ s.

In 1995, Guglielmetti et al. [19] have experimentally studied cluster radioactivity of ^{114}Ba isotope which was produced in ^{58}Ni + ^{58}Ni reactions. Using the on-line mass separator located at the GSI Unilac, they have detected new barium isotopes having mass number, A = 114 - 116 and 118. They have observed the emission of ^{12}C cluster from ^{114}Ba isotope with the help of barium phosphate glass detectors and measured half-lives for ^{4}He decay and ^{12}C decay and are given as T > 500 s and T ≈ 1.7 x 10^4 s respectively. They have mentioned that their experimentally measured half-life values for cluster emission from $^{115-118}$Ba isotopes match well with those predicted using theoretical models. It was found that the branching ratios for the emission of carbon with respect to alpha emission is 8 orders of magnitude larger than those for actinide nuclei.

In 1995, Guglielmetti et al. [20] continued their efforts and studied the cluster decay in ^{114}Ba nucleus that was produced through the reaction, ^{58}Ni(^{58}Ni,2n)^{114}Ba. They have measured the production cross section of ^{114}Ba isotope. Using track detectors they have measured half-life for the emission of ^{12}C cluster from ^{114}Ba isotope and it is given as $T_c \geq 1.1 \times 10^3$ s. They have stated that the detection of ^{12}C decay from ^{114}Ba isotope would help in understanding the cluster radioactivity in nuclei which are in the trans-tin region. Further, they have concluded that this would give information regarding the significance of nearly double shell closure in ^{102}Sn that is far away from the stability line.

Hourani et al. [21] have investigated ^{223}Ra nuclear spectroscopy in the emission of ^{14}C cluster. They have estimated the energy spectrum for ^{14}C cluster emitted from ^{223}Ra source, with the spectrometer SOLENO at ISOLDE. They have obtained the highest statistics of 899 events and best resolution for energy in their measurements. They have measured hindrance

factors for the transition to ground state and to first excited state of ^{209}Pb daughter nucleus.

Tretyakova and Mikheev [22] have provided all experimental data of cluster decay probabilities for atomic nuclei which were measured by them. They have also investigated further possibilities of detecting various other modes of cluster decay experimentally. It was mentioned that experimental studies are motivated to investigate the competition between cluster decay and spontaneous fission and to study the dependence of the probability of cluster decay on the neutron number of parent nucleus. They have presented a complete list of cluster decay data which were experimentally measured.

Guglielmetti et al. [23], in1997, had produced ^{114}Ba in the reaction, ^{58}Ni(^{58}Ni,2n)^{114}Ba using on-line mass separator. They have searched for ^{12}C cluster radioactivity in ^{114}Ba isotope by separating the isotope as a beam containing $^{114}Ba^{19}F^{+}$ and implanting it into a stopper foil located at the centre of a group of track detectors. They have implanted $(5.4 \pm 1.7) \times 10^{4}$ ^{114}Ba atoms but no event of the emission of ^{12}C cluster was observed. They have obtained the branching ratio with an upper limit of 3.4×10^{-5} for the emission of ^{12}C cluster from ^{114}Ba isotope which is considerably lower when compared to the limits observed in previous experiments.

In the same year, Guglielmetti [24] had presented a brief review of the experimental investigation carried out in the area of cluster radioactivity. He had also described about the experimental techniques which were widely used. It had also discussed the problems that are unsolved and the possible experiments related to them.

Ardisson et al. [25], in 1998, reported ^{50}Sc cluster emission from ^{249}Cf. They conducted experiments with phosphate glass detectors and multiple HPGe detectors and measured the probability of cluster decay.

Ogloblin et al. [26], in 2000, had detected ^{34}Si cluster emission from ^{242}Cm parent, with track-recording phosphate glass detectors. For this decay mode, they had obtained the partial half-life and is given as (1.4 + 0.5/-0.3) x 10^{23} s. The corresponding branching ratio with respect to alpha particle emission is 1.0 x 10^{-16} and that with respect to spontaneous fission is given as 1.6 x 10^{-9}. They had also provided the comparison of predictions by semi-empirical systematics and different theoretical models with experimental results.

Tretyakova and Sagaidak [27], in 2003, suggested measurements of fusion-fission and elastic scattering cross sections of the decay products in cluster decay to investigate the mechanism of cluster decay. Their experimental data on ^{12}C + ^{208}Pb permitted them to choose the best one among different theoretical models. They had also discussed cluster radioactivity of ^{112}Ba parent.

In the same year, Tretyakova and Ogloblin [28] presented a report on the advances in cluster decay studies. They had provided experimental data on spontaneous fission and cluster decay attained by scientific groups from Moscow, Milan and Dubna in the previous years. In their own experiments they had used solid state track detectors as the detecting medium.

In 2007, Bonetti and Guglielmetti [29] had presented another report on the current status of experimental studies in the area of cluster radioactivity. They had also discussed about various theoretical approaches and made a comparison between their results on ^{22}Ne and ^{34}Si cluster emissions and the available experimental data.

3.2 Review of theoretical work on cluster radioactivity

Here is presented the developments of various theories related to cluster radioactivity in a chronological order as can be seen from the bibliography. As is generally seen, the theoretical explanation for new observations always motivates researchers to pursue further. In addition to this, new theoretical predictions act as a guidance for carrying out new experiments. Thus theory and experiments always support each other.

Theoretically, the phenomenon called cluster radioactivity was first predicted by Sandulescu, Poenaru and Greiner in 1980 [30]. This phenomenon was experimentally discovered by Rose and Jones in 1984 [1]. Later, Poenaru et al. [31] modified the model to fit cluster decay rates with experimental data. Sandulescu and his collaborators explained intermediate mass systematics and alpha decay systematics using analytical super asymmetric fission model (ASAFM) within the unified framework. On the basis of quantum mechanical fragmentation theory (QMFT), they predicted that cluster decay might occur among nuclei with atomic number (Z) greater than 88. These predictions were based on the fact that there are cold rearrangements of a large number of nucleons from the ground state of the parent nucleus to the ground state of the daughter and the emitted cluster is such that one of the partners is or around the doubly magic nucleus ^{208}Pb.

Employing a formalism extended from the fission model of alpha decay, Poenaru et al. [31] have evaluated lifetime of some heavy nuclei exhibiting cluster radioactivity in the lead region. They observed that the probability of emission of a cluster is high for those cluster decay modes which lead to the generation of a daughter nucleus with neutron number, N = 126, which is a magic number. However, the proton number is not always magic like Z = 82, instead it could be 83, 84, 85 or 86. They have stated that the neutron shell effects dominate over the proton shell effects in the lead

region. Also, they have observed that pairing effect plays a crucial role in the cluster radioactivity exhibited by heavy nuclei. It is also found that the probability for even-Z cluster decay is more than that for odd-Z cluster decay from heavy parent nuclei. They have viewed that spontaneous heavy cluster emission can be taken as a very asymmetric fission.

Poenaru et al. [32] have investigated heavy cluster emission from trans-zirconium stable nuclei. By using ASAFM, they have shown that all stable nuclei which are lighter than lead with atomic number greater than 40 were metastable with respect to the spontaneous cluster decay. They included even-odd effect in the zero point vibration energy and obtained half-lives of the order 10^{40} - 10^{50} s for nuclei with atomic number greater than 62. They have further remarked that the area of metastability against predicted cluster decay modes was offered beyond that for α decay. They have noticed that, in some cases, the rate of decay for clusters were larger than that for alpha decay. They predicted emission of clusters such as ^{12}C, ^{16}O, $^{30,32}Si$, $^{48,50}Ca$ and ^{68}Ni for the stable nuclei with proton number exceeding 60.

Sandulescu et al. [33] have studied cluster decay of ^{223}Ra isotope emitting ^{14}C cluster. They interpreted cluster radioactivity as a highly mass-asymmetric fission. They mentioned that the Coulomb interaction barrier rises considerably with the rise in proton number of the emitted cluster. As a result, the barrier penetrability of the cluster will be very low. They have argued that, as a result of the nuclear shell effects for some parent-cluster combinations, the barrier penetrability becomes compatible with that in alpha decay. They have evaluated barrier penetrabilities for different cluster decay modes with proton number (Z) = 4 to 30 from different heavy parent nuclei. In those calculations, the preformation probability of cluster was not included due to the fact that there had been no experimental observation of such cluster decay modes. They stated that the preformation probability of heavy clusters in the

parent nucleus was comparatively lower than that of alpha particle. They mentioned that the probability of cluster decay would be maximum only for those decay modes resulting in the production of doubly magic daughter nucleus. They suggested some other possible candidates for cluster radioactivity such as ^{14}C radioactivity of ^{226}Ra, ^{24,25}Ne radioactivity of ^{233}U, ^{26}Ne radioactivity of ^{232}Th and ^{30}Mg radioactivity of ^{237}Np isotopes. They concluded that the predicted cluster decay modes would provide proofs for nuclear clustering and importance of shell effects in cluster radioactivity.

With the help of proximity plus Coulomb potential (PPCPM) model, Shi and Swiatecki [34] have evaluated lifetimes for exotic decay of heavy nuclei through the emanation of alpha particles and clusters such as ^{14}C. In their calculations, the radioactive decay lifetime was taken as the product of two components, i.e., Gamow penetrability factor for deformation energy barrier and frequency factor of the range of collective nuclear oscillations. They have provided a closed formula for the Gamow penetrability factor and gave explanation for experimentally estimated branching ratios between ^{14}C and alpha particle emission from ^{222,223,224}Ra isotopes. Also they applied this method to evaluate branching ratios for Ne and O emissions from ^{222,223,224}Ra isotopes.

Poenaru et al. [35] have evaluated kinetic energies and half-lives for spontaneous heavy ion decay from different nuclei. They listed nuclides with atomic number (Z) = 47 - 106 and total half-lives greater than 1 s which consists of the most probable decay modes by the emission of heavy ions. Using the ASAFM model, they have established a semi-empirical formula for alpha decay lifetimes.

By introducing an appropriate collective asymmetry co-ordinate, Herrmann et al. [36] described in a unified way, the intrinsic odd multi-pole moment in the nuclear ground states and the fission by cluster emission and

cluster configurations. This approach was based on the methods of standard collective potential energy used in fission theory.

By using ASAFM model, Poenaru et al. [37] have estimated decay half-lives of heavy clusters from various parent nuclei, within the trans-lead region. They have given a unified description for alpha decay, cluster radioactivity and nuclear fission process. They have reported that the calculated decay lifetimes of more than 140 clusters from various parent nuclei, with proton number, Z = 2 - 24 and neutron number, N = 3 - 31 are less than 10^{30} s. They also mentioned that some stable nuclei with proton number (Z) > 40 were found to be metastable in respect of various new cluster decay modes.

By employing microscopic wave functions, Blendowske et al. [38] have evaluated the probability of detecting ^{14}C from Ra parent nuclei.

By considering the shell effects as well as the nuclear ground-state deformations, Shi and Swiatecki [39] have determined the lifetimes of cluster decay of a large number of nuclei. These corrections are found to be of the order of 10^{1}. They have observed that the inclusion of shell effects as well as nuclear deformations doesn't change the agreement between experimentally measured values and theoretically calculated values. The authors have studied the odd-even effect in the nuclear exotic decay. Here, the emitted cluster was presumed to be spherical and the parent and/or daughter nucleus were considered to possess an axially symmetric deformation. They suggested that since the masses of daughter nucleus, emitted cluster and parent nucleus contain shell effects, the resulting barrier penetrabilities and interacting potential barrier should exhibit the shell effects directly. This was the reason for the strong shell effect displayed by ^{208}Pb daughter nucleus. They remarked that the relative indifference of deformations in exotic decay of nuclei was due to the fact that majority of the interaction barrier relates to separated

fragments and the deformation of parent nucleus affects only the region of pre-scission of potential barrier, that is relatively small.

Using a microscopic approach, Blendowske and Walliser [40] have estimated the decay constant for cluster decay, which is determined by the product of preformation probability and Gamow penetrability. They showed that the preformation probability has a simple mass dependence on the cluster emitted. Their calculated values are found to agree well with the experimental data. Few predictions have also been made by these authors.

Ivascu and Silisteanu [41] have suggested a microscopic approach to find the rates of cluster decay. They have analysed the rare decay modes with the help of a simple theory of microscopic decay. They have estimated the absolute decay rates by using resonance formation factors, shell model and optical model penetrability. They have deduced the resonance formation factors from the form of strong interaction, in which the wave function of the internal region is depicted with regard to compound nucleus decay.

In 1988, Sandulescu [42] made an analysis of magic radioactivity. The author described in a unified way, various decay modes such as cluster decay, alpha decay and new form of symmetric fission, where one or both decay products have proton number or neutron number equal to or nearly equal to magic numbers. He considered only the static prospect of the nuclear evolution which is based on the shell effects. For the inertia parameters, simple assumptions were made and dissipation was not included.

On the basis of open quantum nuclear dynamics, where few collective modes are used as open quantum systems, Sandulescu [43] discussed about the new natural radioactivities accompanied by the emanation of ^{14}C, ^{24}Ne and ^{28}Mg clusters. Neglecting the dissipation, the author has predicted different valleys like Pb valley for cluster decay, alpha valley in the case of

alpha decay and Sn valley for cold fission on the potential energy surfaces. As a result of this observation, the decay modes which were mentioned above could be described in a unified way as spontaneous decay modes, where one or both the decay products have neutron number or proton number equal to or almost equal to magic numbers. This has been regarded as magic radioactivity. The author has concluded that all the phenomena which are subjected to large rearrangements of nucleons could be described as open quantum systems.

With the help of ASAFM model, Poenaru et al. [44] have obtained some significant results regarding alpha decay, cluster radioactivities and cold fission. The authors have obtained the half-life values in the range 10^{11} to 10^{26} s for ^{14}C, ^{24,25,26}Ne, ^{28,30}Mg and ^{32}Si cluster emissions from different heavy parent nuclei. It was stated that the branching ratios with respect to alpha decay have been observed in the range 10^{-16} - 10^{-9}. They concluded that shell effects in the neighbourhood of ^{208}Pb nucleus are responsible for cold fusion reactions and cluster decay of parent in the trans-lead region. They mentioned that though the nuclear shell effects of ^{132}Sn are not as powerful as those of ^{208}Pb, it plays a significant role for cold fission processes.

Malik and Raj Gupta [45] have suggested a new model to illustrate the mechanism of cluster radioactivity in radioactive nuclei. In their model they have described the mechanism of formation of cluster and its penetration through the interaction barrier in radioactive nuclei. The probability of cluster formation is considered as a quantum mechanical fragmentation process and an analytical equation for WKB penetrability has been obtained. Using their model they have analysed the emission of ^{14}C from $^{222-224}$Ra isotopes and the emission of ^{24}Ne cluster from ^{232}U isotope. They have observed that the branching ratio for ^{24}Ne cluster decay of ^{232}U is comparatively larger than that

for ^{14}C decay of ^{232}U. They have made a comparison between the branching ratios for ^{24}Ne emission and that for ^{14}C emission from ^{232}U.

Buck and Merchant [46] have studied alpha decay as well as exotic decay from heavy nuclei as a phenomenon of quantum tunneling. This is done within the framework of semi-classical approximation by employing a cluster model where they used effective cluster-core potential on the basis of the folding procedure. They have obtained good agreement with all the available experimental results of the half-lives for ^{14}C and ^{24}Ne emissions from heavy nuclei.

Barranco et al. [47] have evaluated lifetimes for α decay, Ne decay, Mg decay and spontaneous fission using superfluid tunneling model, without free parameter. They have reported that the calculated values agree with the experimental ones. They have concluded that for ^{234}U isotope, α decay, cluster decay and spontaneous fission can be described in a unified way by superfluid tunneling model without free parameter.

Sobiczewski et al. [48] have investigated deformed even-even nuclei in the superheavy region, with neutron number (N) = 152 - 210 and proton number (Z) = 112 - 130. They have studied equilibrium deformation, fission barrier, ground-state potential energy and half-lives of alpha decay and spontaneous fission. In addition to the spherical nuclei, they have reported the existence of superdeformed superheavy nuclei having half-lives which are long enough to observe experimentally. They have mentioned that the superdeformed nuclei might be synthesized easily in the laboratory since they are near to the already known nuclides.

Shanmugam and Kamalaharan [49] have investigated the effect of deformation on the half-lives of exotic decay of some heavier nuclei which belong to the trans-lead region. They have considered the deformations of

parent and daughter and emitted cluster has been assumed as spherical. Despite the fact that deformation has negligible effect on the decay lifetime, branching ratios of exotic decays are found to be reduced as a result of the incorporation of fragment deformations. For even-A parent, they noticed that the addition of deformation effects in the decay half-life calculations lowers the evaluated half-lives. They have also noted that the influence of parent deformations on the decay half-life values dominates over the effect of daughter deformations. They have noticed that, as a result of nuclear shell effects, the apparent preference of emitted cluster and daughter is to be spherical.

Buck and Merchant [50], in 1990, had investigated the size effects in the alpha decay and exotic decay of heavy nuclei using a cluster model that employed an effective cluster-core potential. They had confirmed that their cluster model offers a consistent theory to evaluate the lifetimes for cluster emission with clusters ranging from α to Mg and Si. They have reported that the experimental half-lives can be reproduced within an order of magnitude by using this model with a fixed set of parameters.

By incorporating the deformation effect to alpha decay studies, Shanmugam and Kamalaharan [51] have extended their cluster decay model. They mentioned that in the exotic decay of nuclei, the charge-to-mass ratio of both the emitted fragment and the parent nucleus is almost the same. This indicates that for a given fragment mass, the redistribution of charge is very small and can be neglected. But for alpha decay, this term has to be considered. Therefore, in the post-scission region, they have made some suitable modifications to the Yukawa plus exponential potential. By using this modified model, they have evaluated half-lives of alpha decay for even-even nuclei with and without the incorporation of charge distribution and have compared their results with the experimental data. They have also evaluated

lifetimes of alpha decay for even-even Ra, Th, U and Pu isotopes and have compared the results with the experimental values.

Buck et al. [52] have proposed a unified model for α decay and cluster decay of heavy nuclei. To evaluate exotic decays to an almost similar degree of accuracy, they have extended their model for alpha decay of some even-even nuclei. They have concluded that with fixed parameters, their model reproduces all the experimental partial lifetimes of some even-even nuclei.

Poenaru and Greiner [53] have shown that fission-like models and preformed cluster models are equivalent and they can be used to provide a unified description of alpha decay and cluster radioactivity. They have interpreted the cluster preformation probability as the probability of penetration of the pre-scission region of the interaction barrier. They have also got linearized universal curves for different cluster decays and have observed that the obtained formula explains the general trend of deviation of experimental result.

Poenaru and Greiner [54] have mentioned that the parameter Z^2/A can only be applied in the case of symmetric fission and based on the theory of heavy ion fusion reactions, a similar parameter can be obtained in the case of asymmetric fission. They have stated that the logarithmic half-lives of symmetric fission evaluated using liquid drop model is a function of fissility and for cluster radioactivities, they have obtained a different dependence of logarithm of half-lives of asymmetric fission. They have reiterated that the parameter Z^2/A provides no information about an asymmetric fission.

By incorporating odd-even effect into the ASAFM model, Poenaru et al. [55] have presented disintegration energy and evaluated partial half-lives for possible cluster decay modes of the nuclei with proton number

(Z) = 52 - 122. They have also included the nuclei far away from the beta-stability line and superheavy nuclei. They have chosen only those parent nuclei where the branching ratio corresponding to alpha particle emission is greater than 10^{-18} and the half-life for cluster decay is less than 10^{30} s.

Raj Gupta et al. [56] have stated that nuclear structure effects regarding the stability of deformed shell have been found to be contained in exotic decays. They have found that the superdeformed ^{78}Sr is very stable against all exotic decay modes whereas the adjacent and equally deformed ^{80}Sr is unstable atleast for some exotic decay modes. They have interpreted this result as a reinforcement shell gap effect of proton number ≈ 38 deformed shell on neutron number ≈ 38 deformed shell.

Raj Gupta et al. [57] have studied the effect of diffuseness of nuclear surface on half-lives of cluster decay using the preformed cluster model (PCM). They have found that even for spherical nuclei, the influence of nuclear surface diffuseness is much larger when compared to the effect of deformation of the parent and daughter nuclei. They have stated that these two effects act in opposite direction and are of similar order. Further, they have noticed that due to the cluster emission, the nuclear surface effects were observed to be significant for both the penetration and preformation probabilities. They have reported that if the emitted cluster has a mass number larger than 20, the effects of surface diffuseness were observed to be small for the evaluations of half-lives.

Sandulescu and Greiner [58] have discussed the spontaneous cluster decay of C, O, Ne, Mg and Si from various nuclei using two extreme approaches, i.e., fission-like or alpha-decay-like theories. They have mentioned that the phenomenological formulations which very well reproduce experimental data provide information about nuclear structure that is useful for the prediction of new decay modes. The authors have interpreted cluster

decays as a new collective motion with large amplitude. They have reviewed cold fusion and cold fission and have also provided new path for the formation of spherical superheavy nuclei.

Sarbjit Singh et al. [59] have investigated synthesis of superheavy elements through cluster decay. Using preformed cluster model they have studied cluster decay of heavy and superheavy nuclei produced in heavy-ion reactions. They have reported that in the case of some exotic decay modes from excited to excited or ground to ground states, the evaluated half-lives were observed to be within the experimental limits. They have found that in the selection of most probable exotic decay modes and cold fusion reactions, the effects of shell stabilization due to both the deformed and spherical shell closure play a significant role.

Using ASAFM model, Poenaru et al. [60] predicted new region of neutron-deficient parent nuclei showing cluster radioactivity. They have calculated branching ratios and half-lives for ^{12}C, ^{16}O and ^{28}Si decay and some other cluster decay modes of parent nuclei with neutron number (N) and proton number (Z) in the range N = 58 - 72 and Z = 56 - 64. They have concluded that these parent nuclei can be formed in reactions which are induced by radioactive beams. They have stated that the exotic decay from these neutron-deficient parent nuclei leads to the production of doubly magic daughter nucleus ^{100}Sn or nuclei in the neighbourhood of it.

Raj Gupta et al. [61] have studied the instabilities against exotic decays in stable nuclei with neutron number (N) and proton number (Z) in the vicinity of various deformed and spherical closed shells. Using PCM, they have investigated the possible exotic decay modes of some nuclei, in the proton number range $50 < Z < 82$. They have mentioned that certain deformed nuclei in the vicinity of spherical magic shell with proton number (Z) = 50 and 82 and the deformed shell with neutron number (N) = 108 are unstable

against different heavy cluster decay modes. They have reported half-lives for ^{8}Be decay of ^{186}Hg and ^{12}C and ^{16}O decay of ^{120}Ba and they are found to be less than the experimental upper limit ($T_{1/2} < 10^{30}$s).

By extending their model of alpha decay, Buck et al. [62] have investigated the cluster decay of some even-even nuclei and other odd-A nuclei. Their model has explained the exotic decays from even-even nuclei as transitions from ground state to ground state but the exotic decay of odd-A nuclei seems to have an excited final state. Their evaluated half-lives for exotic decay from even-even nuclei matches well with the experimental data. They have also investigated the emission of ^{12}C cluster from ^{114}Ba isotope.

Using PCM model, Satish Kumar and Raj Gupta [63] have studied the cluster radioactivity of $^{112\text{-}120}$Ba isotopes. They have calculated half-lives for alpha particle emission and ^{8}Be, ^{12}C, ^{16}O and ^{20}Ne cluster emissions. With half-life $T_{1/2} \approx 10^{4}$ s, it was found that for ^{112}Ba isotope, ^{4}He and ^{12}C cluster emissions are the most probable decay modes. They have pointed out that the minimum value of half-life for ^{12}C decay of ^{112}Ba isotope depicts the importance of the role of doubly magic daughter nucleus ^{100}Sn in trans-tin region of cluster radioactivity.

Satish Kumar et al. [64] have studied the cluster radioactivity of some proton-rich Xe - Gd parent nuclei using PCM model in the trans-tin region. Their calculated half-lives and preformation probabilities implies that the emission of alpha-like clusters (A = 4n, Z = N) such as ^{8}Be, ^{12}C, ^{16}O, ^{20}Ne, ^{24}Mg and ^{28}Si from nuclei with proton number (Z) = neutron number (N) are the most feasible exotic decay modes. They have found that most of the exotic decay modes were within the upper limit of experimental measurements, which points to the significance of daughter nucleus ^{100}Sn in the trans-tin region of cluster radioactivity. They have also found that ^{100}Sn radioactivity is related to alpha-like cluster decays and ^{208}Pb radioactivity is related to non-

alpha-like cluster decays. They have also mentioned that the probability of emission of A = 4n clusters is more than that of A = 4n + 2 clusters.

Through their continued investigations, Satish Kumar et al. [65] have shown the cluster radioactivity of proton-deficient ^{146}Ba, ^{152}Ce, ^{156}Nd, ^{160}Sm and ^{164}Gd isotopes using PCM model. They have observed that evaluation of Q values for chosen decay modes based on shell effects and their corresponding preformation probabilities depicts that the chosen nuclei are stable against the emission of ^{4}He and ^{10}Be. Further, they have found that the probability of emission of non-alpha-like cluster is more for other decay modes. They have found that the most probable decay modes are those which lead to the production of ^{132}Sn daughter nucleus that is doubly magic.

Poenaru et al. [66] have investigated the cluster decay of even-even neutron-deficient Ba, Ce, Nd, Sm and Gd parent nuclei using ASAFM model. They have found that the cluster decay of these nuclei leads to the production of doubly magic daughter nucleus ^{100}Sn or in the neighbourhood of it. They have reported large branching ratios corresponding to beta decay and alpha decay and short half-lives for the emission of ^{16}O cluster from ^{118,120}Ce and ^{122}Nd isotopes and for ^{28}Si decay from ^{126}Sm and ^{132}Gd isotopes and also for ^{12}C emission from ^{114}Ba isotope.

Poenaru et al. [67] have suggested that in even-even nuclei, the strongest cluster or alpha transition takes place from the ground level of the parent nucleus to the ground level of the daughter nucleus. In this work, they have systematically investigated the transitions in parent nuclei with odd number of neutrons and/or protons. They have found that ^{221}F and ^{225}Ac act like even-even nuclei. These nuclei are found to be ^{24}Ne cluster emitters and ^{24}Ne transition is from ground state to ground state. However, they have mentioned that transition of ^{24}Ne from ^{233}U is restricted.

Bonetti et al. [68] have evaluated hindrance factors in alpha decay as well as cluster (Ne and Mg) decay of ^{233}U parent within the framework of one level R-matrix approach by incorporating the structure of internal wave functions. For alpha decay, their estimated values match well with experimental ones. They have also observed small branching ratio between ^{24}Ne and ^{28}Mg cluster emissions.

Shanmugam and Kamalaharan [69] have formulated cubic-plus-Yukawa-plus exponential model (CYEM) with fixed barrier height of the interacting potential. Shell effects at ground states have also been included in this model. In this model, zero-point vibration energy is included explicitly without breaking the energy conservation and the shape of interaction barrier in the region of overlap is considered as a polynomial of third order. They have also incorporated the inertial mass co-efficient that depends on the distance of centre of mass. Using CYEM, they have evaluated branching ratio for ^{14}C cluster emission from ^{231}Pa and ^{232,233}U isotopes. They have compared their calculated values of barrier height with those evaluated using liquid drop model and also with experimental values.

Later, Shanmugam and Carmel Vigila Bai [70] have investigated the distinction between cluster decay by nuclear fission and preformed cluster emission. Using CYEM model, they have made a comparison between the cluster mode and fission mode of cluster decay to find the point of transition from cluster mode to fission mode in the trans-tin region. Here, the parent nucleus and the emitted cluster have been considered as spheroid whereas daughter nucleus is taken as spherical. They have found that the fission model can be applied to all cluster decays whereas the preformed cluster model can be applied to lighter cluster emissions. They have mentioned that transition occurs from cluster mode to fission mode for the emitted cluster with mass number, A = 16. Santhosh et al. [71] had also done a work related to this.

Raj Gupta et al. [72] have studied cluster radioactivity and cold fission exhibited by ^{234,236,238}U isotopes. They have made the calculations on the basis of preformed cluster model, saddle point fission model and quantum mechanical fragmentation theory. They have mentioned that in the case of super-asymmetric mass region of cluster decay, the probability of cold fission process is more than that of exotic decay process and hot fission process. They have found that exotic decay and cold fission processes become identical for the emitted cluster with mass number $A \geq 46$.

Santhosh and Joseph [73] have evaluated logarithmic half-lives for alpha particle emission and ^{12}C cluster emission from Ba isotopes by taking interacting potential as Coulomb plus proximity potential (CPPM). They have reported the calculated half-life for ^{12}C decay of ^{112}Ba and also stated that the most probable emission is the emission of ^{12}C cluster from ^{114}Ba. Their calculated half-lives agree well with the corresponding values calculated using Yukawa plus exponential model. They have also compared their logarithmic half-life values with those evaluated using PCM and ASAFM models.

In another work, Santhosh and Joseph [74] have investigated the cluster radioactivity of cerium isotopes using CPPM model. They have evaluated the half-lives for ^{8}Be, ^{12}C, ^{16}O, ^{20}Ne, ^{24}Mg and ^{28}Si-emissions from different cerium isotopes. It is reported that the emission of ^{12}C and ^{16}O from ^{116}Ce isotope and that of ^{16}O from ^{118}Ce isotope are the most favourable modes of cluster decay. They have also found that the lowest half-life for the emission of ^{16}O cluster is from ^{116}Ce isotope, which depicts the significance of ^{100}Sn (doubly magic) nucleus in the trans-tin region of cluster radioactivity. Since the Geiger-Nuttall plots for various cluster decays were linear in nature, they concluded that the addition of proximity potential to the interacting

potential does not cause any variation to the linear nature of Geiger-Nuttall plots, other than reducing the barrier height.

Tretyakova et al. [75] have discussed about the current status of research in cluster radioactivity. They have evaluated the mass distributions for the energetically feasible decays of parent nuclei having mass number (A) > 112. They mentioned that the present experimental data denote that the transition between adiabatic and sudden mechanisms of the formation of fragment takes place at the fragment mass number (A) ≈ 35 - 40. They have stated that a sensitive tool for the study of decay mechanism is the investigation of fusion-fission reaction or elastic scattering. Also, they have provided a list of new experiments to be conducted.

In another study, Santhosh and Joseph [76] have investigated cluster radioactivity of xenon isotopes. They have calculated the half-lives for the emission of alpha particle, ^{8}Be, ^{12}C and ^{16}O clusters. They have obtained the lowest half-life for the emission of ^{8}Be cluster from ^{108}Xe isotope which points out the significance of ^{100}Sn nucleus (doubly magic) in the trans-tin region of cluster radioactivity. They have found that the excess of neutrons in the parent nucleus slows down the process of cluster emission. They have obtained the half-life for ^{4}He decay of ^{110}Xe which matches well with the measured values.

Raj Gupta et al. [77] have studied the decay of ^{56}Ni* produced in the ^{32}S + ^{24}Mg reaction at the incident energies E = 51.6 MeV and 60.5 MeV using the dynamical cluster-decay model (DCM). This model is usually used for the study of decay of hot and rotating compound nuclei produced in light heavy-ion reactions. They have considered the light particles and complex intermediate mass fragments as the dynamical collective motion of preformed clusters through the interaction barrier. Using this model, they have shown that the characteristics of light particles are different from those of

intermediate mass fragments. The systematic variations of light particle and intermediate mass fragment cross sections calculated using DCM match well with those evaluated using statistical fission model. They have compared their average total kinetic energy spectra with the experimental data and found that they are in good agreement, favoring asymmetric mass distributions. They have shown that light particle emission cross section has a strong dependence on the type of particles emitted and on their multiplicities.

Greiner [78] had presented a new insight for the decay modes of heavy parent nuclei. He had given a brief review about the fission approach used in the theory of alpha decay and heavy-particle radioactivities. Employing macroscopic-microscopic method, he had obtained the potential barrier for the emission of ^{14}C from ^{222}Ra isotope. He had stated that the plot of potential energy surface against the mass asymmetry and the distance of separation between fragments for ^{222}Ra shows the cluster decay and fission valleys formed by the shell effects caused by ^{132}Sn and ^{208}Pb fragments. He had mentioned that the half-lives calculated using ASAFM agree well with the experimental data for various exotic decay modes.

Biju et al. [79] have studied the exotic decay of $^{248-254}Cf$ isotopes based on cold valley in cold fusion and cold fission. They have located the minima corresponding to alpha particle, S, Ar and Ca clusters. On the basis of their study, it was reported that these parent nuclei are unstable against heavy clusters and stable against light clusters. They have found that the most probable decays are ^{46}Ar and $^{48,50}Ca$ cluster emissions, which points to the significance of doubly magic clusters in exotic decay. They have extended their model to the symmetric region and observed that symmetric fission is also probable which points out the significance of ^{132}Sn nucleus, which is doubly magic. They have reported that odd-A cluster emission is favourable from parent nuclei with odd mass number.

Sushil Kumar [80] has studied the cluster radioactivity in $^{118\text{-}132,140\text{-}170}$Ce nuclei. He has studied the closed shells corresponding to the Sn daughter nucleus. He had obtained the minimum value of half-lives for the emission of oxygen cluster when the number of neutrons of the daughter nucleus is 50 and 82, which are magic numbers. He has concluded that minimum value of half-lives for decay modes resulting in ^{100}Sn and ^{132}Sn daughters denotes their high stability against cluster emissions except at these configurations.

Joseph and Girija [81] have investigated cluster decay of proton-rich Er isotopes within the framework of fission model approach. Employing fission model potential, they have calculated the half-lives of exotic decay of Er isotopes in the mass number range A = 150 - 190. They have studied the instability against various cluster decays and have fixed the measurable range of half-life at 10^{40} s. They have stated that the minimum value of half-lives for a particular exotic decay mode implies the significance of closed shell effects.

Bao et al. [82] have evaluated half-lives for different cluster decay modes of isotopes in the trans-lead region with the help of generalized liquid drop model (GLDM). They have explained cluster decay process as an asymmetric spontaneous fission and have evaluated half-lives of exotic decay modes using WKB barrier penetration probability. They have constructed the potential barrier by considering mass asymmetry, nuclear proximity energy, an accurate nuclear radius, microscopic shell correction and phenomenological pairing correction. The decay half-lives calculated using GLDM are found to agree well with the corresponding experimental data.

Santhosh and Biju [83] have investigated the stability of $^{248\text{-}254}$Cf nuclei against alpha decay and cluster decay using CPPM model. They have mentioned that these isotopes are unstable against heavy cluster decays and stable against light cluster decays. They have observed that cluster emissions

from these nuclides result in the production of doubly magic daughter nucleus ^{208}Pb or neighbouring one. They have studied the effect of quadrupole deformation and hexadecapole deformation of parent, daughter and emitted cluster on decay half-lives. They have reported that due to quadrupole deformation, the barrier height and width reduces and therefore half-life decreases.

Using CPPM model, Santhosh and Priyanka [84] have investigated the feasibility for heavy particle decay and alpha particle emission from even-even superheavy nuclei having atomic number, Z = 116 - 124. The cluster formation probability is observed to be maximum for the heavy particle decay accompanying ^{298}114. Accordingly the minimum half-life is obtained for the heavy particle decay resulting in the production of ^{298}114.

Recently, Kuklin et al. [85] have proposed a unified description of alpha decay and cluster radioactivity of cold nuclei using dinuclear system model. They have determined the spectroscopic factor and barrier penetrability of the nucleus-nucleus interaction potential. They have suggested a new method for evaluating the spectroscopic factor and have studied the hindrance factors in the presence of orbital angular momentum. They have found a genuine reason for the deviation of half-life from the Geiger-Nuttall law in alpha decay of proton-rich ^{194,196}Rn isotopes. They have predicted and characterized the fine structure of alpha decays of uranium and thorium isotopes. Using this model, they have described alpha particle emissions from the rotational band of nuclei with even-Z and even-N. They have also discussed the cluster radioactivity in excited nuclei. Finally, they have analysed the relation of cluster decay to highly deformed nuclear states and spontaneous fission.

In a different approach, Adel and Alharbi [86] have investigated nuclear cluster radioactivity using microscopic potentials within WKB

approximation of quantum tunneling by incorporating the Bohr-Sommerfield quantization condition. They have numerically constructed the microscopic cluster-daughter potential in the double-folding model. They have considered a realistic form of M3Y-Paris NN interaction with zero-range exchange NN force and finite-range exchange part. They have investigated the effect of nuclear deformations on the half-lives of cluster decay. On the basis of available experimental data, they have extracted the cluster preformation factors from the experimental and the calculated half-lives of cluster decay. They have made some useful predictions about cluster decay half-lives for emissions of already known clusters from possible nuclei, which may help in future experiments.

References

1. H. J. Rose and G. A. Jones, *Nature* **307**, 245 (1984).

2. D. V. Aleksandrov, A. F. Belyatskii, A. Yu. Glukhov, E. Yu. Nikol'skii, B. G. Novataskii, A. A. Ogloblin and D. N. Stepanov, *Pis'ma Zh. Eksp. Theor. Fiz.* **40**, 152 (1984).

3. P. B. Price, J. D. Stevenson, S. W. Barwick and H. L. Ravn, *Phys. Rev. Lett.* **54**, 297 (1985).

4. S. W. Barwick, P. B. Price and J. D. Stevenson, *Phys. Rev. C* **31**, 1984 (1985).

5. W. Kutschera, I. Ahmad, S. G. Armato, A. M. Friedman, J. E. Gindler, W. Henning, T. Ishii, M. Paul and K. E. Rehm, *Phys. Rev. C* **32**, 2036 (1985).

6. S. W. Barwick, P. B. Price, H. L. Ravn, E. Hourani and M. Hussonnois, *Phys. Rev. C* **34**, 362 (1986).

7. K. J. Moody, E. K. Hulet, Shicheng Wang, P. B. Price and S. W. Barwick, *Phys. Rev. C* **36**, 2710 (1987).

8. P. B. Price, *Nucl. Phys. A* **502**, 41c (1989).

9. A. A. Ogloblin, N. I. Venikov, S. K. Lisin, S. V. Pirozhkov, V. A. Pchelin, Yu. F. Rodionov, V. M. Semochkin, V. A. Shabrov, I. K. Shvetsov, V. M. Shubko, S. P. Tretyakova and V. L. Mikheev, *Phys. Lett. B* **235**, 35 (1990).

10. S. P. Tretyakova, *Nucl. Tracks Radiat. Meas.* **19**, 667 (1991).

11. R. Bonetti, C. Chiesa, A. Guglielmetti, C. Migliorino, A. Cesana, M. Terrani and P. B. Price, *Phys. Rev. C* **44**, 888 (1991).

12. K. J. Moody, E. K. Hulet and P. B. Price, *Phys. Rev. C* **45**, 1392 (1992).

13. P. B. Price, R. Bonetti, A. Guglielmetti, C. Chiesa, R. Matheoud, C. Migliorino and K. J. Moody, *Phys. Rev. C* **46**, 1939 (1992).

14. R. Bonetti, C. Chiesa, A. Guglielmetti, C. Migliorino, A. Cesana and M. Terrani, *Nucl. Phys. A* **556**, 115 (1993).

15. R. Bonetti, C. Chiesa, A. Guglielmetti, R. Matheoud, C. Migliorino, A. L. Pasinetti and H. L. Ravn, *Nucl. Phys. A* **562**, 32 (1993).

16. R. Bonetti, C. Chiesa, A. Guglielmetti, C. Migliorino, P. Monti, A. L. Pasinetti and H. L. Ravn, *Nucl. Phys. A* **576**, 21 (1994).

17. S. P. Tretyakova, V. L. Mikheev, V. A. Ponomarenko, A. N. Golovchenko, A. A. Ogloblin and V. A. Shigin, *JEPT. Lett.* **59**, 397 (1994).

18. Yu. Ts. Oganessian, Yu. A. Lazarev, V. L. Mikheev, Yu. A. Muzychka, V. Shirokovsky, S. P. Tretyakova and V. K. Utyonkov, *Z. Phys. A : Hadrons Nucl.* **349**, 34 (1994).

19. A. Guglielmetti, R. Bonetti, G. Poli, P. B. Price, A. J. Westphal, Z. Janas, H. Keller, R. Kirchner, O. Klepper, A. Piechaczek, E. Roeckl, K. Schmidt, A. Plochoki, J. Szerypo and B. Blank, *Phys. Rev. C* **52**, 740 (1995).

20. A. Guglielmetti, B. Blank, R. Bonetti, Z. Janas, H. Keller, R. Krichner, O. Klepper, A. Piechaczek, A. Plochocki, G. Poli, P. B. Price, E. Roeckl, K. Schmidt, J. Szerypo and A. J. Westphal, *Nucl. Phys. A* **583**, 867 (1995).

21. E. Hourani, G. Berrier-Ronsin, A. Elayi, P. Hoffmann-Rothe, A. C. Mueller, L. Rosier, G. Rotbard, G. Renou, A. Lie'be, D. N. Poenaru and H. L. Ravn, *Phys. Rev. C* **52**, 267 (1995).

22. S. P. Tretyakova and V. L. Mikheev, *IL NUOVO CIMENTO* **110A**, 1043 (1997).

23. A. Guglielmetti, R. Bonetti, G. Poli, R. Collatz, Z. Hu, R. Kirchner, E. Roeckl, N. Gunn, P. B. Price, B. A. Weaver, A. Westphal and J. Szerypo, *Phys. Rev. C* **56**, R2912 (1997).

24. A. Guglielmetti, *IL NUOVO CIMENTO* **110A**, 1039 (1997).

25. G. Ardisson, A. A. Koua and G. Barci-Funel, *J. Radioanal. Nucl. Chem.* **227**, 177 (1998).

26. A. A. Ogloblin, R. Bonetti, V. A. Denisov, A. Guglielmetti, M. G. Itkis, C. Mazzocchi, V. L. Mikheev, Yu. Ts. Oganessian, G. A. Pik-Pichak, G. Poli, S. M. Pirozhkov, V. M. Semochkin, V. A. Shigin, I. K. Shvetsov and S. P. Tretyakova, *Phys. Rev. C* **61**, 034301 (2000).

27. A. A. Ogloblin, S. P. Tretyakova and R. N. Sagaidak, *Heavy Ion Physics* **18**, 339 (2003).

28. S. P. Tretyakova and A. A. Ogloblin, *Heavy Ion Physics* **18**, 333 (2003).

29. R. Bonetti and A. Guglielmetti, *Rom. Rep. in Phys.* **59**, 301 (2007).

30. A. Sandulescu, D. N. Poenaru and W. Greiner, *Sov. J. Part. Nucl.* **11**, 528 (1980).

31. D. N. Poenaru, M. Ivascu, A. Sandulescu and W. Greiner, *J. Phys. G : Nucl. Phys.* **10**, L183 (1984).

32. D. N. Poenaru, W. Greiner, M. Ivascu and A. Sandulescu, *Phys. Rev. C* **32**, 2198 (1985).

33. A. Sandulescu, D. N. Poenaru and W. Greiner, *Phys. Rev. Lett.* **54**, 490 (1985).

34. Shi Yi-Jin and W. J. Swiatecki, *Nucl. Phys. A* **438**, 450 (1985).

35. D. N. Poenaru, W. Greiner, K. Depta, M. Ivascu, D. Mazilu and A. Sandulescu, *At. Data Nucl. Data Tables* **34**, 423 (1986).

36. R. Herrmann, J. A. Maruhn and W. Greiner, *J. Phys. G : Nucl. Part. Phys.* **12**, L285 (1986).

37. D. N. Poenaru, M. Ivascu and W. Greiner, *Nuclear Tracks* **12**, 313 (1986).

38. R. Blendowske, T. Fliessbach and H. Walliser, *Nucl. Phys. A* **464**, 75 (1987).

39. Shi Yi-Jin and W. J. Swiatecki, *Nucl. Phys. A* **464**, 205 (1987).

40. R. Blendowske and H. Walliser, *Phys. Rev. Lett.* **61**, 1930 (1988).

41. M. Ivascu and I. Silisteanu, *Nucl. Phys. A* **485**, 93 (1988).

42. A. Sandulescu, *Phys. Scr. T* **23**, 43 (1988).

43. A. Sandulescu, *J. Phys. G : Nucl. Part. Phys.* **15**, 529 (1989).

44. D. N. Poenaru, W. Greiner and M. Ivascu, *Nucl. Phys. A* **502**, 59c (1989).

45. S. S. Malik and Raj K. Gupta, *Phys. Rev. C* **39**, 1992 (1989).

46. B. Buck and A. C. Merchant, *J. Phys. G : Nucl. Part. Phys.* **15**, 615 (1989).

47. F. Barranco, E. Vigezzi and R. A. Broglia, *Phys. Rev. C* **39**, 2101 (1989).

48. A. Sobiczewski, Z. Patyk and S. Cwiok, *Phys. Lett. B* **224**, 1 (1989).

49. G. Shanmugam and B. Kamalaharan, *Phys. Rev. C* **41**, 1184 (1990).

50. B. Buck and A. C. Merchant, *J. Phys. G : Nucl. Part. Phys.* **16**, L85 (1990).

51. G. Shanmugam and B. Kamalaharan, *Phys. Rev. C* **41**, 1742 (1990).

52. B. Buck, A. C. Merchant and S. M. Perez, *J. Phys. G : Nucl. Part. Phys.* **17**, L91 (1991).

53. D. N. Poenaru and W. Greiner, *Phys. Scr.* **44**, 427 (1991).

54. D. N. Poenaru and W. Greiner, *J. Phys. G : Nucl. Part. Phys.* **17**, S443 (1991).

55. D. N. Poenaru, D. Schnabel, W. Greiner, D. Mazilu and R. Gherghescu, *At. Data Nucl. Data Tables* **48**, 231 (1991).

56. Raj K. Gupta, Werner Scheid and W. Greiner, *J. Phys. G : Nucl. Part. Phys.* **17**, 1731 (1991).

57. Raj K. Gupta, Sarbjit Singh, Rajeev K. Puri, A. Sandulescu, W. Greiner and Werner Scheid, *J. Phys. G : Nucl. Part. Phys.* **18**, 1533 (1992).

58. A. Sandulescu and W. Greiner, *Rep. Prog. Phys.* **55**, 1423 (1992).

59. Sarbjit Singh, Raj K. Gupta, Werner Scheid and W. Greiner, *J. Phys. G : Nucl. Phys.* **18**, 1243 (1992).

60. D. N. Poenaru, W. Greiner and R. Gherghescu, *Phys. Rev. C* **47**, 2030 (1993).

61. Raj K. Gupta, Sarbjit Singh, Rajeev K. Puri and Werner Scheid, *Phys. Rev. C* **47**, 561 (1993).

62. B. Buck, A. C. Merchant, S. M. Perez and P. Tripe, *J. Phys. G : Nucl. Part. Phys.* **20**, 351 (1994).

63. Satish Kumar and Raj K. Gupta, *Phys. Rev. C* **49**, 1922 (1994).

64. Satish Kumar, Dharam Bir and Raj K. Gupta, *Phys. Rev. C* **51**, 1762 (1995).

65. Satish Kumar, J. S. Batra and Raj K. Gupta, *J. Phys. G : Nucl. Part. Phys.* **22**, 215 (1996).

66. D. N. Poenaru, W. Greiner and E. Hourani, *J. Phys. G : Nucl. Part. Phys.* **22**, 621 (1996).

67. D. N. Poenaru, W. Greiner, E. Hourani and R. A. Gherghescu, *IL NUOVO CIMENTO* **110A**, 1049 (1997).

68. R. Bonetti, Iosif Bulboaca, Florin Carstoiu, Ovidiu Dumitrescu, *Phys. Lett. B* **396**, 15 (1997).

69. G. Shanmugam and B. Kamalaharan, *Phys. Rev. C* **38**, 1377 (1998).

70. G. Shanmugam and G. M. Carmel Vigila Bai, *Pramana J. Phys.* **53**, 443 (1999).

71. K. P. Santhosh and Antony Joseph, *Pramana J. Phys.* **59**, 599 (2002).

72. Raj K. Gupta, Dharam Bir, M. Balasubramaniam and Werner Scheid, *J. Phys. G : Nucl. Part. Phys.* **26**, 1373 (2000).

73. K. P. Santhosh and Antony Joseph, *Pramana J. Phys.* **55**, 375 (2000).

74. K. P. Santhosh and Antony Joseph, *Pramana J. Phys.* **59**, 679 (2002).

75. S. P. Tretyakova, A. A. Ogloblin and G. A. Pik-Pichak, *Phys. At. Nucl.* **66**, 1618 (2003).

76. K. P. Santhosh and Antony Joseph, *Pramana J. Phys.* **62**, 957 (2004).

77. Raj K. Gupta, M. Balasubramaniam, Rajesh Kumar, Dalip Singh, C. Beck and W. Greiner, *Phys. Rev. C* **71**, 014601 (2005).

78. W. Greiner, *Rom. Rep. in Phys.* **59**, 193 (2007).

79. R. K. Biju, Sabina Sahadevan, K. P. Santhosh and Antony Joseph, *Pramana J. Phys.* **70**, 617 (2008).

80. Sushil Kumar, *Proc. Int. Sym. Nucl. Phys.* **54**, 204 (2009).

81. Antony Joseph and K. K. Girija, *Proc. DAE Symp. Nucl. Phys.* **56**, 398 (2011).

82. B. J. Bao, H. F. Zhang, B. S. Hu, G. Royer and J. Q. Li, *J. Phys. G : Nucl. Part. Phys.* **39**, 095103 (2012).

83. K. P. Santhosh and R. K. Biju, *Annals of Physics* **334**, 280 (2013).

84. K. P. Santhosh and B. Priyanka, *Nucl. Phys. A* **929**, 20 (2014).

85. S. N. Kuklin, G. G. Adamian and N. V. Antonenko, *Phys. Part. Nuclei* **47**, 206 (2016).

86. A. Adel and T. Alharbi, *Nucl. Phys. A* **958**, 187 (2017).

CHAPTER 4

EXOTIC DECAY IN TUNGSTEN ISOTOPES

4.1 Probable exotic decay modes

The decay half-lives have been evaluated for probable decays in proton-deficient and neutron-deficient isotopes of tungsten, using the effective liquid drop model (ELDM). All probable blends of cluster and parent, for which the Q value is positive, have been analysed. Within the measurable range, i.e., for $T_{1/2} < 10^{30}$ s, the possible decay modes in proton-rich tungsten isotopes are observed as alpha decay and certain alpha-like cluster (A = 4n, Z = N) decays such as ^{8}Be, ^{12}C and ^{16}O decays. The mass ranges of W isotopes exhibiting alpha decay and various cluster decays for which $T_{1/2} < 10^{30}$ s have been shown in Table 4.1. It is observed that both alpha decay and observed cluster decays slow down with the rise in mass number of parent nucleus and therefore, these emissions are found to be absent in the case of proton-deficient isotopes of tungsten.

Table 4.1. Mass ranges of W isotopes showing alpha and different cluster decays with half-lives in the range $T_{1/2} < 10^{30}$ s.

Decays with $T_{1/2} < 10^{30}$ s	Mass range (A)
Alpha decay	158 – 180
^{8}Be decay	158 – 165
^{12}C decay	157 – 168
^{16}O decay	158 – 167

4.2 Comparison study of decay half-lives

The comparison study of logarithmic half-life values calculated using ELDM and UDL (universal decay law) [1,2] has been shown in tables 4.2 – 4.5, for various decay modes in W isotopes. For alpha decay, it is observed that the calculated decay half-lives agree well with the experimental half-life values [3]. Therefore, the effective liquid drop model is applied to predict the half-lives of possible cluster decays. When compared with the universal decay law model, the ELDM half-life values for alpha decay and ^{8}Be, ^{12}C and ^{16}O cluster decays are found to lie near the range of UDL values. Again cluster decays are found to diminish with the increase in the number of neutrons. From the calculated half-lives of all decays, it is found that alpha decay from ^{158}W isotope is the most probable decay mode in W isotopes, since it has the lowest logarithmic half-life of -2.8932. Also, ^{12}C emission from ^{162}W isotope is found to be the most probable cluster decay mode, since it has the lowest logarithmic half-life of 17.3833 among cluster decays.

Standard rms deviation (σ) of $\log_{10}T_{1/2}$ values for alpha decay is calculated and it is found that, within ELDM model, σ = 0.2609 and within UDL model, σ = 0.5406. The smaller the value of σ, better is the corresponding model.

Table 4.2. Comparison study of decay half-lives calculated using ELDM and UDL models for alpha decay of W isotopes.

Mass number of W	Daughter	$Log_{10}T_{1/2}$ ($T_{1/2}$ in seconds)		
		ELDM (present)	UDL	Experiment [3]
158	^{154}Hf	-2.8932	-3.5702	-3.05
159	^{155}Hf	-2.3548	-3.0008	-2.14
160	^{156}Hf	-0.9566	-1.5293	-1.00
161	^{157}Hf	-0.3787	-0.9207	-0.30
162	^{158}Hf	0.5980	0.1024	0.48
163	^{159}Hf	1.2887	0.8248	0.83
164	^{160}Hf	2.3962	1.9806	-
165	^{161}Hf	3.6345	3.2686	> 3.40
166	^{162}Hf	4.5471	4.2166	4.67
167	^{163}Hf	5.1820	4.8758	-
168	^{164}Hf	6.5978	6.3417	6.20
169	^{165}Hf	7.9153	7.7025	-
170	^{166}Hf	8.9213	8.7406	-
171	^{167}Hf	10.2725	10.1316	-
172	^{168}Hf	11.1708	11.0556	-
173	^{169}Hf	13.4573	13.4021	-
174	^{170}Hf	13.1119	13.0501	-
175	^{171}Hf	15.2048	15.1936	-
176	^{172}Hf	15.5581	15.5566	-
177	^{173}Hf	16.0384	16.0498	-
178	^{174}Hf	18.9565	19.0296	-
179	^{175}Hf	22.0260	22.1580	-
180	^{176}Hf	25.4949	25.6870	-

Table 4.3. Comparison study of decay half-lives calculated using ELDM and UDL models for ^{8}Be decay of W isotopes.

Mass number of W	Daughter	$Log_{10}T_{1/2}$ ($T_{1/2}$ in seconds)	
		ELDM (present)	UDL
158	^{150}Yb	27.0789	28.5368
159	^{151}Yb	21.8553	23.1056
160	^{152}Yb	18.2100	19.2959
161	^{153}Yb	19.3020	20.4461
162	^{154}Yb	22.2588	23.5428
163	^{155}Yb	23.7446	25.0971
164	^{156}Yb	26.4106	27.8754
165	^{157}Yb	28.7894	30.3490

Table 4.4. Comparison study of decay half-lives calculated using ELDM and UDL models for ^{12}C decay of W isotopes.

Mass number of W	Daughter	$Log_{10}T_{1/2}$ ($T_{1/2}$ in seconds)	
		ELDM (present)	UDL
157	^{145}Er	29.9272	31.8849
158	^{146}Er	26.0024	27.7339
159	^{147}Er	24.5129	26.1566
160	^{148}Er	21.7852	23.2518
161	^{149}Er	18.9856	20.2553
162	^{150}Er	17.3833	18.5370
163	^{151}Er	18.4615	19.7053
164	^{152}Er	21.1454	22.5953
165	^{153}Er	22.8442	24.4202
166	^{154}Er	25.3234	27.0710
167	^{155}Er	27.0934	28.9589
168	^{156}Er	29.5568	31.5764

Table 4.5. Comparison study of decay half-lives calculated using ELDM and UDL models for ^{16}O decay of W isotopes.

Mass number of W	Daughter	$Log_{10}T_{1/2}$ ($T_{1/2}$ in seconds)	
		ELDM (present)	UDL
158	^{142}Dy	28.2240	29.9145
159	^{143}Dy	27.5684	29.2166
160	^{144}Dy	26.3601	27.9189
161	^{145}Dy	25.2188	26.6921
162	^{146}Dy	23.3129	24.6303
163	^{147}Dy	21.7643	22.9509
164	^{148}Dy	21.0295	22.1570
165	^{149}Dy	22.5431	23.8178
166	^{150}Dy	25.4773	27.0160
167	^{151}Dy	27.1299	28.8153

4.3 Half-lives and β_2 values

Tables 4.6 and 4.7 show the deformation parameter β_2 of parent and daughter along with the half-life for ^{8}Be and ^{12}C cluster decays of W isotopes. β_2 values are taken from the Nuclear Data Table by Möller et al. [4]. Here we can see that minimum value of half-life is obtained for minimum β_2 value of daughter (β_2 = 0.000 for ^{8}Be decay and β_2 = 0.011 for ^{12}C decay) which corresponds to spherical and nearly spherical daughters. This implies that the probability of cluster decay will be high if the daughter nucleus has spherical or nearly spherical shape. It is evident that the shape of the daughter nucleus influences the cluster decay half-lives more than that of the parent nucleus.

Table 4.6. Half-lives and β_2 values of parent and daughter for ^{8}Be decay of W isotopes.

Parent	β_2 (Parent)	Daughter	β_2 (Daughter)	$Log_{10}T_{1/2}$(ELDM) ($T_{1/2}$ in seconds)
^{158}W	0.085	^{150}Yb	-0.167	27.0789
^{159}W	0.107	^{151}Yb	-0.125	21.8553
^{160}W	0.128	^{152}Yb	0.000	18.2100
^{161}W	0.139	^{153}Yb	-0.052	19.3020
^{162}W	0.150	^{154}Yb	-0.104	22.2588
^{163}W	0.162	^{155}Yb	0.118	23.7446
^{164}W	0.173	^{156}Yb	0.139	26.4106
^{165}W	0.173	^{157}Yb	0.161	28.7894

Table 4.7. Half-lives and β_2 values of parent and daughter for ^{12}C decay of W isotopes.

Parent	β_2 (Parent)	Daughter	β_2 (Daughter)	$Log_{10}T_{1/2}$(ELDM) ($T_{1/2}$ in seconds)
^{157}W	-0.063	^{145}Er	0.219	29.9272
^{158}W	0.085	^{146}Er	-0.187	26.0024
^{159}W	0.107	^{147}Er	-0.187	24.5129
^{160}W	0.128	^{148}Er	-0.146	21.7852
^{161}W	0.139	^{149}Er	-0.094	18.9856
^{162}W	0.150	^{150}Er	0.011	17.3833
^{163}W	0.162	^{151}Er	-0.063	18.4615
^{164}W	0.173	^{152}Er	-0.084	21.1454
^{165}W	0.173	^{153}Er	0.129	22.8442
^{166}W	0.184	^{154}Er	0.150	25.3234
^{167}W	0.195	^{155}Er	0.172	27.0934
^{168}W	0.206	^{156}Er	0.205	29.5568

4.4 Plots of half-life and Q versus neutron number of daughter

Figures 4.1 – 4.4 show the profiles of N_d (neutron number of daughter nucleus) against $\log_{10}T_{1/2}$ and Q. In the plots of Q versus N_d and $\log_{10}T_{1/2}$ versus N_d for alpha decay and ^{8}Be, ^{12}C and ^{16}O cluster decays, there is a decrease in Q value corresponding to an increase in $\log_{10}T_{1/2}$ with the rise in N_d and that results in the appearance of the plots, with one appearing as the mirror reflection of the other. Since barrier penetrability factor is inversely proportional to decay half-life, the probability of decay decreases with the rise in $\log_{10}T_{1/2}$. Therefore, the probability of cluster emissions decreases with the increase in neutron number of daughter. In the plots for ^{8}Be, ^{12}C and ^{16}O cluster decays, a dip in $\log_{10}T_{1/2}$ can be observed at $N_d = 82$, a magic number. At this point, the probability of cluster emissions will be high, which in turn points to the significant role played by neutron magicity in cluster radioactivity.

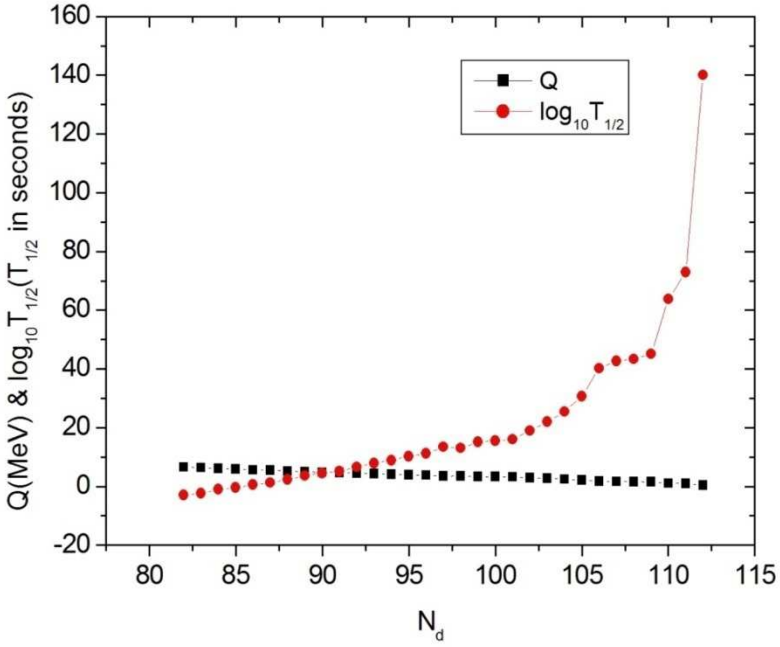

Fig. 4.1. Plots of $\log_{10}T_{1/2}$ and Q against N_d for alpha decay of W isotopes.

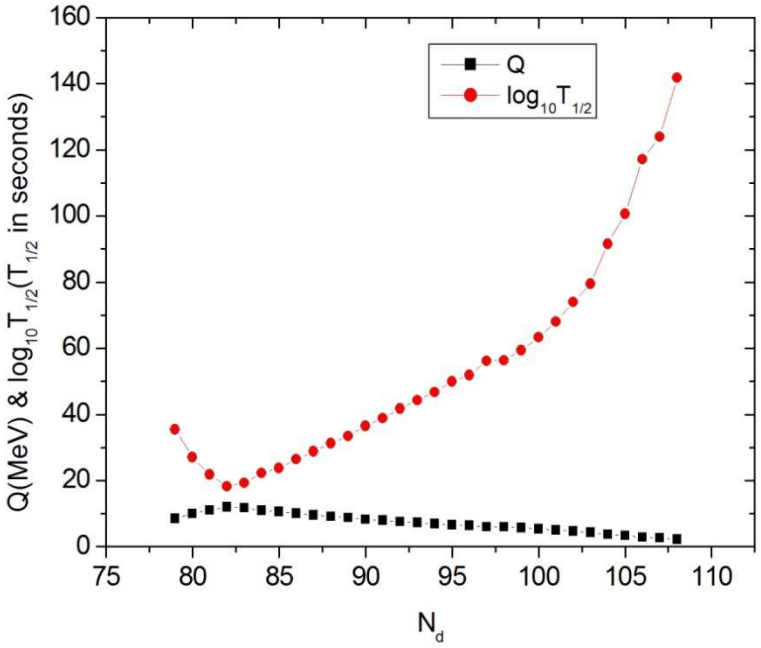

Fig. 4.2. Plots of $\log_{10}T_{1/2}$ and Q against N_d for ^{8}Be decay of W isotopes.

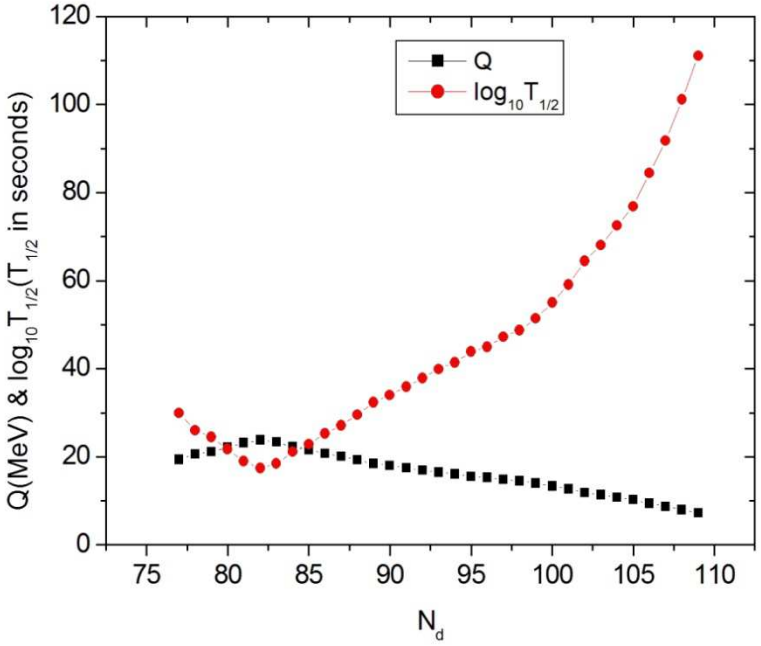

Fig. 4.3. Plots of $\log_{10}T_{1/2}$ and Q against N_d for ^{12}C decay of W isotopes.

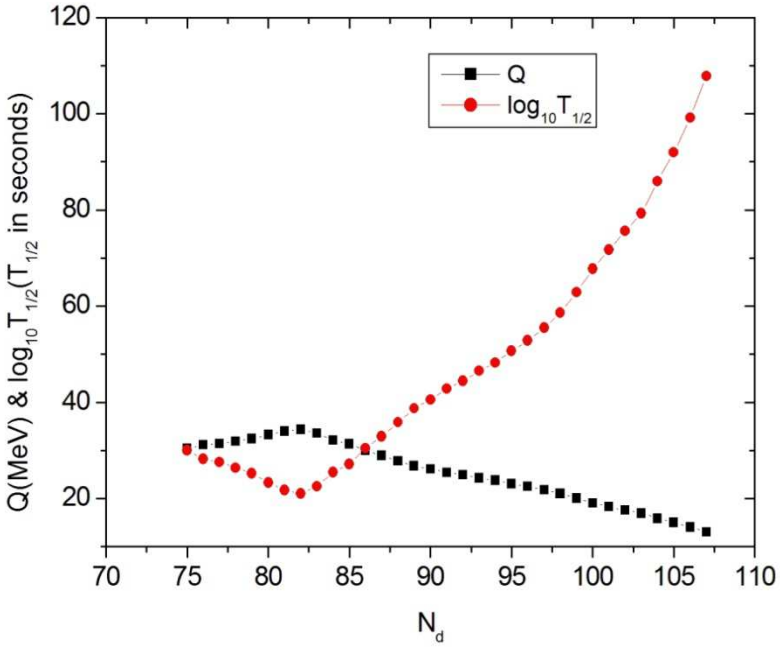

Fig. 4.4. Plots of $\log_{10}T_{1/2}$ and Q against N_d for ^{16}O decay of W isotopes.

4.5 Plot of half-life versus neutron number of parent

Fig. 4.5 shows the combined plot of half-life versus N_p (neutron number of parent nucleus) for alpha decay and ^{8}Be, ^{12}C and ^{16}O cluster decays of W isotopes. The general trend of these plots is that as the parent becomes rich in the number of neutrons, half-life increases, which in turn, slows down the alpha and cluster emissions. When compared to other emissions, half-lives of alpha emission are found to be minimum for a large range of N_p values, favoring high probability of alpha particle emission from these isotopes. For ^{8}Be, ^{12}C and ^{16}O cluster emissions, it is found that the minimum value of half-life shifts towards the higher N_p values. Also, decay characteristics are found to be similar for ^{12}C and ^{16}O cluster decays.

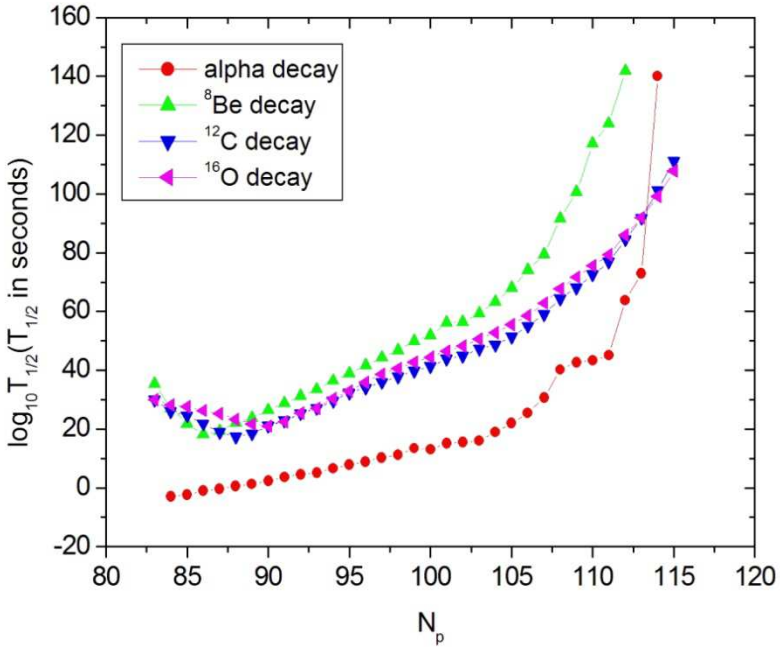

Fig. 4.5. Plot of $\log_{10}T_{1/2}$ against N_p for various decays of W isotopes.

4.6 Geiger-Nuttall plots

Figures 4.6 – 4.9 show the Geiger-Nuttall (G-N) plots, i.e., $\log_{10}T_{1/2}$ versus $Q^{-1/2}$ graphs for alpha decay and observed cluster decays. All the plots show linear behaviour which emphasizes the fact that the inclusion of surface potential in the interaction potential does not cause any variation to the linear nature that is usually observed in G-N plot for the system under pure Coulomb potential. The intercepts and slopes of G-N plots for various decays exhibited by W isotopes are shown in table 4.8. Apparent changes in the slopes and intercepts are due to the shell effects and surface potential included in the interaction barrier.

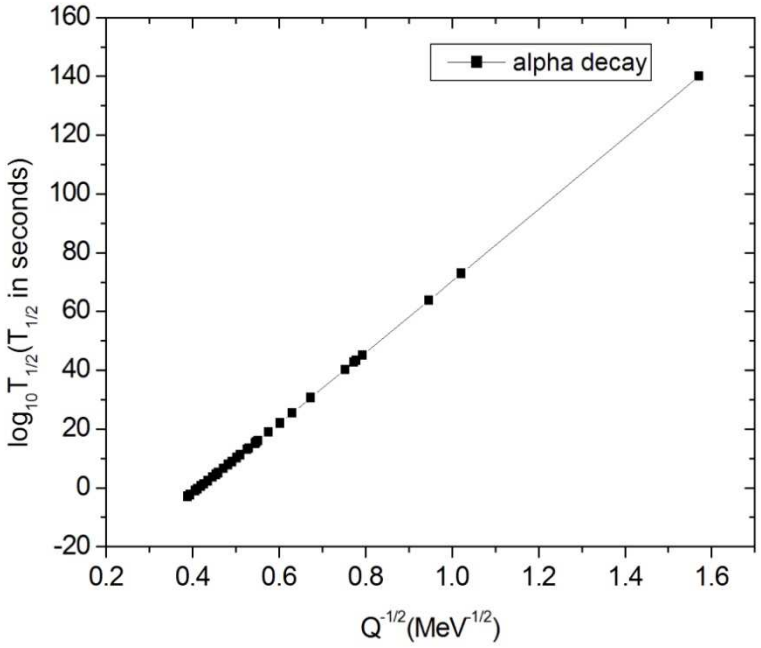

Fig. 4.6. G-N plot for alpha decay of W isotopes.

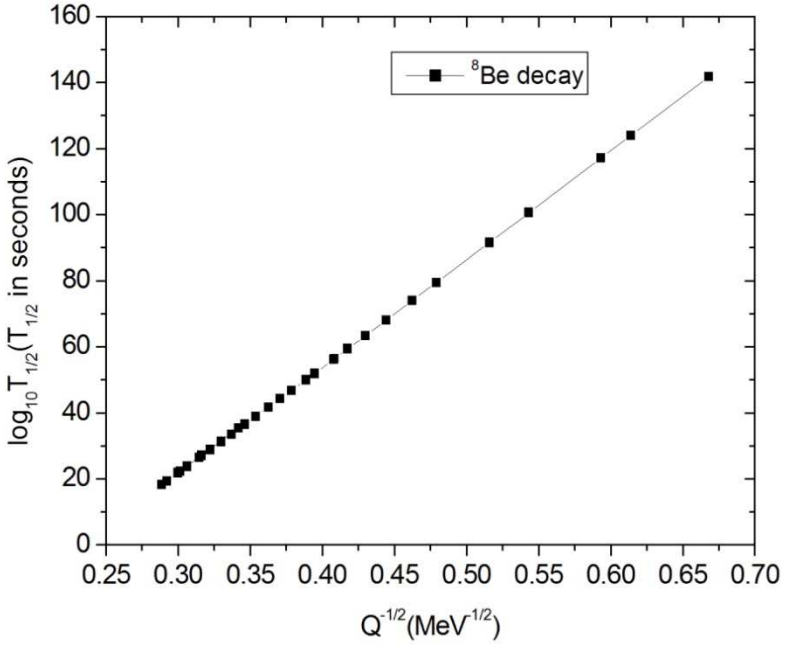

Fig. 4.7. G-N plot for ^{8}Be decay of W isotopes.

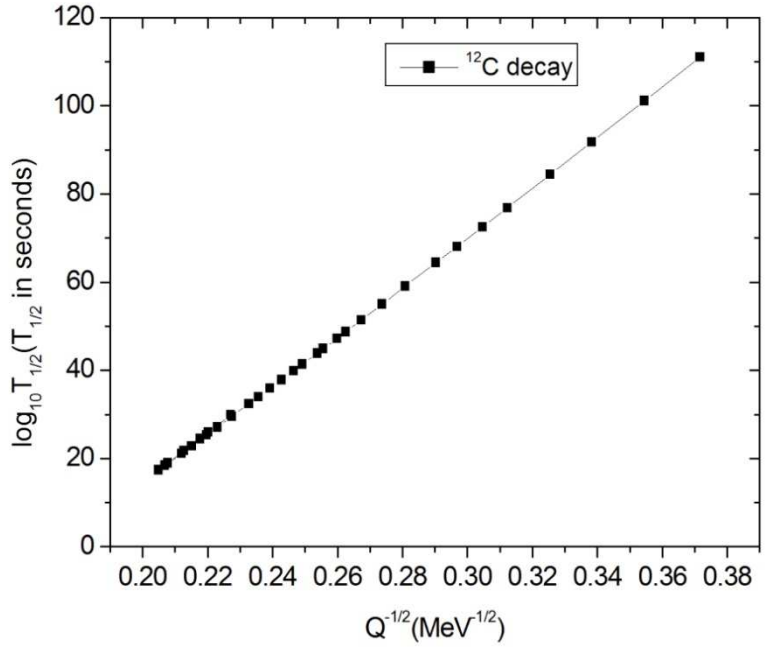

Fig. 4.8. G-N plot for ^{12}C decay of W isotopes.

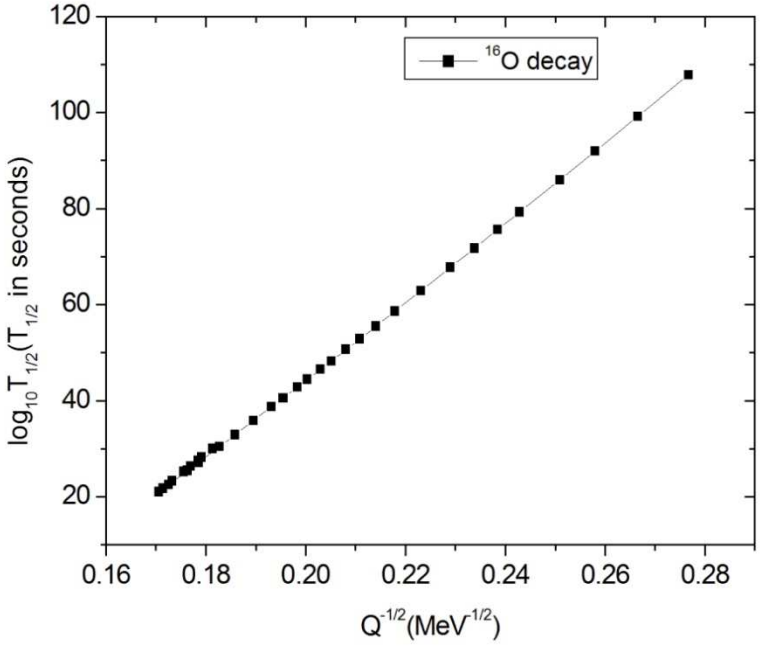

Fig. 4.9. G-N plot for ^{16}O decay of W isotopes.

Table 4.8. Slopes and intercepts of G-N plots for various decays of W isotopes.

Cluster emitted	Slope (X)	Intercept (Y)
^{4}He	120.7642	-50.3663
^{8}Be	325.3257	-76.1436
^{12}C	558.9839	-97.5513
^{16}O	811.0089	-117.6139

4.7 Half-life in terms of atomic number of cluster

From the slopes and intercepts of G-N plots and atomic number of the corresponding emitted cluster (Z_1), we have obtained a general equation for logarithmic half-life, which can be applied to all clusters emitted from various W isotopes, i.e.,

$$\log_{10}T_{1/2} = \frac{X(Z_1)}{\sqrt{Q}} + Y(Z_1) \quad (4.1)$$

where

$$X(Z_1) = -0.2235Z_1^3 + 6.3196Z_1^2 + 70.6225Z_1 - 43.9707 \quad (4.2)$$

$$Y(Z_1) = -0.0630Z_1^3 + 1.3023Z_1^2 - 18.9383Z_1 - 17.1949 \quad (4.3)$$

References

1. C. Qi, F. R. Xu, R. J. Liotta and R. Wyss, *Phys. Rev. Lett.* **103**, 072501 (2009).

2. C. Qi, F. R. Xu, R. J. Liotta, R. Wyss, M. Y. Zhang, C. Asawatangtrakuldee and D. Hu, *Phys. Rev. C* **80**, 044326 (2009).

3. S. B. Duarte, O. A. P. Tavares, F. Guzman and A. Dimarco, *At. Data Nucl. Data Tables* **80**, 235 (2002).

4. P. Möller, A. J. Sierk, T. Ichikawa and H. Sagawa, *At. Data Nucl. Data Tables* **109**, 1 (2016).

CHAPTER 5

EXOTIC DECAY IN RHENIUM ISOTOPES

5.1 Probable exotic decay modes

Using the effective liquid drop model (ELDM), the decay half-lives are evaluated for proton decay, alpha decay and cluster radioactivity in proton-rich and neutron-rich isotopes of rhenium. All possible combinations of parent and cluster have been considered for which the Q value is positive. The half-lives for proton, alpha, ^{8}Be, ^{12}C and ^{16}O decays are observed to be well within the measurable range ($T_{1/2} < 10^{30}$ s) and therefore, they are predicted to be the possible decay modes in proton-rich rhenium isotopes. Table 5.1 shows the mass ranges of Re isotopes exhibiting proton decay, alpha decay and various cluster decays with $T_{1/2} < 10^{30}$ s. It is also noticed that the cluster emissions slow down with the rise in the number of neutrons and hence no cluster radioactivity is spotted in the case of neutron-rich isotopes.

Table 5.1. Mass ranges of Re isotopes exhibiting proton, alpha and various cluster emissions with half-lives in the measurable range.

Decays with $T_{1/2} < 10^{30}$ s	Mass range (A)
Proton decay	159 – 163, 165
Alpha decay	160 – 182
^{8}Be decay	159 – 167
^{12}C decay	159 – 170
^{16}O decay	159 – 169

5.2 Comparison study of decay half-lives

Tables 5.2 – 5.6 show the comparison study of logarithmic half-lives calculated using ELDM and UDL (universal decay law) [1,2] models for different decay modes in Re isotopes. It has been observed that the evaluated half-lives of proton decay and alpha decay are in good agreement with the available experimental data [3,4]. When compared with the UDL model, it is found that the present formalism (ELDM) is the better tool for reproducing the experimental data. Hence, the use of ELDM is extended for cluster decay studies. The calculated half-lives of proton and alpha decays and of ^{8}Be, ^{12}C and ^{16}O cluster decays lie close to those predicted using UDL model. It is evident from the calculations that the probability of cluster emissions diminishes with increasing neutron number. From the calculated half-lives of all decays, it is found that proton decay from ^{159}Re isotope is the most probable decay mode in Re isotopes, since it has the lowest logarithmic half-life of -7.9352. Also, ^{12}C emission from ^{163}Re isotope is found to be the most probable cluster decay mode, since it has the lowest logarithmic half-life of 16.2729 among cluster decays.

Standard rms deviation (σ) of $\log_{10}T_{1/2}$ values for alpha decay is calculated and it is found that, within ELDM model, σ = 0.3739 and within UDL model, σ = 0.7667.

Table 5.2. Comparison study of half-lives using ELDM and UDL models for proton decay of Re isotopes.

Mass number of Re	Daughter	$Log_{10}T_{1/2}$ ($T_{1/2}$ in seconds)		
		ELDM (present)	UDL	Experiment [3]
159	^{158}W	-7.9352	-10.0249	-
160	^{159}W	-4.3786	-6.4232	-3.046
161	^{160}W	-3.5829	-5.6197	-3.432
162	^{161}W	3.5629	-1.5773	-
163	^{162}W	5.2335	-3.2556	-
165	^{164}W	25.8259	23.9070	-

Table 5.3. Comparison study of half-lives using ELDM and UDL models for alpha decay of Re isotopes.

Mass number of Re	Daughter	$Log_{10}T_{1/2}$ ($T_{1/2}$ in seconds)		
		ELDM (present)	UDL	Experiment [4]
160	^{156}Ta	-2.7984	-3.4494	-2.06
161	^{157}Ta	-1.5031	-2.0827	-1.82
162	^{158}Ta	-1.2225	-1.7861	< 0.52
163	^{159}Ta	-0.3321	-0.8497	-0.39
164	^{160}Ta	0.0025	-0.4974	0.18
165	^{161}Ta	1.2390	0.7965	1.26
166	^{162}Ta	1.9817	1.5730	-
167	^{163}Ta	2.9246	2.5561	2.79
168	^{164}Ta	3.9106	3.5818	-
169	^{165}Ta	4.1770	3.8605	-
170	^{166}Ta	5.5998	5.3362	-
171	^{167}Ta	6.0449	5.7984	-
172	^{168}Ta	7.4943	7.2974	-
173	^{169}Ta	8.3203	8.1505	-
174	^{170}Ta	10.2242	10.1115	-
175	^{171}Ta	10.4527	10.3487	-
176	^{172}Ta	11.7212	11.6531	-
177	^{173}Ta	12.8551	12.8174	-
178	^{174}Ta	13.1806	13.1527	-
179	^{175}Ta	15.5851	15.6157	-
180	^{176}Ta	18.5948	18.6910	-
181	^{177}Ta	22.6733	22.8477	-
182	^{178}Ta	23.2735	23.4605	-

Table 5.4. Comparison study of half-lives using ELDM and UDL models for ^{8}Be decay of Re isotopes.

Mass number of Re	Daughter	$Log_{10}T_{1/2}$ ($T_{1/2}$ in seconds)	
		ELDM (present)	UDL
159	^{151}Lu	25.9684	27.4209
160	^{152}Lu	20.9429	22.1874
161	^{153}Lu	16.9067	17.9595
162	^{154}Lu	18.0064	19.1205
163	^{155}Lu	20.6157	21.8611
164	^{156}Lu	21.8862	23.1945
165	^{157}Lu	23.6820	25.0734
166	^{158}Lu	25.9496	27.4383
167	^{159}Lu	28.1876	29.7690

Table 5.5. Comparison study of half-lives using ELDM and UDL models for ^{12}C decay of Re isotopes.

Mass number of Re	Daughter	$Log_{10}T_{1/2}$ ($T_{1/2}$ in seconds)	
		ELDM (present)	UDL
159	^{147}Tm	25.4027	27.1305
160	^{148}Tm	23.6732	25.2944
161	^{149}Tm	20.5940	22.0067
162	^{150}Tm	18.1122	19.3437
163	^{151}Tm	16.2729	17.3636
164	^{152}Tm	17.4039	18.5939
165	^{153}Tm	19.5083	20.8686
166	^{154}Tm	21.4983	23.0127
167	^{155}Tm	23.4542	25.1117
168	^{156}Tm	25.5116	27.3134
169	^{157}Tm	27.5862	29.5253
170	^{158}Tm	29.2344	31.2803

Table 5.6. Comparison study of half-lives using ELDM and UDL models for ^{16}O decay of Re isotopes.

Mass number of Re	Daughter	$Log_{10}T_{1/2}$ ($T_{1/2}$ in seconds)	
		ELDM (present)	UDL
159	^{143}Ho	27.5876	29.2556
160	^{144}Ho	26.7037	28.3093
161	^{145}Ho	25.4487	26.9585
162	^{146}Ho	24.3131	25.7341
163	^{147}Ho	22.1897	23.4301
164	^{148}Ho	20.7203	21.8318
165	^{149}Ho	19.6173	20.6314
166	^{150}Ho	21.3971	22.5892
167	^{151}Ho	23.9048	25.3338
168	^{152}Ho	25.9187	27.5316
169	^{153}Ho	28.5738	30.4133

5.3 Half-lives and β_2 values

Tables 5.7 and 5.8 show the deformation parameter β_2 of parent and daughter along with the half-life for ^{8}Be and ^{12}C cluster decays of Re isotopes. β_2 values are taken from the Nuclear Data Table by Möller et al. [5]. Here we can see that minimum value of half-life is obtained for minimum β_2 value of daughter (β_2 = -0.021 for ^{8}Be decay and β_2 = 0.021 for ^{12}C decay) which corresponds to nearly spherical daughter. This implies that the probability of cluster decay will be high if the daughter nucleus has nearly spherical shape. It is evident that the shape of the daughter nucleus influences the cluster decay half-lives more than that of the parent nucleus.

Table 5.7. Half-lives and β_2 values of parent and daughter for ^{8}Be decay of Re isotopes.

Parent	β_2 (Parent)	Daughter	β_2 (Daughter)	$Log_{10}T_{1/2}$(ELDM) ($T_{1/2}$ in seconds)
^{159}Re	0.064	^{151}Lu	-0.167	25.9684
^{160}Re	0.107	^{152}Lu	-0.105	20.9429
^{161}Re	0.118	^{153}Lu	-0.021	16.9067
^{162}Re	0.129	^{154}Lu	-0.084	18.0064
^{163}Re	0.150	^{155}Lu	0.096	20.6157
^{164}Re	0.151	^{156}Lu	0.118	21.8862
^{165}Re	0.162	^{157}Lu	0.139	23.6820
^{166}Re	0.173	^{158}Lu	0.161	25.9496
^{167}Re	0.173	^{159}Lu	0.172	28.1876

Table 5.8. Half-lives and β_2 values of parent and daughter for ^{12}C decay of Re isotopes.

Parent	β_2 (Parent)	Daughter	β_2 (Daughter)	$Log_{10}T_{1/2}$(ELDM) ($T_{1/2}$ in seconds)
^{159}Re	0.064	^{147}Tm	-0.187	25.4027
^{160}Re	0.107	^{148}Tm	-0.177	23.6732
^{161}Re	0.118	^{149}Tm	-0.166	20.5940
^{162}Re	0.129	^{150}Tm	-0.125	18.1122
^{163}Re	0.150	^{151}Tm	0.021	16.2729
^{164}Re	0.151	^{152}Tm	-0.073	17.4039
^{165}Re	0.162	^{153}Tm	-0.104	19.5083
^{166}Re	0.173	^{154}Tm	0.128	21.4983
^{167}Re	0.173	^{155}Tm	0.150	23.4542
^{168}Re	0.184	^{156}Tm	0.172	25.5116
^{169}Re	0.196	^{157}Tm	0.194	27.5862
^{170}Re	0.206	^{158}Tm	0.205	29.2344

5.4 Plots of half-life and Q versus neutron number of daughter

Figures 5.1 – 5.5 show the profiles of calculated half-lives and Q values for proton, alpha and probable cluster emissions of neutron-deficient Re isotopes against neutron number of daughter N_d. In the case of proton decay, the probability of decay is found to be high for daughter having even number of neutrons. It is observed that the plots for alpha, ^{8}Be, ^{12}C and ^{16}O decays are similar and appear almost as mirror reflected images. Proton decay is an exception in this case. The plots show a decrease in the Q value corresponding to an increase in $\log_{10}T_{1/2}$ with the rise in N_d. Since barrier penetrability factor is inversely proportional to decay half-life, the probability of decay decreases with the rise in $\log_{10}T_{1/2}$. Therefore, the probability of cluster emissions decreases with the increase in neutron number of daughter. The profiles for ^{8}Be, ^{12}C and ^{16}O emissions indicate the shell closure at N_d = 82, which points out the significance of neutron magicity in cluster decay.

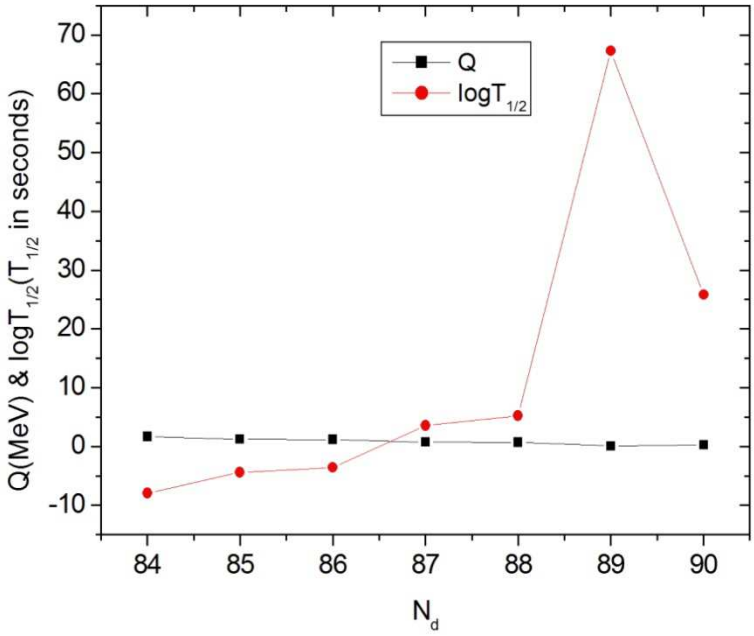

Fig. 5.1. Plots of $\log_{10}T_{1/2}$ and Q against N_d for proton decay of Re isotopes.

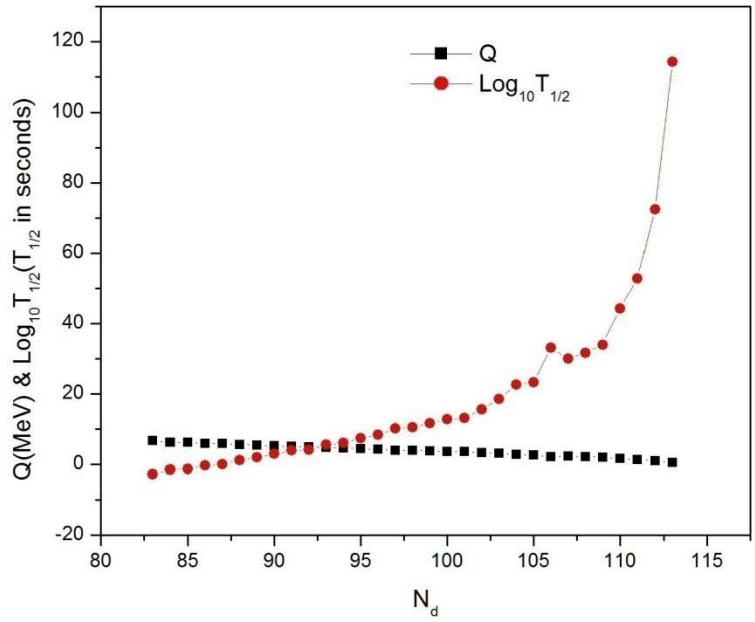

Fig. 5.2. Plots of $\log_{10}T_{1/2}$ and Q against N_d for alpha decay of Re isotopes.

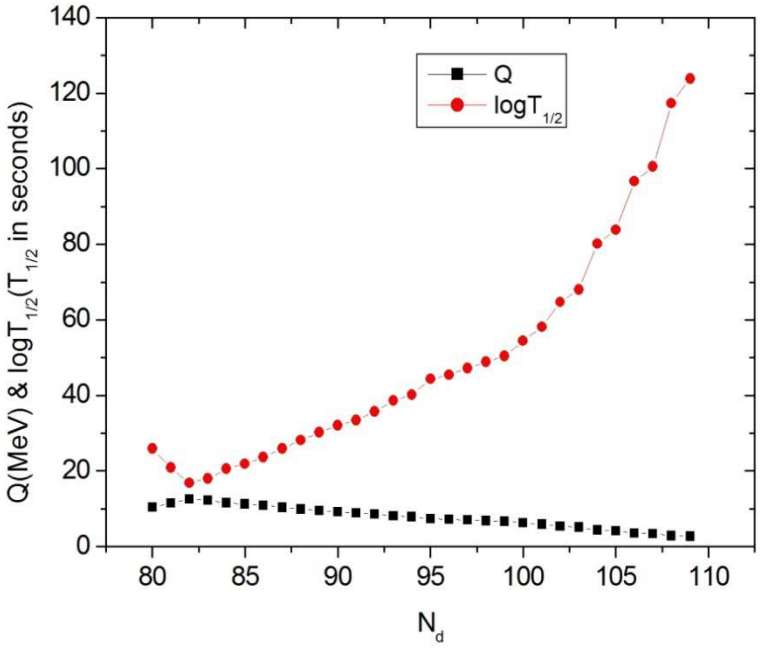

Fig. 5.3. Plots of $\log_{10}T_{1/2}$ and Q against N_d for ^{8}Be decay of Re isotopes.

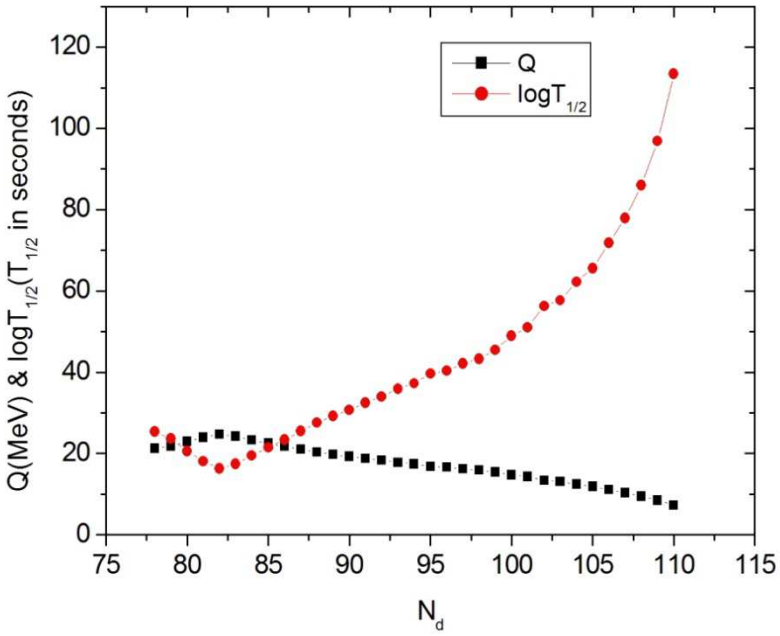

Fig. 5.4. Plots of $\log_{10}T_{1/2}$ and Q against N_d for ^{12}C decay of Re isotopes.

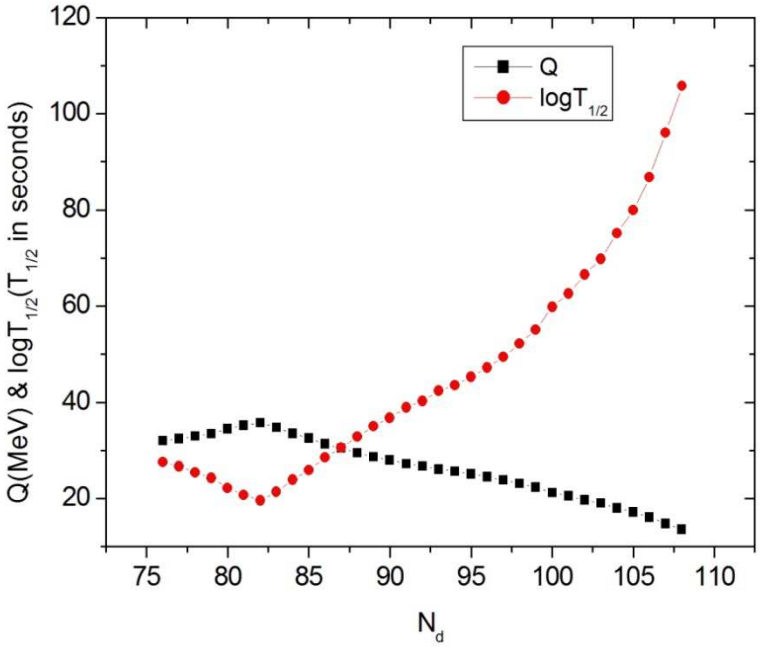

Fig. 5.5. Plots of $\log_{10}T_{1/2}$ and Q against N_d for ^{16}O decay of Re isotopes.

5.5 Plot of half-life versus neutron number of parent

Fig. 5.6 shows the combined plot of half-life versus N_p (neutron number of parent nucleus) for proton and alpha decays and ^{8}Be, ^{12}C and ^{16}O cluster decays of Re isotopes. The general trend of these plots is that as the parent becomes rich in the number of neutrons, half-life increases, which in turn, slows down the alpha and cluster emissions. When compared to other emissions, half-lives of alpha emission are found to be minimum for a large range of N_p values, favoring high probability of alpha particle emission from these isotopes. For ^{8}Be, ^{12}C and ^{16}O cluster emissions, it is found that the minimum value of half-life shifts towards the higher N_p values. Also, decay characteristics are found to be similar for ^{12}C and ^{16}O cluster decays. The decay characteristics of proton decay are found to be much different from those of other decays.

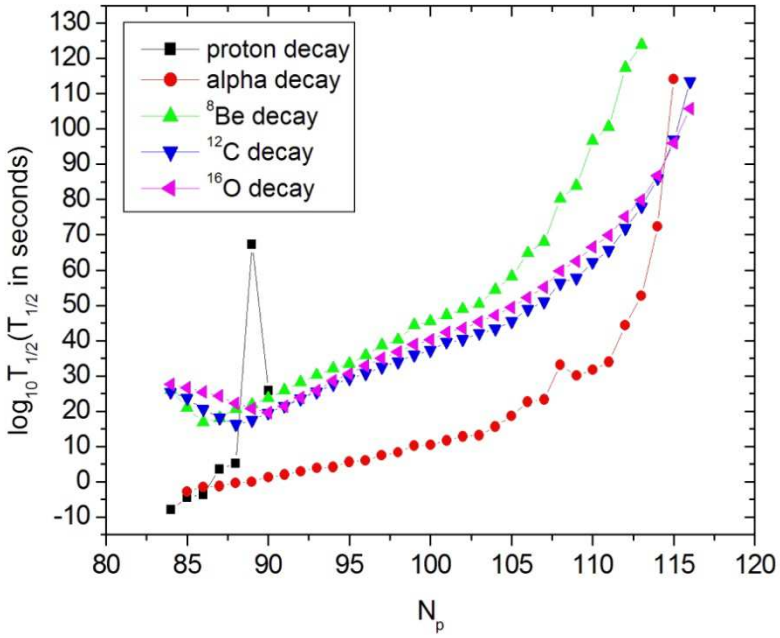

Fig. 5.6. Plot of $\log_{10}T_{1/2}$ against N_p for various decays of Re isotopes.

5.6 Geiger-Nuttall plots

Figures 5.7 – 5.11 show the Geiger-Nuttall (G-N) plots for proton, alpha, ^{8}Be, ^{12}C and ^{16}O decays of Re isotopes. Obviously, they all show linear behaviour and it is already known that G-N law is, in general, applicable to the system under pure Coulomb potential. The obtained data plots indicate that the inclusion of surface potential produces no remarkable variation to the linear nature. Table 5.9 shows the intercepts and slopes of G-N plots for various decays of Re isotopes. The apparent shifts in slopes and intercepts of G-N plots for different decays mark the presence of surface potential and shell effects in the nuclear configuration of rhenium isotopes.

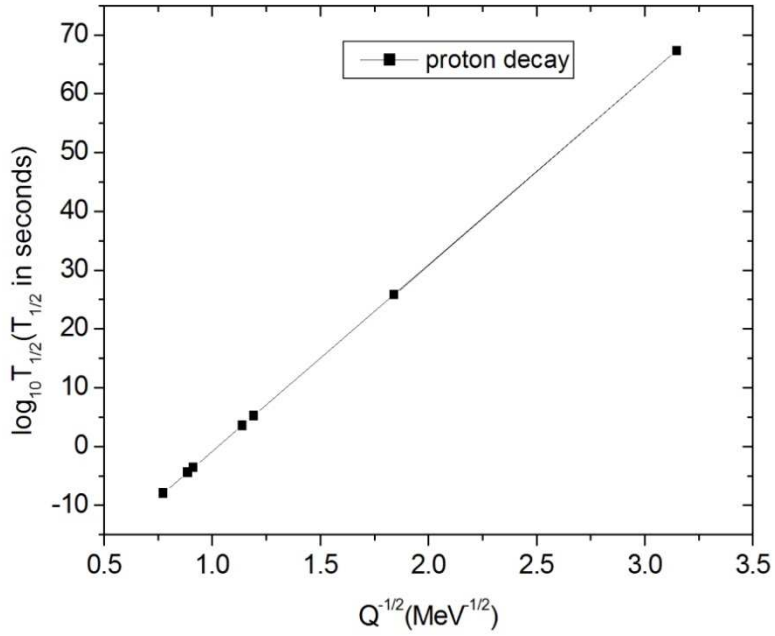

Fig. 5.7. G-N plot for proton decay of Re isotopes.

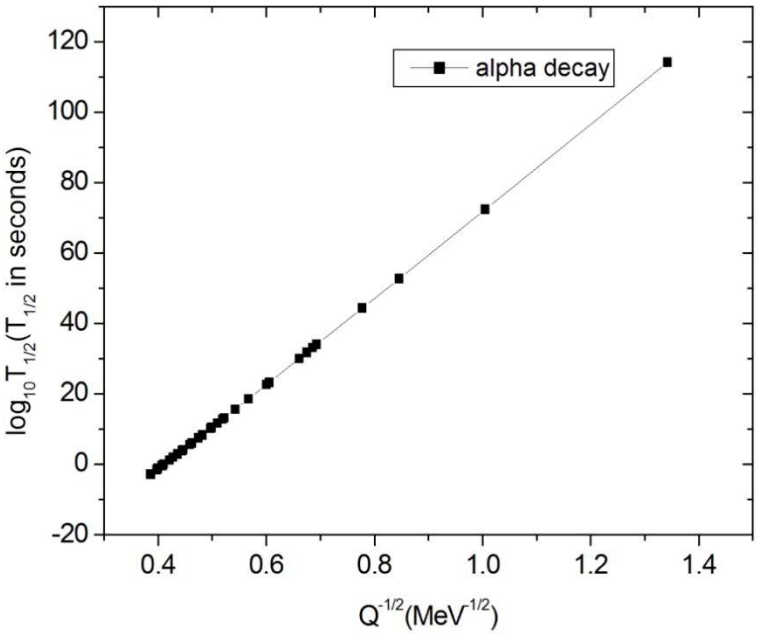

Fig. 5.8. G-N plot for alpha decay of Re isotopes.

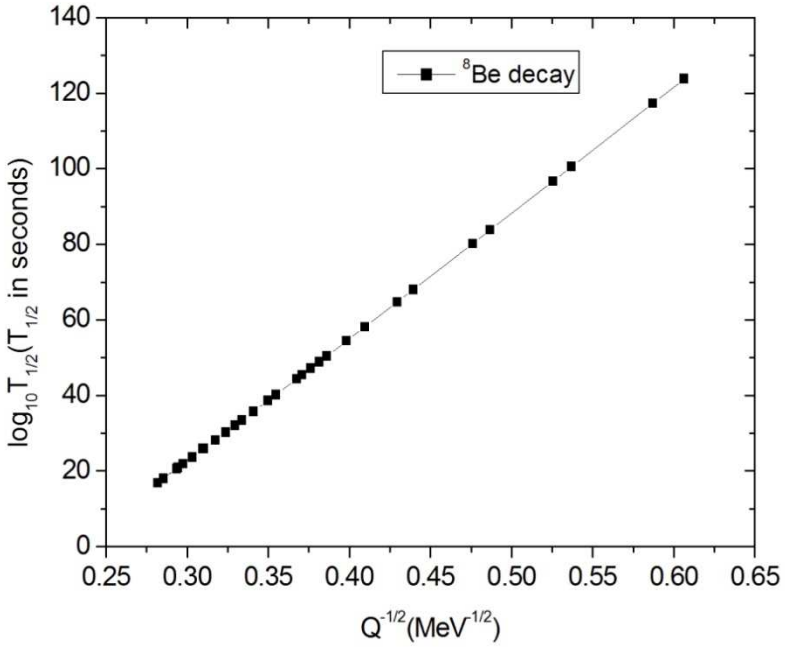

Fig. 5.9. G-N plot for ^{8}Be decay of Re isotopes.

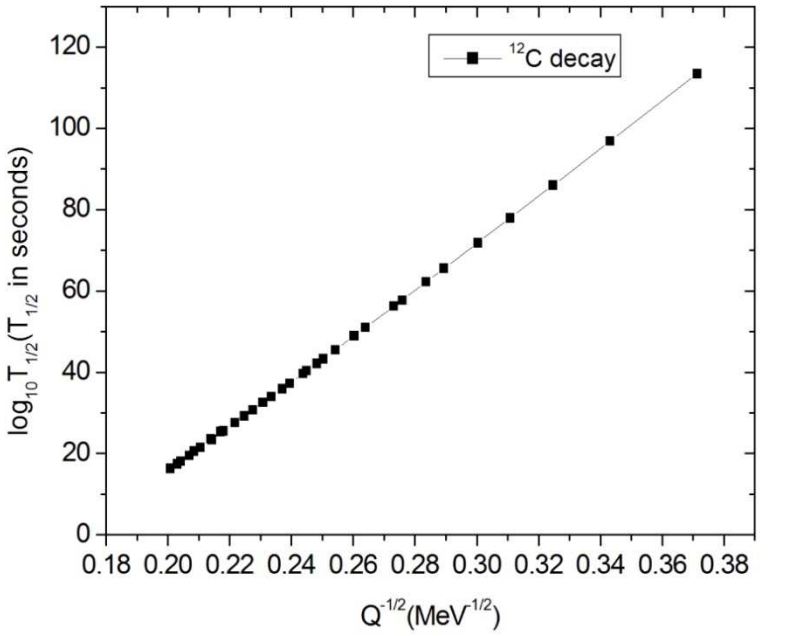

Fig. 5.10. G-N plot for ^{12}C decay of Re isotopes.

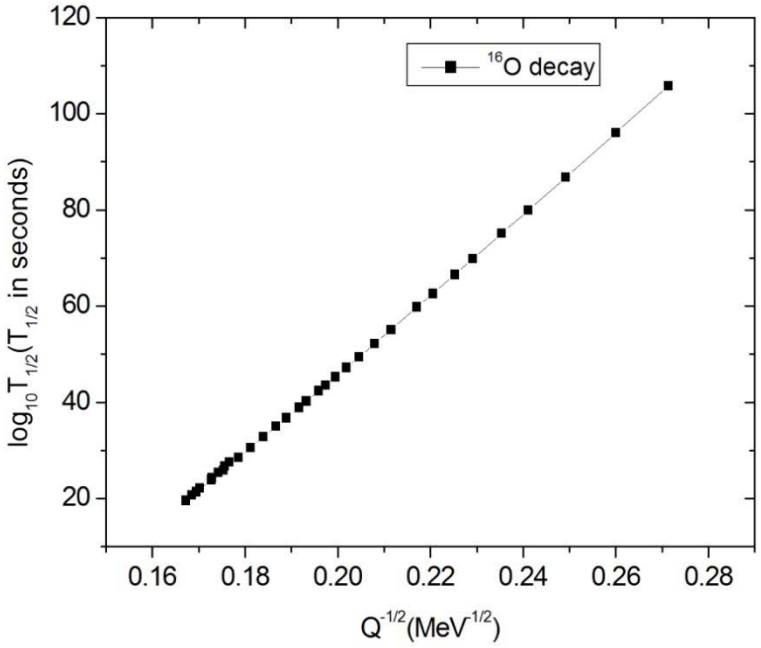

Fig. 5.11. G-N plot for ^{16}O decay of Re isotopes.

Table 5.9. Slopes and intercepts of G-N plots for various decays of Re isotopes.

Cluster emitted	Slope (X)	Intercept (Y)
^{1}H	31.7242	-32.5368
^{4}He	122.1261	-50.4371
^{8}Be	329.0765	-76.2906
^{12}C	566.2301	-98.0024
^{16}O	820.7718	-118.0070

5.7 Half-life in terms of atomic number of cluster

From the slopes and intercepts of G-N plots and atomic number of the corresponding emitted cluster (Z_1), we have obtained a general equation for logarithmic half-life, which can be applied to all clusters emitted from various Re isotopes, i.e.,

$$\log_{10}T_{1/2} = \frac{X(Z_1)}{\sqrt{Q}} + Y(Z_1) \quad (5.1)$$

where

$$X(Z_1) = -0.2176Z_1^3 + 6.2077Z_1^2 + 72.7216Z_1 - 46.8052 \quad (5.2)$$

$$Y(Z_1) = -0.1088Z_1^3 + 2.0352Z_1^2 - 22.5599Z_1 - 12.1180 \quad (5.3)$$

References

1. C. Qi, F. R. Xu, R. J. Liotta and R. Wyss, *Phys. Rev. Lett.* **103**, 072501 (2009).

2. C. Qi, F. R. Xu, R. J. Liotta, R. Wyss, M. Y. Zhang, C. Asawatangtrakuldee and D. Hu, *Phys. Rev. C* **80**, 044326 (2009).

3. J. M. Dong, H. F. Zhang and G. Royer, *Phys. Rev. C* **79**, 054330 (2009).

4. S. B. Duarte, O. A. P. Tavares, F. Guzman and A. Dimarco, *At. Data Nucl. Data Tables* **80**, 235 (2002).

5. P. Möller, A. J. Sierk, T. Ichikawa and H. Sagawa, *At. Data Nucl. Data Tables* **109**, 1 (2016).

CHAPTER 6

EXOTIC DECAY IN IRIDIUM ISOTOPES

6.1 Probable exotic decay modes

Employing the effective liquid drop model (ELDM), the half-lives are estimated for alpha decay, proton decay and cluster decays in neutron-deficient and proton-deficient isotopes of iridium. All feasible combinations of cluster and parent have been studied where the Q value is found to be positive. Within the measurable range, the admissible decay modes in neutron-deficient iridium isotopes are found to be proton and alpha decays and cluster decays like ^{8}Be, ^{12}C, ^{14}N, ^{16}O, ^{20}Ne and ^{24}Mg, which have $T_{1/2} < 10^{30}$ s. Table 6.1 shows the mass ranges of Ir isotopes displaying proton decay, alpha decay and different cluster decays with decay half-lives in the range $T_{1/2} < 10^{30}$s. Both proton and alpha decays and cluster emissions are observed to slow down with the increase in mass number and as a result, these decays are not observed for neutron-rich isotopes of iridium.

Table 6.1. Mass ranges of Ir isotopes exhibiting proton, alpha and various cluster decays with half-lives in the range $T_{1/2} < 10^{30}$ s .

Decays with $T_{1/2} < 10^{30}$ s	Mass range (A)
Proton decay	164 – 169
Alpha decay	164 – 190
^{8}Be decay	164 – 175
^{12}C decay	164 – 177
^{14}N decay	164 – 168, 170
^{16}O decay	164 – 175
^{20}Ne decay	165 – 171
^{24}Mg decay	164 – 172

6.2 Comparison study of decay half-lives

Tables 6.2 – 6.9 show the comparison study of decay half-lives using effective liquid drop model and universal decay law (UDL) model [1,2] for the respective decay modes in iridium isotopes. The estimated half-lives of alpha decay are observed to agree well with the available experimental data [3]. ELDM values are compared with the UDL values and found that the former model is an effective tool to reproduce the experimental data. Therefore, the effective liquid drop model is employed for cluster decay studies. The estimated half-lives for proton and alpha decays and ^{8}Be, ^{12}C, ^{14}N, ^{16}O, ^{20}Ne and ^{24}Mg cluster decays are observed to lie close to the UDL values. Evidently, the probability of cluster decays diminishes with the rise in neutron number. From the calculated half-lives of all decays, it is found that proton decay from ^{164}Ir isotope is the most probable decay mode in Ir isotopes, since it has the lowest logarithmic half-life of -6.5904. Also, ^{12}C emission from ^{165}Ir isotope is found to be the most probable cluster decay mode, since it has the lowest logarithmic half-life of 13.9789 among cluster decays.

Standard rms deviation (σ) of $\log_{10}T_{1/2}$ values for alpha decay is calculated and it is found that, within ELDM model, $\sigma = 0.58$ and within UDL model, $\sigma = 0.56$.

Table 6.2. Comparison study of decay half-lives for proton decay of Ir isotopes using ELDM and UDL models.

Mass number of Ir	Daughter	$\text{Log}_{10}T_{1/2}$ ($T_{1/2}$ in seconds)	
		ELDM (present)	UDL
164	^{163}Os	-6.5904	-8.6409
165	^{164}Os	-6.4303	-8.4791
166	^{165}Os	-2.4768	-4.4818
167	^{166}Os	-1.2304	-3.2254
168	^{167}Os	13.7383	11.8165
169	^{168}Os	8.6140	6.6736

Table 6.3. Comparison study of decay half-lives for alpha decay of Ir isotopes using ELDM and UDL models.

Mass number of Ir	Daughter	$Log_{10}T_{1/2}$ ($T_{1/2}$ in seconds)		
		ELDM (present)	UDL	Experiment [3]
164	^{160}Re	-2.9116	-3.5278	-
165	^{161}Re	-2.4640	-3.0528	-
166	^{162}Re	-2.1409	-2.7096	> -2.30
167	^{163}Re	-1.3724	-1.8981	≥ -1.29
168	^{164}Re	-0.9119	-1.4124	-
169	^{165}Re	-0.0215	-0.4753	-0.40
170	^{166}Re	0.1043	-0.3422	0.15
171	^{167}Re	0.5361	0.1119	0.18
172	^{168}Re	0.5583	0.1369	-
173	^{169}Re	1.7021	1.3346	-
174	^{170}Re	2.1007	1.7521	-
175	^{171}Re	2.9935	2.6840	3.04
176	^{172}Re	3.8976	3.6255	2.58
177	^{173}Re	4.7404	4.5017	4.70
178	^{174}Re	5.1898	4.9703	-
179	^{175}Re	6.3832	6.2073	-
180	^{176}Re	7.1124	6.9630	-
181	^{177}Re	8.9567	8.8670	-
182	^{178}Re	10.3172	10.2697	-
183	^{179}Re	11.9632	11.9624	-
184	^{180}Re	13.2188	13.2526	-
185	^{181}Re	13.5494	13.5927	-
186	^{182}Re	12.7740	12.7997	-
187	^{183}Re	12.8634	12.8934	-
188	^{184}Re	16.3402	16.4551	-
189	^{185}Re	21.9304	22.1610	-
190	^{186}Re	24.4127	24.6892	-

Table 6.4. Comparison study of decay half-lives for ^{8}Be decay of Ir isotopes using ELDM and UDL models.

Mass number of Ir	Daughter	$Log_{10}T_{1/2}$ ($T_{1/2}$ in seconds)	
		ELDM (present)	UDL
164	^{156}Ta	15.1894	16.2168
165	^{157}Ta	16.8821	18.0075
166	^{158}Ta	17.4814	18.6436
167	^{159}Ta	19.1133	20.3642
168	^{160}Ta	19.9053	21.1998
169	^{161}Ta	21.9896	23.3872
170	^{162}Ta	22.8103	24.2506
171	^{163}Ta	24.1308	25.6336
172	^{164}Ta	25.0344	26.5799
173	^{165}Ta	26.5202	28.1317
174	^{166}Ta	28.2215	29.9052
175	^{167}Ta	29.5973	31.3378

Table 6.5. Comparison study of decay half-lives for ^{12}C decay of Ir isotopes using ELDM and UDL models.

Mass number of Ir	Daughter	$Log_{10}T_{1/2}$ ($T_{1/2}$ in seconds)	
		ELDM (present)	UDL
164	^{152}Lu	15.9080	17.0146
165	^{153}Lu	13.9789	14.9232
166	^{154}Lu	14.7704	15.7912
167	^{155}Lu	16.6402	17.8291
168	^{156}Lu	17.5762	18.8490
169	^{157}Lu	19.0305	20.4276
170	^{158}Lu	20.2479	21.7456
171	^{159}Lu	21.6013	23.2059
172	^{160}Lu	22.5840	24.2660
173	^{161}Lu	24.1264	25.9241
174	^{162}Lu	24.9980	26.8609
175	^{163}Lu	26.5597	28.5320
176	^{164}Lu	28.3432	30.4350
177	^{165}Lu	29.4974	31.6669

Table 6.6. Comparison study of decay half-lives for ^{14}N decay of Ir isotopes using ELDM and UDL models.

Mass number of Ir	Daughter	$Log_{10}T_{1/2}$ ($T_{1/2}$ in seconds)	
		ELDM (present)	UDL
164	^{150}Yb	24.9108	26.6080
165	^{151}Yb	27.7593	29.6798
166	^{152}Yb	20.6428	22.0063
167	^{153}Yb	27.0679	28.9537
168	^{154}Yb	24.4199	26.1118
170	^{156}Yb	27.4822	29.4225

Table 6.7. Comparison study of decay half-lives for ^{16}O decay of Ir isotopes using ELDM and UDL models.

Mass number of Ir	Daughter	$Log_{10}T_{1/2}$ ($T_{1/2}$ in seconds)	
		ELDM (present)	UDL
164	^{148}Tm	21.9044	23.1542
165	^{149}Tm	19.9371	21.0066
166	^{150}Tm	18.2566	19.1648
167	^{151}Tm	17.2169	18.0263
168	^{152}Tm	18.2867	19.2152
169	^{153}Tm	20.2878	21.4267
170	^{154}Tm	21.8258	23.1203
171	^{155}Tm	23.4594	24.9157
172	^{156}Tm	24.9479	26.5456
173	^{157}Tm	26.9804	28.7623
174	^{158}Tm	28.3266	30.2296
175	^{159}Tm	29.7745	31.8036

Table 6.8. Comparison study of decay half-lives for ^{20}Ne decay of Ir isotopes using ELDM and UDL models.

Mass number of Ir	Daughter	$Log_{10}T_{1/2}$ ($T_{1/2}$ in seconds)	
		ELDM (present)	UDL
165	^{145}Ho	29.2299	30.6401
166	^{146}Ho	28.4026	29.7421
167	^{147}Ho	26.8971	28.0988
168	^{148}Ho	25.7808	26.8783
169	^{149}Ho	25.1608	26.2045
170	^{150}Ho	26.8398	28.0664
171	^{151}Ho	29.3035	30.7838

Table 6.9. Comparison study of decay half-lives for ^{24}Mg decay of Ir isotopes using ELDM and UDL models.

Mass number of Ir	Daughter	$Log_{10}T_{1/2}$ ($T_{1/2}$ in seconds)	
		ELDM (present)	UDL
164	^{140}Tb	28.6632	29.3550
165	^{141}Tb	28.6421	29.3426
166	^{142}Tb	28.0608	28.7100
167	^{143}Tb	27.7670	28.3939
168	^{144}Tb	27.2001	27.7739
169	^{145}Tb	26.2192	26.6948
170	^{146}Tb	25.8596	26.3051
171	^{147}Tb	25.8933	26.3535
172	^{148}Tb	27.6464	28.3160

6.3 Half-lives and β_2 values

Tables 6.10 and 6.11 show the deformation parameter β_2 of parent and daughter along with the half-life for ^{12}C and ^{14}N cluster decays of Ir isotopes. β_2 values are taken from the Nuclear Data Table by Möller et al. [4]. Here we can see that minimum value of half-life is obtained for minimum β_2 value of daughter (β_2 = -0.021 for ^{12}C decay and β_2 = 0.000 for ^{14}N decay) which

corresponds to nearly spherical and spherical daughters. This implies that the probability of cluster decay will be high if the daughter nucleus has spherical or nearly spherical shape. It is evident that the shape of the daughter nucleus influences the cluster decay half-lives more than that of the parent nucleus.

Table 6.10. Half-lives and β_2 values of parent and daughter for ^{12}C decay of Ir isotopes.

Parent	β_2 (Parent)	Daughter	β_2 (Daughter)	$Log_{10}T_{1/2}$(ELDM) ($T_{1/2}$ in seconds)
^{164}Ir	0.107	^{152}Lu	-0.105	15.9080
^{165}Ir	0.118	^{153}Lu	-0.021	13.9789
^{166}Ir	0.129	^{154}Lu	-0.084	14.7704
^{167}Ir	0.140	^{155}Lu	0.096	16.6402
^{168}Ir	0.140	^{156}Lu	0.118	17.5762
^{169}Ir	0.151	^{157}Lu	0.139	19.0305
^{170}Ir	0.162	^{158}Lu	0.161	20.2479
^{171}Ir	0.162	^{159}Lu	0.172	21.6013
^{172}Ir	0.173	^{160}Lu	0.183	22.5840
^{173}Ir	0.173	^{161}Lu	0.206	24.1264
^{174}Ir	0.184	^{162}Lu	0.206	24.9980
^{175}Ir	0.195	^{163}Lu	0.228	26.5597
^{176}Ir	0.239	^{164}Lu	0.239	28.3432
^{177}Ir	0.240	^{165}Lu	0.239	29.4974

Table 6.11. Half-lives and β_2 values of parent and daughter for ^{14}N decay of Ir isotopes.

Parent	β_2 (Parent)	Daughter	β_2 (Daughter)	$Log_{10}T_{1/2}$(ELDM) ($T_{1/2}$ in seconds)
^{164}Ir	0.107	^{150}Yb	-0.167	24.9108
^{165}Ir	0.118	^{151}Yb	-0.125	27.7593
^{166}Ir	0.129	^{152}Yb	0.000	20.6428
^{167}Ir	0.140	^{153}Yb	-0.052	27.0679
^{168}Ir	0.140	^{154}Yb	-0.104	24.4199
^{170}Ir	0.162	^{156}Yb	0.139	27.4822

6.4 Plots of half-life and Q versus neutron number of daughter

Figures 6.1 – 6.8 show the plots of $\log_{10}T_{1/2}$ and Q versus the neutron number of daughter nucleus N_d for various decays of Ir isotopes. In the case of proton and ^{14}N decays, the probability of decay is found to be high for daughter having even number of neutrons. The profiles of $\log_{10}T_{1/2}$ versus N_d and Q versus N_d for alpha, ^{8}Be, ^{12}C, ^{16}O, ^{20}Ne and ^{24}Mg decays are found to be similar and appear as mirror reflections. In this case, the plots for proton decay and ^{14}N decay are exceptions. The plots show a decrease in the Q value corresponding to an increase in $\log_{10}T_{1/2}$ with the rise in N_d. Since barrier penetrability factor is inversely proportional to decay half-life, the probability of decay decreases with the rise in $\log_{10}T_{1/2}$. Therefore, the probability of cluster emissions decreases with the increase in neutron number of daughter. In the plots for ^{12}C, ^{14}N, ^{16}O, ^{20}Ne and ^{24}Mg decays, shell closures are observed at or near N_d = 82, which emphasizes the relevance of neutron magicity in cluster emissions. The plot for ^{14}N decay is quite interesting where a large number of minima are observed. This points to the possibility of a large number of emissions of ^{14}N cluster from Ir isotopes. The observation of the emission of ^{14}N, which is an odd-odd cluster, is a rare one, since odd-odd cluster emissions have not been experimentally observed until now [5].

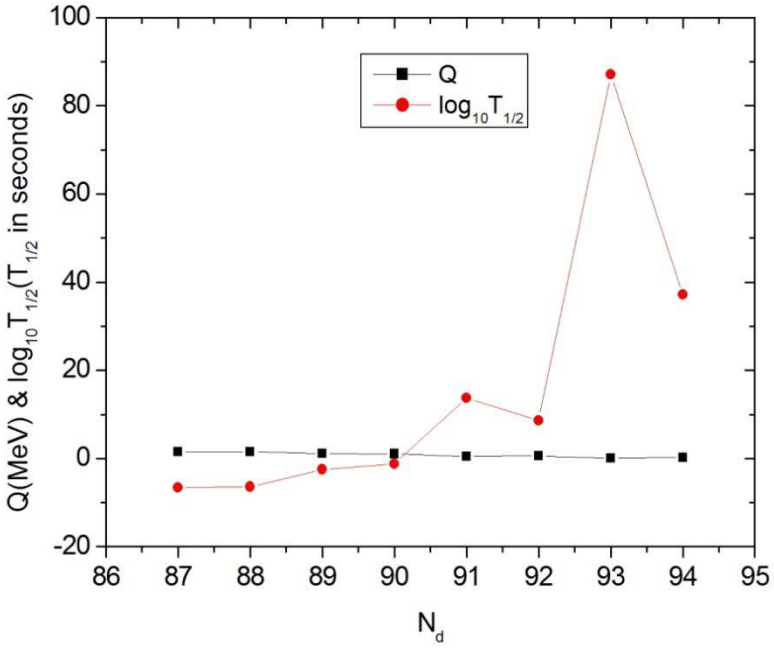

Fig. 6.1. Plots of $\log_{10}T_{1/2}$ and Q against N_d for proton decay of Ir isotopes.

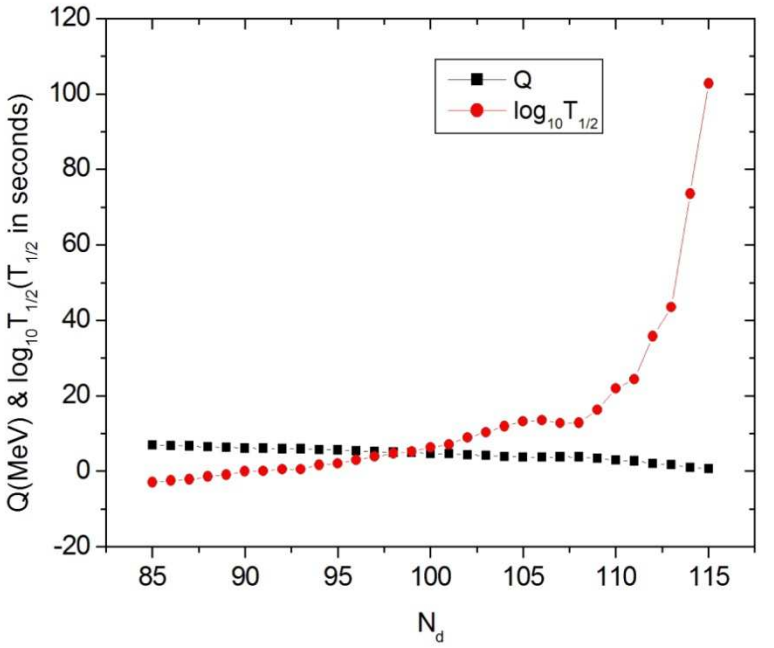

Fig. 6.2. Plots of $\log_{10}T_{1/2}$ and Q against N_d for alpha decay of Ir isotopes.

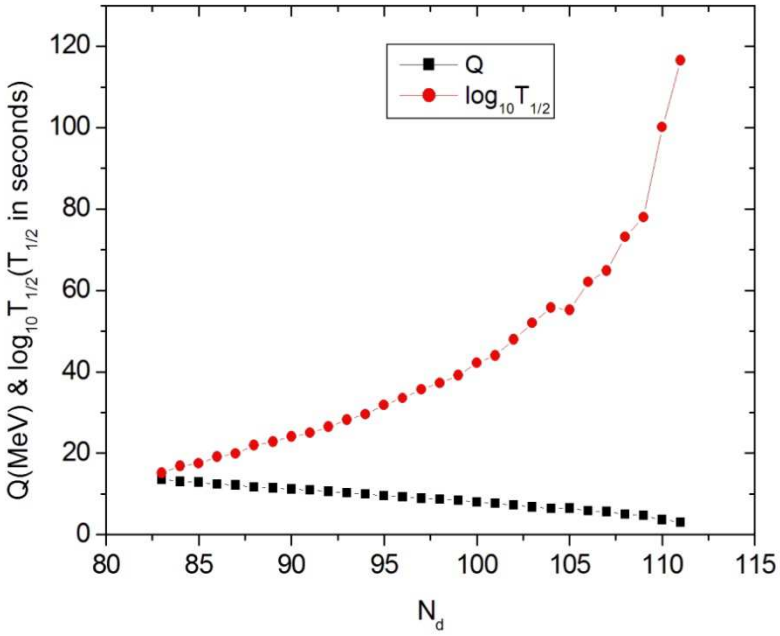

Fig. 6.3. Plots of $\log_{10}T_{1/2}$ and Q against N_d for ^{8}Be decay of Ir isotopes.

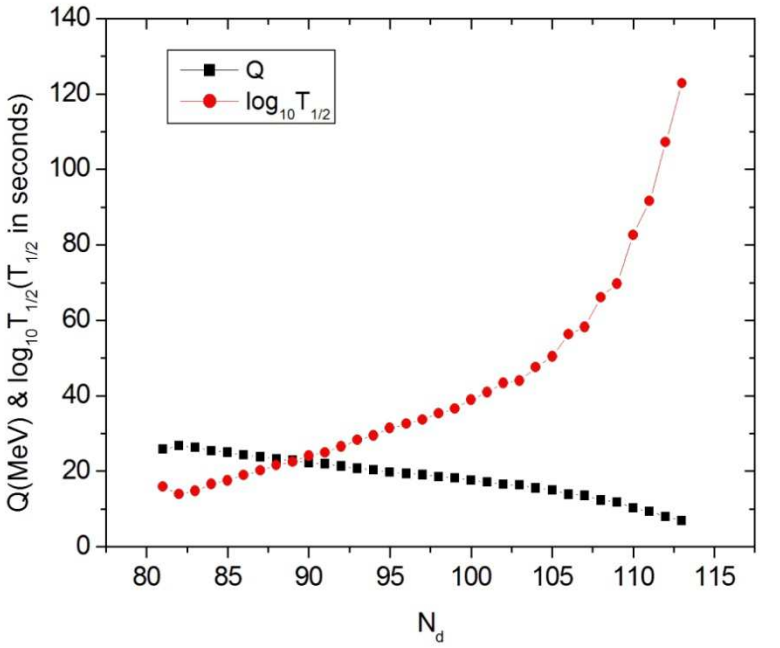

Fig. 6.4. Plots of $\log_{10}T_{1/2}$ and Q against N_d for ^{12}C decay of Ir isotopes.

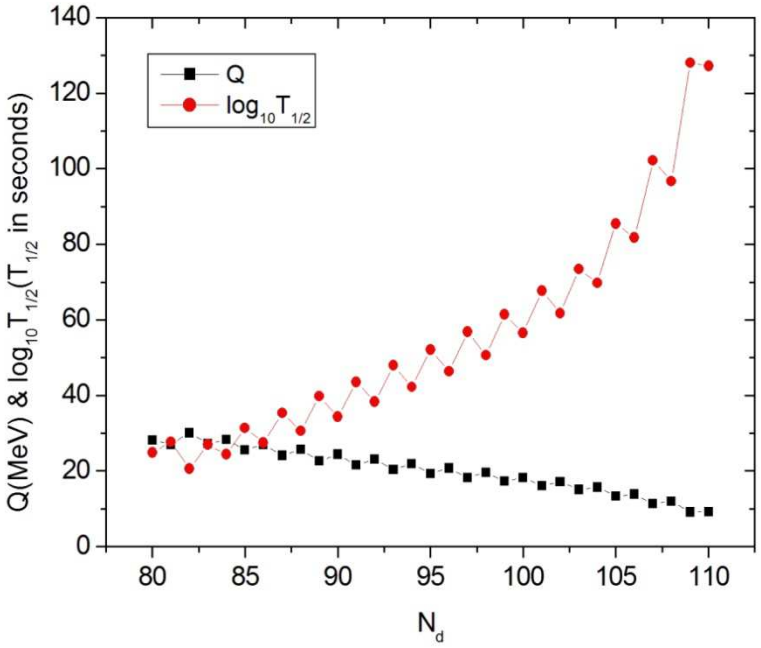

Fig. 6.5. Plots of $\log_{10}T_{1/2}$ and Q against N_d for ^{14}N decay of Ir isotopes.

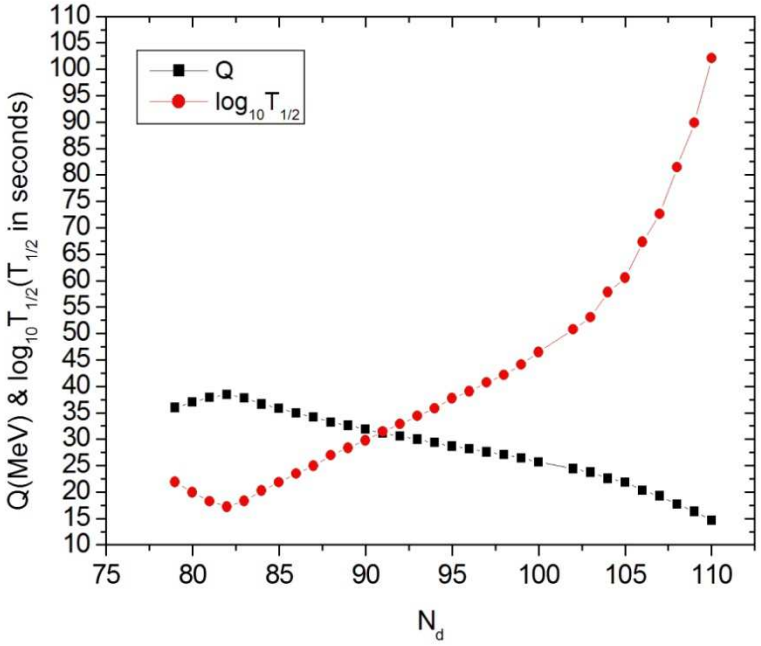

Fig. 6.6. Plots of $\log_{10}T_{1/2}$ and Q against N_d for ^{16}O decay of Ir isotopes.

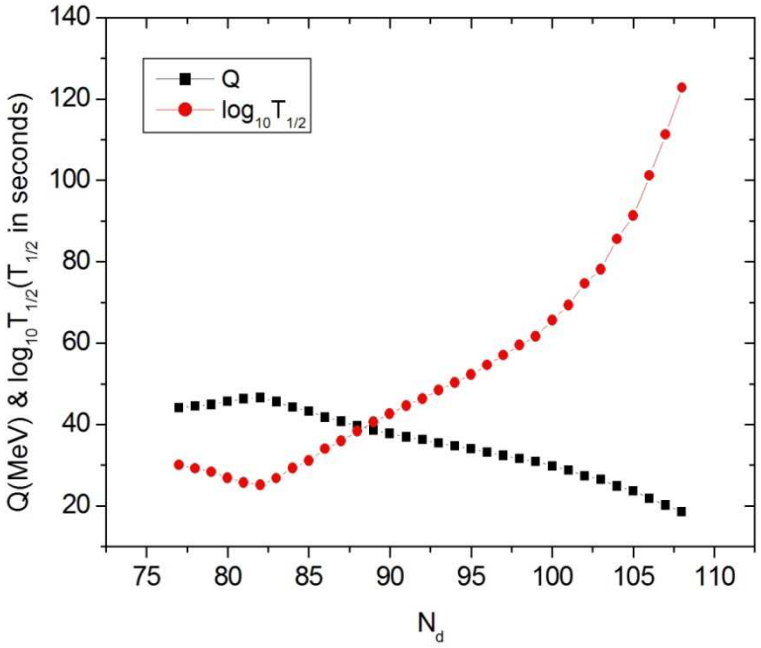

Fig. 6.7. Plots of $\log_{10}T_{1/2}$ and Q against N_d for ^{20}Ne decay of Ir isotopes.

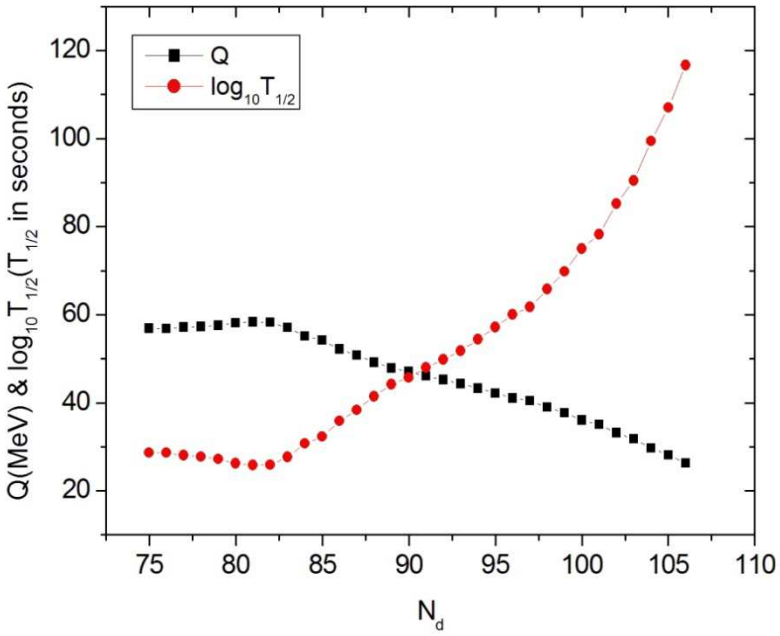

Fig. 6.8. Plots of $\log_{10}T_{1/2}$ and Q against N_d for ^{24}Mg decay of Ir isotopes.

6.5 Plot of half-life versus neutron number of parent

Fig. 6.9 shows the combined plot of half-life versus N_p (neutron number of parent nucleus) for proton and alpha decays and ^{8}Be, ^{12}C, ^{14}N, ^{16}O, ^{20}Ne and ^{24}Mg cluster decays of Ir isotopes. The general trend of these plots is that as the parent becomes rich in the number of neutrons, half-life increases, which in turn, slows down the alpha and cluster emissions. When compared to other emissions, half-lives of alpha emission are found to be minimum for a large range of N_p values, favoring high probability of alpha particle emission from these isotopes. For ^{8}Be, ^{12}C, ^{14}N, ^{16}O, ^{20}Ne and ^{24}Mg cluster emissions, it is found that the minimum value of half-life shifts towards the higher N_p values. A close similarity in the decay characteristics is observed between ^{12}C and ^{16}O cluster decays and also between ^{20}Ne and ^{24}Mg cluster emissions. The decay characteristics of proton decay and ^{14}N cluster decay are found to be much different from those of other decays.

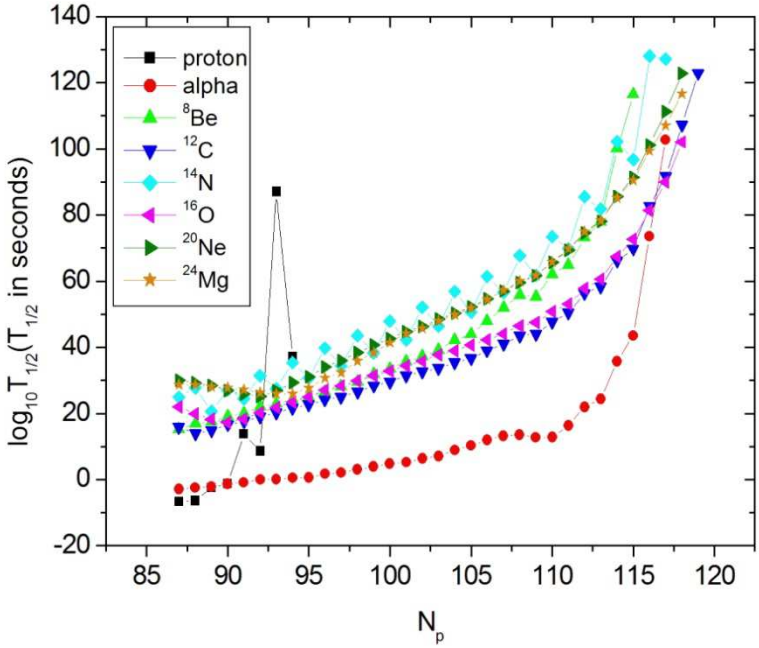

Fig. 6.9. Plot of $\log_{10}T_{1/2}$ against N_p for various decays of Ir isotopes.

6.6 Geiger-Nuttall plots

Figures 6.10 – 6.17 show the Geiger-Nuttall (G-N) plots, i.e., $Q^{-1/2}$ versus $\log_{10}T_{1/2}$ graphs for proton, alpha, ^{8}Be, ^{12}C, ^{14}N, ^{16}O, ^{20}Ne and ^{24}Mg decays. All of them exhibit linear behaviour, which implies that no notable variation in the linear nature is caused by the addition of surface potential, since G-N law is generally applied to the system subjected to pure Coulomb potential. Table 6.12 shows the intercepts and slopes of G-N plots for different decays of Ir isotopes. Apparent shifts observed in the slopes and intercepts are caused by the inclusion of surface potential and shell effects in the nuclear configuration of iridium isotopes.

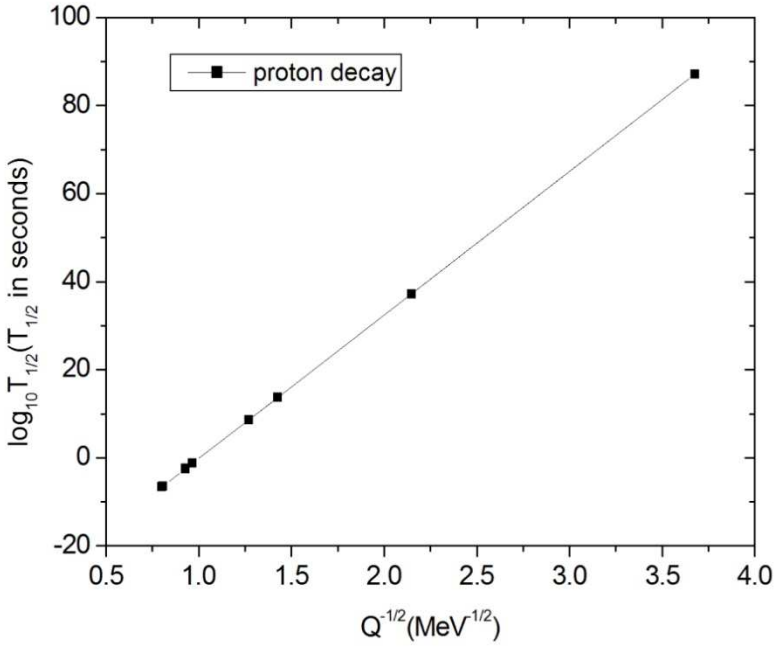

Fig. 6.10. G-N plot for proton decay of Ir isotopes.

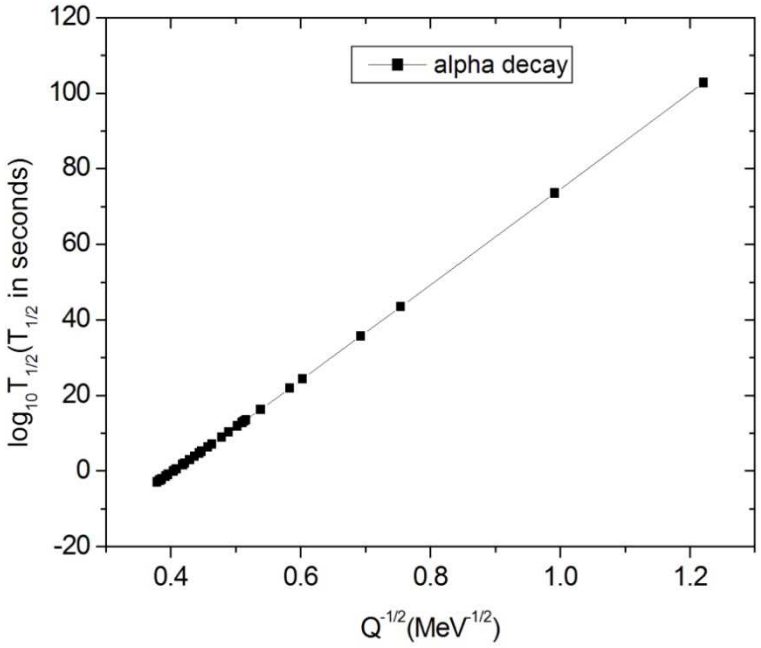

Fig. 6.11. G-N plot for alpha decay of Ir isotopes.

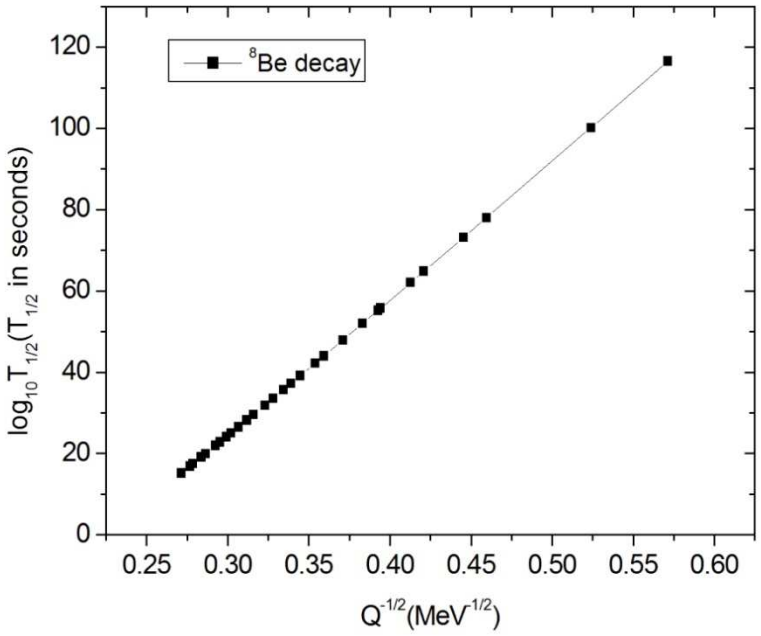

Fig. 6.12. G-N plot for ^{8}Be decay of Ir isotopes.

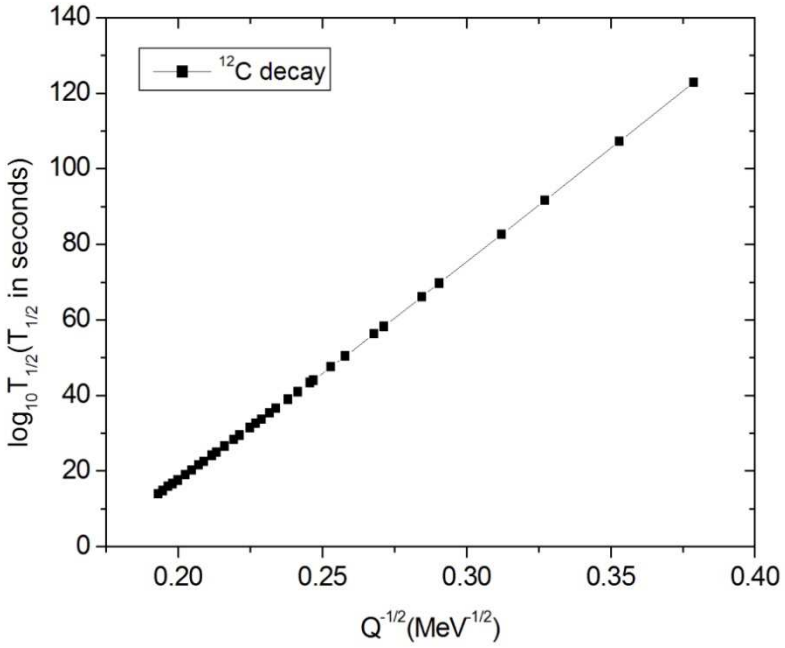

Fig. 6.13. G-N plot for ^{12}C decay of Ir isotopes.

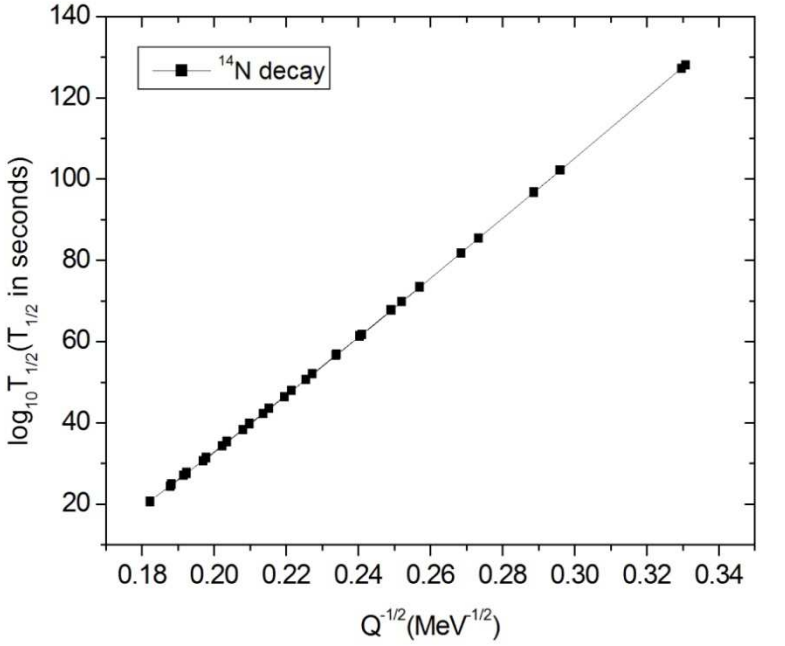

Fig. 6.14. G-N plot for ^{14}N decay of Ir isotopes.

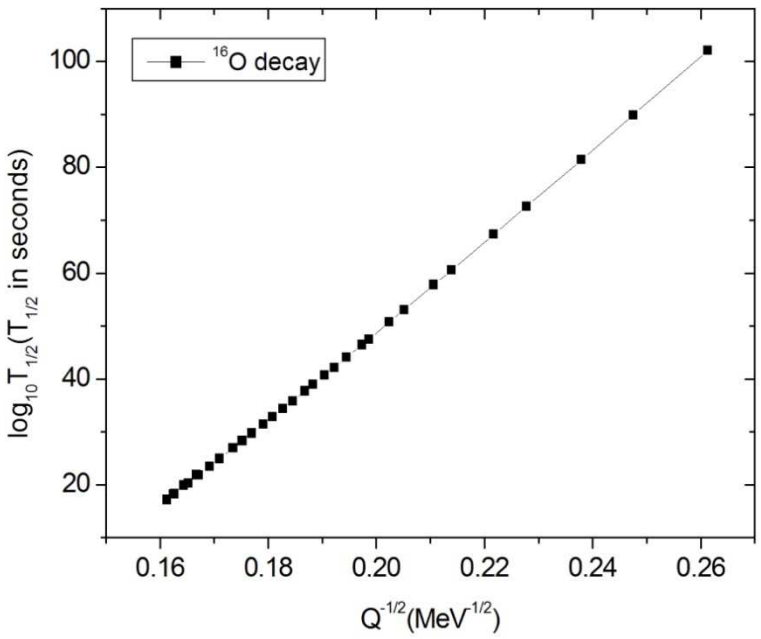

Fig. 6.15. G-N plot for ^{16}O decay of Ir isotopes.

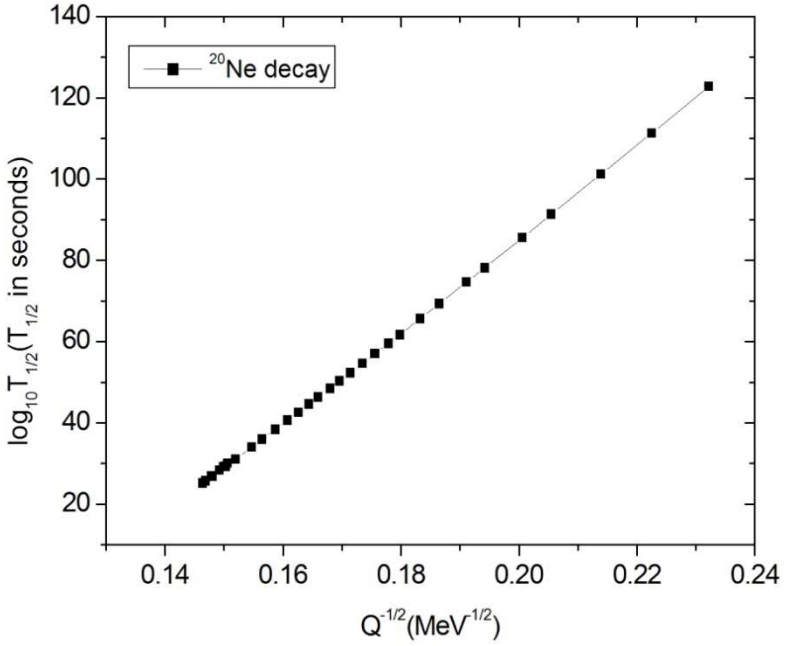

Fig. 6.16. G-N plot for ^{20}Ne decay of Ir isotopes.

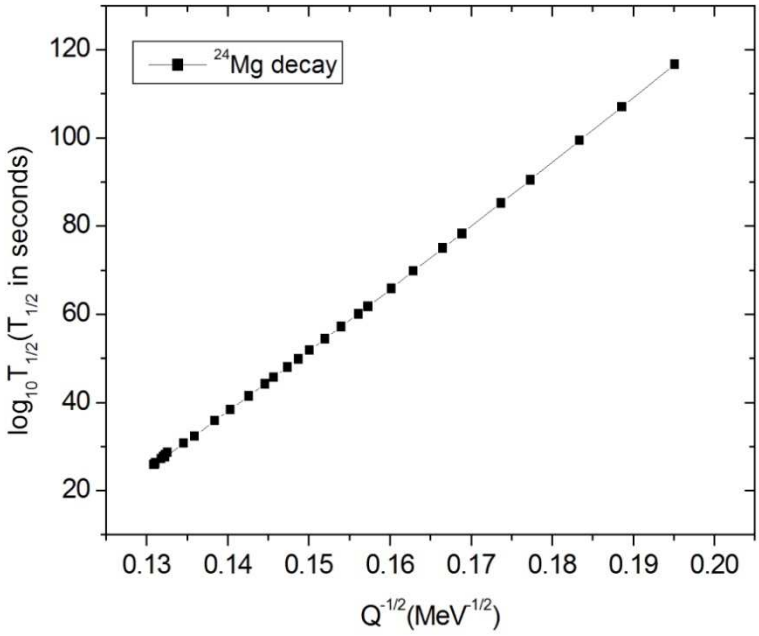

Fig. 6.17. G-N plot for ^{24}Mg decay of Ir isotopes.

Table 6.12. Slopes and intercepts of G-N plots for various decays of Ir isotopes.

Cluster emitted	Slope (X)	Intercept (Y)
^{1}H	32.5943	-32.7329
^{4}He	125.3672	-50.8394
^{8}Be	337.0190	-76.8062
^{12}C	584.2209	-99.7006
^{14}N	721.5385	-111.5861
^{16}O	842.1141	-119.1888
^{20}Ne	1128.0874	-140.5360
^{24}Mg	1399.2949	-157.7140

6.7 Half-life in terms of atomic number of cluster

From the slopes and intercepts of G-N plots and atomic number of the corresponding emitted cluster (Z_1), we have obtained a general equation for

logarithmic half-life, which can be applied to all clusters emitted from various Ir isotopes, i.e.,

$$\log_{10}T_{1/2} = \frac{X(Z_1)}{\sqrt{Q}} + Y(Z_1) \quad (6.1)$$

where

$$X(Z_1) = -0.2260Z_1^3 + 6.6337Z_1^2 + 73.5237Z_1 - 47.1294 \quad (6.2)$$

$$Y(Z_1) = -0.0309Z_1^3 + 0.9240Z_1^2 - 18.4851Z_1 - 15.9705 \quad (6.3)$$

References

1. C. Qi, F. R. Xu, R. J. Liotta and R. Wyss, *Phys. Rev. Lett.* **103**, 072501 (2009).

2. C. Qi, F. R. Xu, R. J. Liotta, R. Wyss, M. Y. Zhang, C. Asawatangtrakuldee and D. Hu, *Phys. Rev. C* **80**, 044326 (2009).

3. S. B. Duarte, O. A. P. Tavares, F. Guzman and A. Dimarco, *At. Data Nucl. Data Tables* **80**, 235 (2002).

4. P. Möller, A. J. Sierk, T. Ichikawa and H. Sagawa, *At. Data Nucl. Data Tables* **109**, 1 (2016).

5. D. N. Poenaru, R. A. Gherghescu and W. Greiner, *Phys. Rev. C* **83**, 014601 (2011).

CHAPTER 7

EXOTIC DECAY IN PLATINUM ISOTOPES

7.1 Probable exotic decay modes

Adopting the effective liquid drop model (ELDM), the decay half-lives are assessed for alpha decay and cluster decays in proton-rich and neutron-rich isotopes of platinum. All possible combinations of parent and cluster have been examined, for which the Q value is positive. The half-lives for alpha, ^{8}Be, ^{12}C, ^{16}O, ^{20}Ne and ^{24}Mg decays are perceived to be well within the measurable range ($T_{1/2} < 10^{30}$ s). So they are predicted to be the admissible decay modes in proton-rich platinum isotopes. Table 7.1 shows the mass ranges of Pt isotopes exhibiting alpha decay and various cluster decays with half-lives in the measurable range. It is also found that the cluster emissions diminish with the rise in the number of neutrons and therefore, no cluster radioactivity is noted in the case of neutron-rich Pt isotopes.

Table 7.1. Mass ranges of Pt isotopes exhibiting alpha decay and various cluster decays with half-lives in the measurable range.

Decays with $T_{1/2} < 10^{30}$ s	Mass range(A)
Alpha decay	166 – 191
^{8}Be decay	166 – 178
^{12}C decay	166 – 180
^{16}O decay	166 – 178
^{20}Ne decay	166 – 173
^{24}Mg decay	166 – 175

7.2 Comparison study of decay half-lives

Tables 7.2 – 7.7 show the comparison study of decay half-lives using ELDM and universal decay law (UDL) model [1,2] for the respective decay modes in Pt isotopes. It has been noticed that the evaluated half-lives of alpha

decay are in remarkable agreement with the experimental data [3]. When compared with the UDL model, it is seen that the present formalism (ELDM) is more effective one for reproducing the experimental data. Therefore, the use of ELDM is adopted here for cluster decay studies. The evaluated half-lives of alpha decay and ^{8}Be, ^{12}C, ^{16}O, ^{20}Ne and ^{24}Mg cluster decays are seen to be very near the range of those predicted using UDL model. It is clearly seen from the calculations that the probability of cluster emissions decreases with increasing neutron number. From the calculated half-lives of all decays, it is found that alpha decay from ^{166}Pt isotope is the most probable decay mode in Pt isotopes, since it has the lowest logarithmic half-life of -3.5519. Also, ^{12}C emission from ^{166}Pt isotope is found to be the most probable cluster decay mode, since it has the lowest logarithmic half-life of 12.6327 among cluster decays.

Standard rms deviation (σ) of $\log_{10}T_{1/2}$ values for alpha decay is calculated and it is found that, within ELDM model, σ = 0.3189 and within UDL model, σ = 0.3588.

Table 7.2. Comparison study of decay half-lives for alpha decay of Pt isotopes using ELDM and UDL models.

Mass number of Pt	Daughter	$Log_{10}T_{1/2}$ ($T_{1/2}$ in seconds)		
		ELDM (present)	UDL	Experiment [3]
166	^{162}Os	-3.5519	-4.1851	-
167	^{163}Os	-3.1622	-3.7704	-
168	^{164}Os	-2.6288	-3.2037	-
169	^{165}Os	-2.2449	-2.7962	-2.60
170	^{166}Os	-1.7154	-2.2361	-2.22
171	^{167}Os	-1.3698	-1.8701	-1.60
172	^{168}Os	-0.8730	-1.3459	-0.96
173	^{169}Os	-0.4860	-0.9374	-0.39
174	^{170}Os	0.1831	-0.2336	0.04
175	^{171}Os	0.1833	-0.2310	-
176	^{172}Os	1.3896	1.0332	1.23
177	^{173}Os	2.4569	2.1489	2.30
178	^{174}Os	2.7660	2.4725	2.43
179	^{175}Os	3.5265	3.2655	-
180	^{176}Os	4.3960	4.1712	4.23
181	^{177}Os	4.8367	4.6301	4.93
182	^{178}Os	5.9147	5.7496	-
183	^{179}Os	6.6448	6.5066	7.48
184	^{180}Os	8.0019	7.9108	8.00
185	^{181}Os	9.0385	8.9813	-
186	^{182}Os	9.8240	9.7925	9.72
187	^{183}Os	8.2558	8.1774	-
188	^{184}Os	12.1493	12.1861	12.53
189	^{185}Os	12.9582	13.0184	-
190	^{186}Os	19.0421	19.2445	19.00
191	^{187}Os	20.7958	21.0351	-

Table 7.3. Comparison study of decay half-lives for ^{8}Be decay of Pt isotopes using ELDM and UDL models.

Mass number of Pt	Daughter	$Log_{10}T_{1/2}$ ($T_{1/2}$ in seconds)	
		ELDM (present)	UDL
166	^{158}W	14.6710	15.7037
167	^{159}W	15.3769	16.4554
168	^{160}W	16.5436	17.6924
169	^{161}W	17.4441	18.6461
170	^{162}W	18.6874	19.9587
171	^{163}W	19.6048	20.9277
172	^{164}W	20.7663	22.1513
173	^{165}W	21.5728	23.0003
174	^{166}W	22.9971	24.4947
175	^{167}W	23.6981	25.2318
176	^{168}W	25.6392	27.2612
177	^{169}W	27.5648	29.2702
178	^{170}W	28.8074	30.5658

Table 7.4. Comparison study of decay half-lives for ^{12}C decay of Pt isotopes using ELDM and UDL models.

Mass number of Pt	Daughter	$Log_{10}T_{1/2}$ ($T_{1/2}$ in seconds)	
		ELDM (present)	UDL
166	^{154}Hf	12.6327	13.4754
167	^{155}Hf	13.3394	14.2552
168	^{156}Hf	14.7774	15.8300
169	^{157}Hf	15.6010	16.7332
170	^{158}Hf	16.8212	18.0665
171	^{159}Hf	17.6921	19.0159
172	^{160}Hf	18.8983	20.3264
173	^{161}Hf	19.9344	21.4500
174	^{162}Hf	21.1650	22.7812
175	^{163}Hf	21.8364	23.5089
176	^{164}Hf	23.5533	25.3558
177	^{165}Hf	25.1841	27.1057
178	^{166}Hf	26.2739	28.2753
179	^{167}Hf	28.1657	30.2964
180	^{168}Hf	28.9528	31.1390

Table 7.5. Comparison study of decay half-lives for ^{16}O decay of Pt isotopes using ELDM and UDL models.

Mass number of Pt	Daughter	$Log_{10}T_{1/2}$ ($T_{1/2}$ in seconds)	
		ELDM (present)	UDL
166	^{150}Yb	18.2603	19.1797
167	^{151}Yb	16.6961	17.4582
168	^{152}Yb	15.7542	16.4222
169	^{153}Yb	16.6164	17.3873
170	^{154}Yb	18.3908	19.3583
171	^{155}Yb	19.3826	20.4595
172	^{156}Yb	20.9176	22.1569
173	^{157}Yb	22.1368	23.5014
174	^{158}Yb	23.6332	25.1459
175	^{159}Yb	24.6918	26.3082
176	^{160}Yb	26.5321	28.3204
177	^{161}Yb	28.1331	30.0659
178	^{162}Yb	29.5152	31.5699

Table 7.6. Comparison study of decay half-lives for ^{20}Ne decay of Pt isotopes using ELDM and UDL models.

Mass number of Pt	Daughter	$Log_{10}T_{1/2}$ ($T_{1/2}$ in seconds)	
		ELDM (present)	UDL
166	^{146}Er	27.0311	28.2409
167	^{147}Er	26.4869	27.6514
168	^{148}Er	25.3448	26.4015
169	^{149}Er	23.9028	24.8163
170	^{150}Er	23.3419	24.2051
171	^{151}Er	24.4794	25.4761
172	^{152}Er	26.8172	28.0691
173	^{153}Er	28.2978	29.7074

Table 7.7. Comparison study of decay half-lives for ^{24}Mg decay of Pt isotopes using ELDM and UDL models.

Mass number of Pt	Daughter	$Log_{10}T_{1/2}$ ($T_{1/2}$ in seconds)	
		ELDM (present)	UDL
166	^{142}Dy	26.5235	26.9885
167	^{143}Dy	26.3921	26.8541
168	^{144}Dy	26.0768	26.5133
169	^{145}Dy	25.6524	26.0522
170	^{146}Dy	24.7933	25.1028
171	^{147}Dy	24.0045	24.2311
172	^{148}Dy	23.8738	24.0963
173	^{149}Dy	25.2704	25.6693
174	^{150}Dy	27.9176	28.6317
175	^{151}Dy	29.3416	30.2252

7.3 Half-lives and β_2 values

Tables 7.8 and 7.9 show the deformation parameter β_2 of parent and daughter along with the half-life for ^{12}C and ^{16}O cluster decays of Pt isotopes. β_2 values are taken from the Nuclear Data Table by Möller et al. [4]. Here we can see that minimum value of half-life is obtained for minimum β_2 value of daughter (β_2 = 0.021 for ^{12}C decay and β_2 = 0.000 for ^{16}O decay) which corresponds to nearly spherical and spherical daughters. This implies that the probability of cluster decay will be high if the daughter nucleus has spherical or nearly spherical shape. It is evident that the shape of the daughter nucleus influences the cluster decay half-lives more than that of the parent nucleus.

Table 7.8. Half-lives and β_2 values of parent and daughter for ^{12}C decay of Pt isotopes.

Parent	β_2 (Parent)	Daughter	β_2 (Daughter)	$Log_{10}T_{1/2}$(ELDM) ($T_{1/2}$ in seconds)
^{166}Pt	-0.105	^{154}Hf	0.021	12.6327
^{167}Pt	0.107	^{155}Hf	-0.063	13.3394
^{168}Pt	0.118	^{156}Hf	-0.084	14.7774
^{169}Pt	0.129	^{157}Hf	0.118	15.6010
^{170}Pt	0.129	^{158}Hf	0.128	16.8212
^{171}Pt	0.140	^{159}Hf	0.150	17.6921
^{172}Pt	0.140	^{160}Hf	0.161	18.8983
^{173}Pt	0.151	^{161}Hf	0.172	19.9344
^{174}Pt	0.162	^{162}Hf	0.183	21.1650
^{175}Pt	0.173	^{163}Hf	0.194	21.8364
^{176}Pt	0.239	^{164}Hf	0.206	23.5533
^{177}Pt	0.250	^{165}Hf	0.217	25.1841
^{178}Pt	0.250	^{166}Hf	0.228	26.2739
^{179}Pt	0.250	^{167}Hf	0.239	28.1657
^{180}Pt	0.251	^{168}Hf	0.251	28.9528

Table 7.9. Half-lives and β_2 values of parent and daughter for ^{16}O decay of Pt isotopes.

Parent	β_2 (Parent)	Daughter	β_2 (Daughter)	$Log_{10}T_{1/2}$(ELDM) ($T_{1/2}$ in seconds)
^{166}Pt	-0.105	^{150}Yb	-0.167	18.2603
^{167}Pt	0.107	^{151}Yb	-0.125	16.6961
^{168}Pt	0.118	^{152}Yb	0.000	15.7542
^{169}Pt	0.129	^{153}Yb	-0.052	16.6164
^{170}Pt	0.129	^{154}Yb	-0.104	18.3908
^{171}Pt	0.140	^{155}Yb	0.118	19.3826
^{172}Pt	0.140	^{156}Yb	0.139	20.9176
^{173}Pt	0.151	^{157}Yb	0.161	22.1368
^{174}Pt	0.162	^{158}Yb	0.183	23.6332
^{175}Pt	0.173	^{159}Yb	0.194	24.6918
^{176}Pt	0.239	^{160}Yb	0.206	26.5321
^{177}Pt	0.250	^{161}Yb	0.217	28.1331
^{178}Pt	0.250	^{162}Yb	0.239	29.5152

7.4 Plots of half-life and Q versus neutron number of daughter

Figures 7.1 – 7.6 show the profiles of evaluated half-lives and Q values for alpha decay and possible cluster emissions from neutron-deficient Pt isotopes against neutron number of daughter N_d. It is found that the plots for alpha, ^{8}Be, ^{12}C, ^{16}O, ^{20}Ne, and ^{24}Mg decays are alike and appear almost like mirror reflected images. The plots show a decrease in the Q value corresponding to an increase in $\log_{10}T_{1/2}$ with the rise in N_d. Since barrier penetrability factor is inversely proportional to decay half-life, the probability of decay decreases with the rise in $\log_{10}T_{1/2}$. Therefore, the probability of cluster emissions decreases with the increase in neutron number of daughter. The profiles for ^{12}C, ^{16}O, ^{20}Ne and ^{24}Mg emissions point to the shell closure at N_d = 82, which is a magic number. Minimum value of half-life indicates an increase in the probability of cluster decays. This sets forth the importance of neutron magicity in cluster radioactivity.

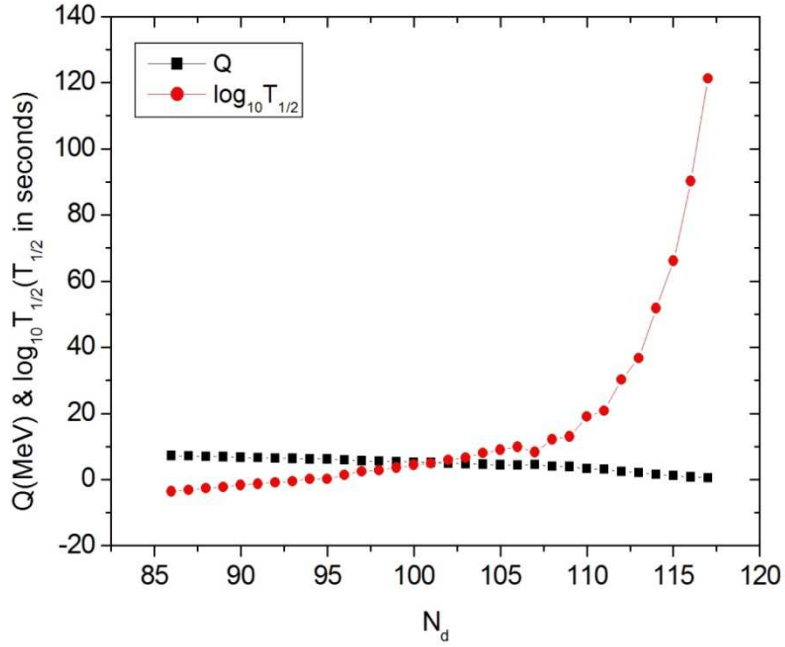

Fig. 7.1. Plots of $\log_{10}T_{1/2}$ and Q against N_d for alpha decay of Pt isotopes.

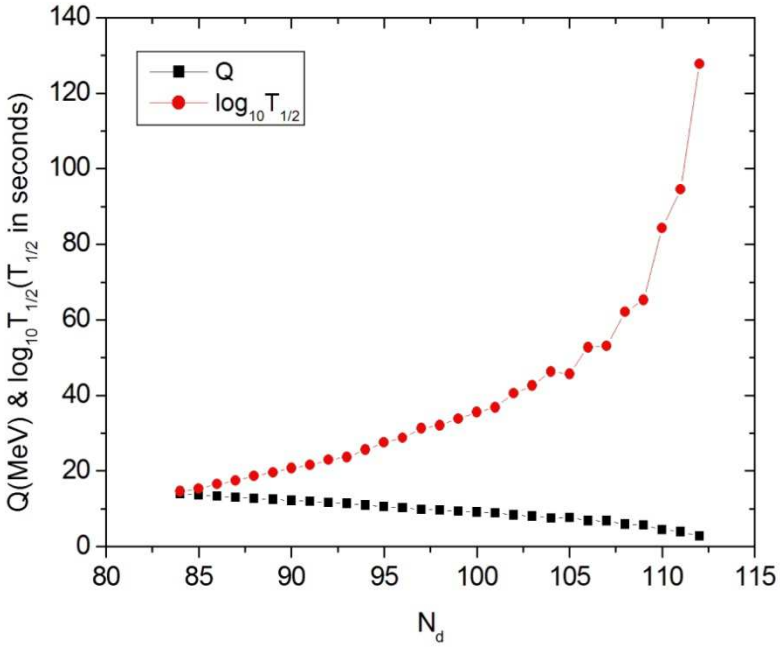

Fig. 7.2. Plots of $\log_{10}T_{1/2}$ and Q against N_d for ^{8}Be decay of Pt isotopes.

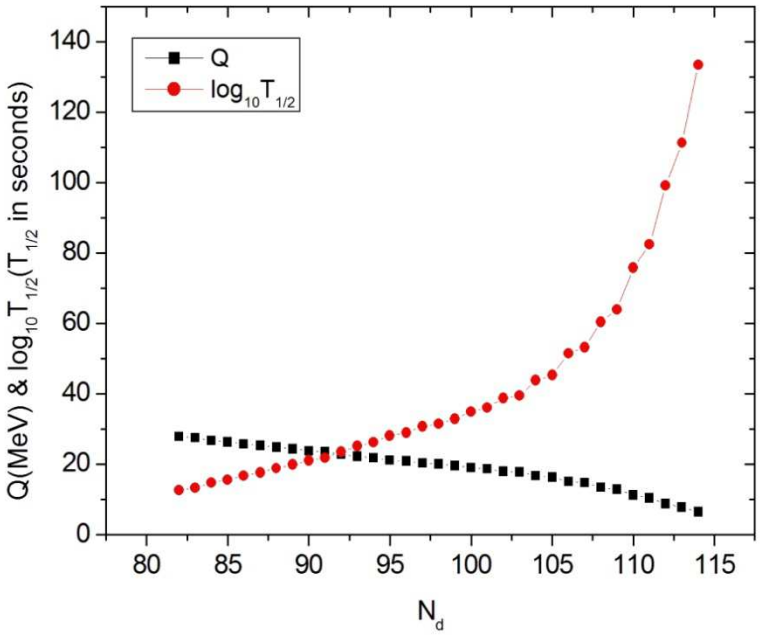

Fig. 7.3. Plots of $\log_{10}T_{1/2}$ and Q against N_d for ^{12}C decay of Pt isotopes.

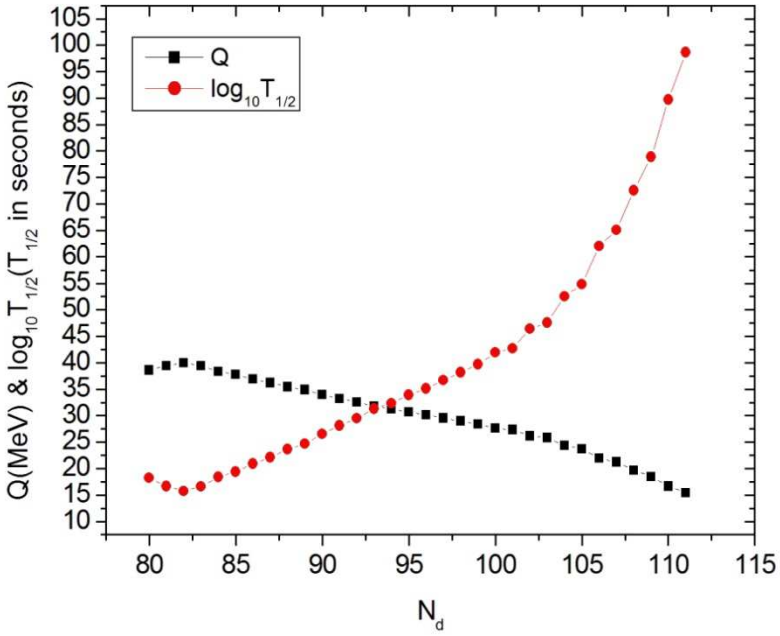

Fig. 7.4. Plots of $\log_{10}T_{1/2}$ and Q against N_d for ^{16}O decay of Pt isotopes.

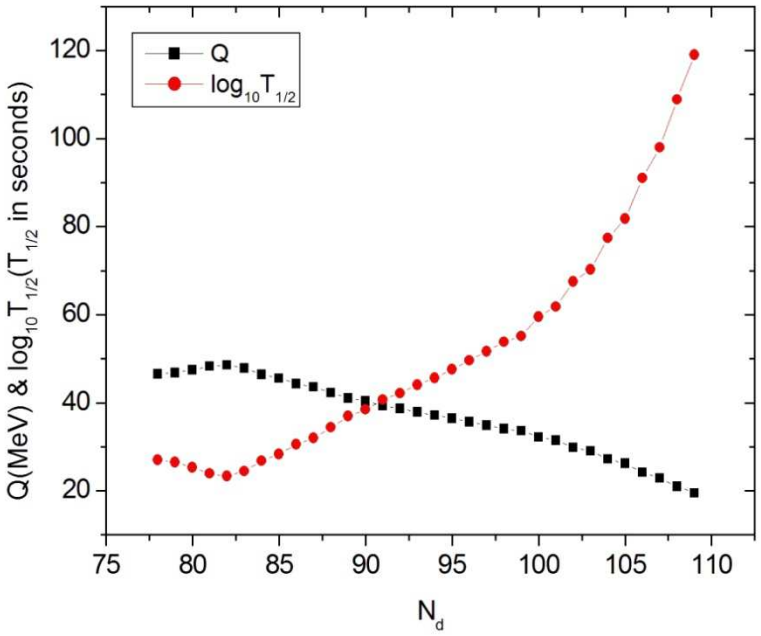

Fig. 7.5. Plots of $\log_{10}T_{1/2}$ and Q against N_d for ^{20}Ne decay of Pt isotopes.

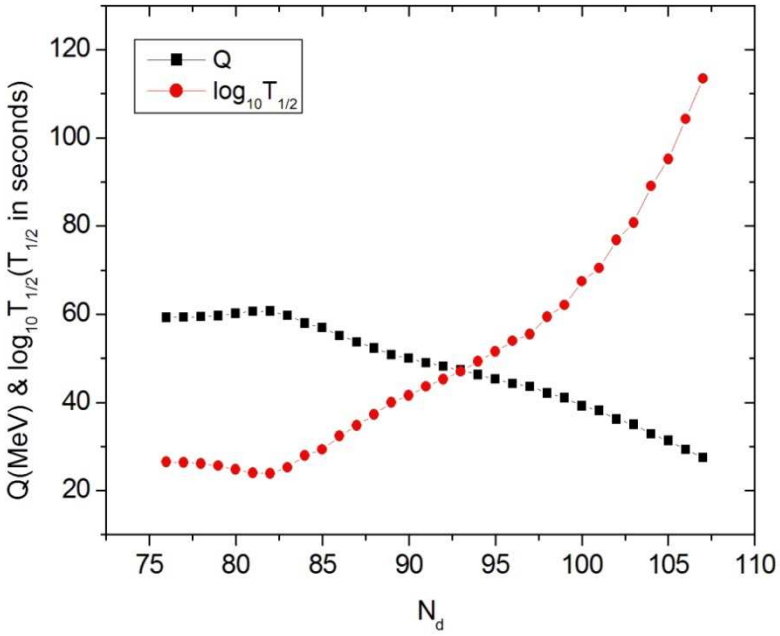

Fig. 7.6. Plots of $\log_{10}T_{1/2}$ and Q against N_d for ^{24}Mg decay of Pt isotopes.

7.5 Plot of half-life versus neutron number of parent

Fig. 7.7 shows the combined plot of half-life versus N_p (neutron number of parent nucleus) for alpha decay and ^{8}Be, ^{12}C, ^{16}O, ^{20}Ne and ^{24}Mg cluster decays of Pt isotopes. The general trend of these plots is that as the parent becomes rich in the number of neutrons, half-life increases, which in turn, slows down the alpha and cluster emissions. When compared to other emissions, half-lives of alpha emission are found to be minimum for a large range of N_p values, favoring high probability of alpha particle emission from these isotopes. For ^{8}Be, ^{12}C, ^{16}O, ^{20}Ne and ^{24}Mg cluster emissions, it is found that the minimum value of half-life shifts towards the higher N_p values. A close similarity in the decay characteristics is observed between ^{12}C and ^{16}O cluster decays and also between ^{20}Ne and ^{24}Mg cluster emissions.

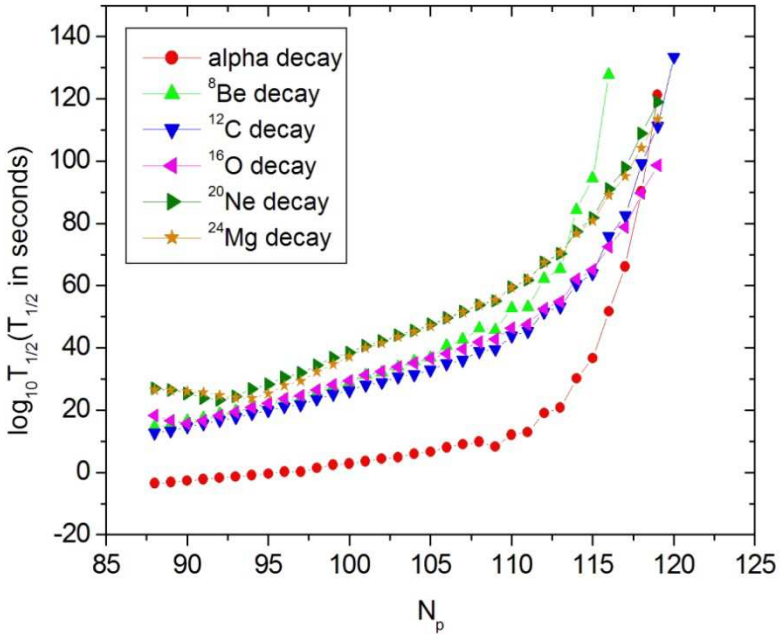

Fig. 7.7. Plot of $\log_{10}T_{1/2}$ against N_p for various decays of Pt isotopes.

7.6 Geiger-Nuttall plots

Figures 7.8 – 7.13 show the Geiger-Nuttall (G-N) plots for the probable decay modes in Pt isotopes. Clearly, they all point to the linear nature and it is already known that G-N law, in general, could be applied to the system under pure Coulomb potential. The data plots reveal the fact that the inclusion of surface potential causes no notable variation to the linear behaviour. Table 7.10 shows the slopes and intercepts of G-N plots for various decays of Pt isotopes. The apparent changes in slopes and intercepts of G-N plots indicate the presence of surface potential and shell effects in the nuclear configuration of platinum isotopes. Similar features have been observed in the cluster decay studies conducted on a few other isotopes [5,6].

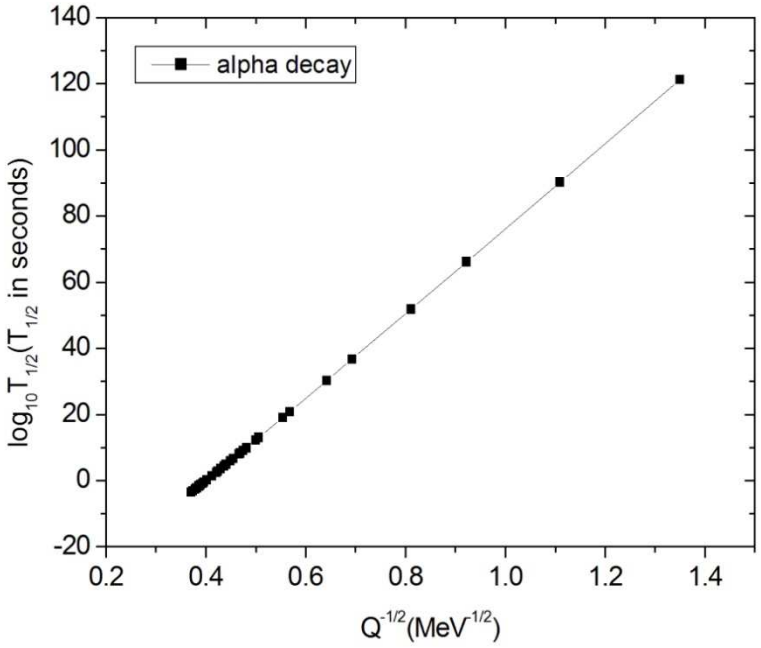

Fig. 7.8. G-N plot for alpha decay of Pt isotopes.

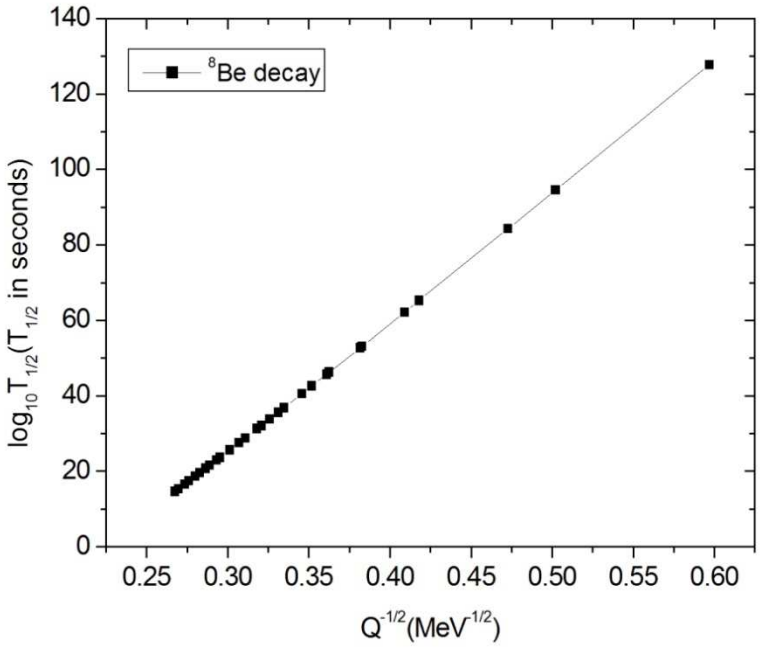

Fig. 7.9. G-N plot for ^{8}Be decay of Pt isotopes.

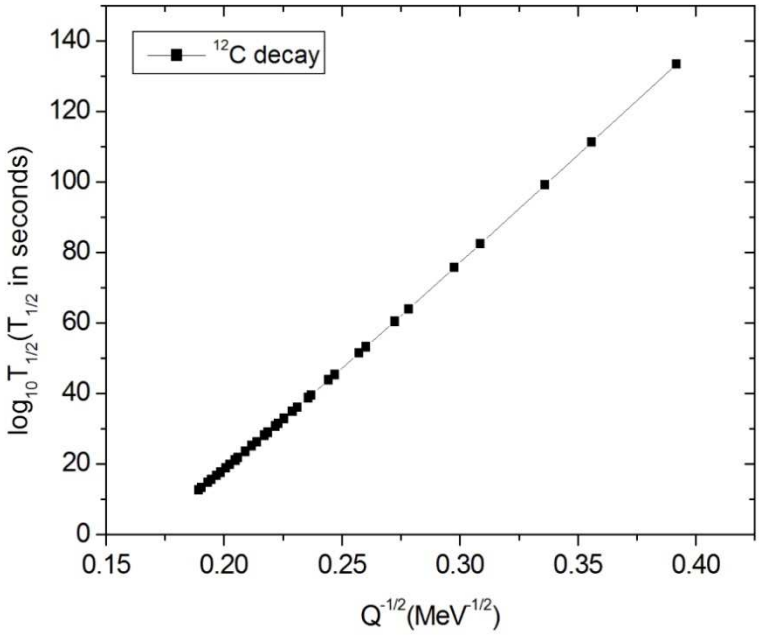

Fig. 7.10. G-N plot for ^{12}C decay of Pt isotopes.

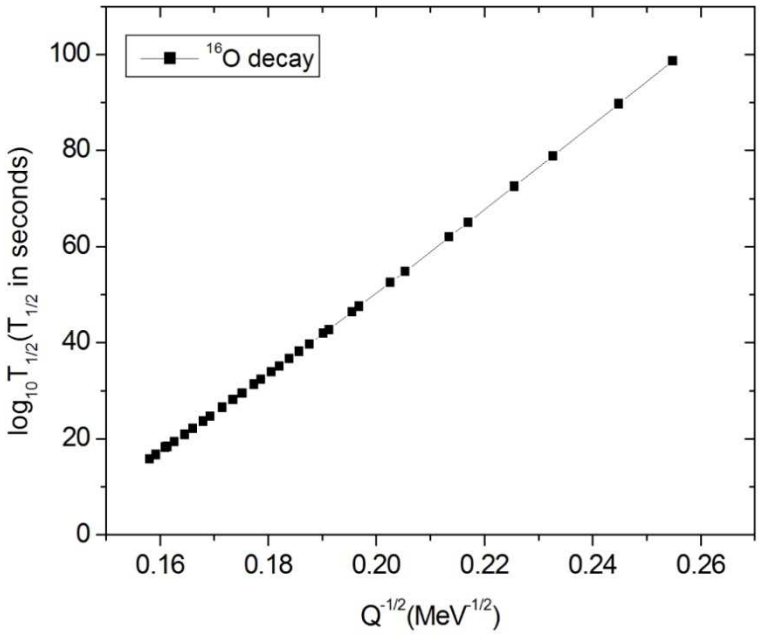

Fig. 7.11. G-N plot for ^{16}O decay of Pt isotopes.

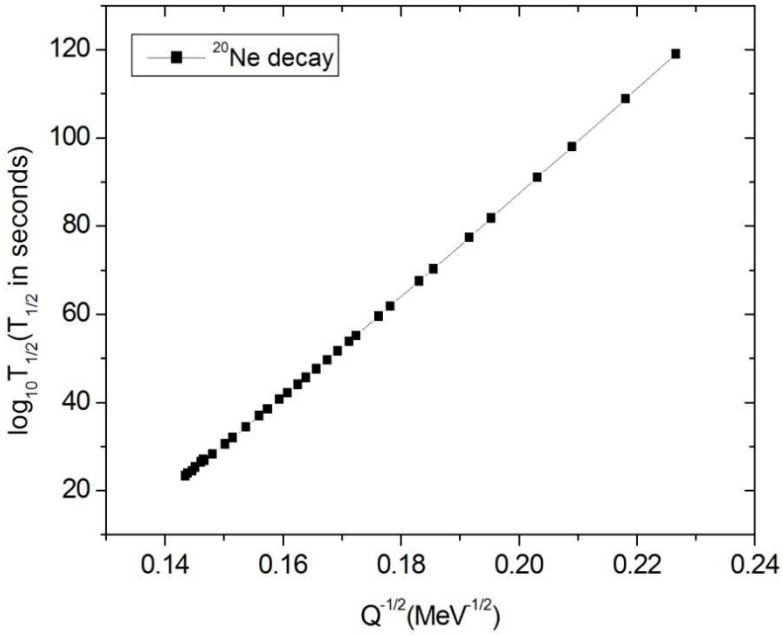

Fig. 7.12. G-N plot for ^{20}Ne decay of Pt isotopes.

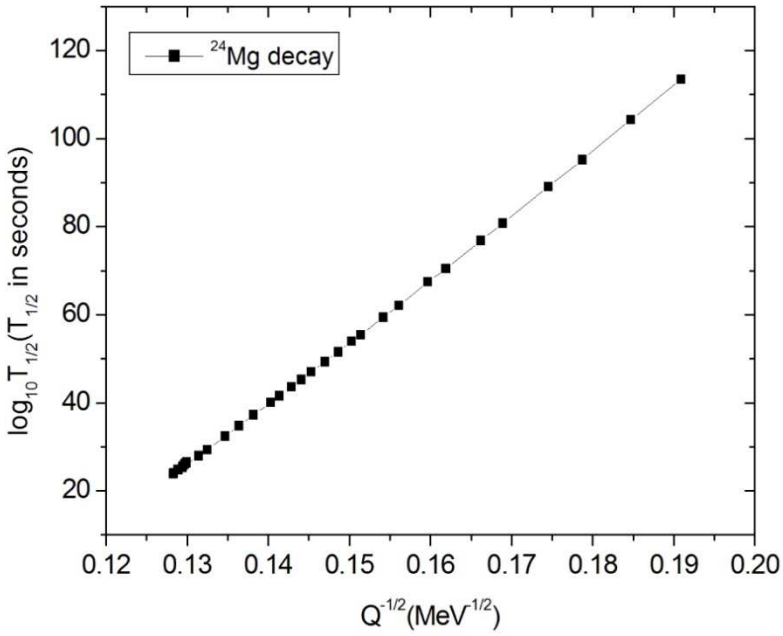

Fig. 7.13. G-N plot for ^{24}Mg decay of Pt isotopes.

Table 7.10. Slopes and intercepts of G-N plots for various decays of Pt isotopes.

Cluster emitted	Slope (X)	Intercept (Y)
^{4}He	127.3040	-51.1751
^{8}Be	342.1204	-77.4235
^{12}C	594.0258	-100.6913
^{16}O	852.0274	-119.6095
^{20}Ne	1142.2109	-141.1249
^{24}Mg	1417.1430	-158.4351

7.7 Half-life in terms of atomic number of cluster

From the slopes and intercepts of G-N plots and atomic number of the corresponding emitted cluster (Z_1), we have obtained a general equation for logarithmic half-life, which can be applied to all clusters emitted from various Pt isotopes, i.e.,

$$\log_{10}T_{1/2} = \frac{X(Z_1)}{\sqrt{Q}} + Y(Z_1) \quad (7.1)$$

where

$$X(Z_1) = -0.2123Z_1^3 + 6.4841Z_1^2 + 74.8288Z_1 - 46.5226 \quad (7.2)$$

$$Y(Z_1) = -0.0170Z_1^3 + 0.5885Z_1^2 - 16.0529Z_1 - 21.3935 \quad (7.3)$$

References

1. C. Qi, F. R. Xu, R. J. Liotta and R. Wyss, *Phys. Rev. Lett.* **103**, 072501 (2009).

2. C. Qi, F. R. Xu, R. J. Liotta, R. Wyss, M. Y. Zhang, C. Asawatangtrakuldee and D. Hu, *Phys. Rev. C* **80**, 044326 (2009).

3. S. B. Duarte, O. A. P. Tavares, F. Guzman and A. Dimarco, *At. Data Nucl. Data Tables* **80**, 235 (2002).

4. P. Möller, A. J. Sierk, T. Ichikawa and H. Sagawa, *At. Data Nucl. Data Tables* **109**, 1 (2016).

5. K. K. Girija and A. Joseph, *Turk. J. Phys.* **37**, 172 (2013).

6. K. P. Santhosh and A. Joseph, *Pramana J. Phys.* **62**, 957 (2004).

CHAPTER 8
SUMMARY AND CONCLUSIONS

8.1 Conclusions

The feasibility of exotic decay in tungsten (W), rhenium (Re), iridium (Ir) and platinum (Pt) isotopes within the mass range $150 < A < 200$ is analysed theoretically. In this systematic study, employing effective liquid drop model (ELDM), the half-lives of proton and alpha decays and probable cluster decays are computed and analysed for different proton-rich and neutron-rich isotopes. The interacting potential is taken as the effective liquid drop one, which is the sum of Coulomb, surface and centrifugal potentials. All possible combinations of parent and cluster have been considered for which the Q value is positive.

Within the measurable range, i.e., for $T_{1/2} < 10^{30}$ s, the possible decay modes in proton-rich W isotopes are observed as alpha decay and certain alpha-like cluster (A = 4n, Z = N) decays such as ^{8}Be, ^{12}C and ^{16}O decays. It is observed that both alpha decay and observed cluster decays slow down with the rise in mass number of parent nucleus and therefore, these emissions are found to be absent in the case of neutron-rich isotopes of tungsten. For alpha decay, it is observed that the calculated decay half-lives agree well with the experimental half-life values. Therefore, ELDM is applied to predict the half-lives of possible cluster decays. When compared with the universal decay law (UDL) model, the ELDM half-life values for the respective decays are found to lie near the range of UDL values. Again, cluster decays are found to diminish with the increase in the number of neutrons. It is found that alpha decay from ^{158}W isotope is the most probable decay mode in W isotopes. Also, ^{12}C emission from ^{162}W isotope is found to be the most probable cluster

decay mode in W isotopes. For ^{8}Be and ^{12}C cluster decays, the decay probability is found to be high if the daughter nucleus has spherical or nearly spherical shape. The plots of Q versus N_d (neutron number of daughter nucleus) and $\log_{10}T_{1/2}$ versus N_d for alpha decay and ^{8}Be, ^{12}C and ^{16}O cluster decays appear almost alike and look like mirror reflected images. It is observed that the probability of cluster emissions decreases with the increase in neutron number of daughter. In these plots, the shell closure is found to be at $N_d = 82$, a magic number, which in turn points to the significant role played by neutron magicity in exotic decay.

For Re isotopes, the half-lives for proton, alpha, ^{8}Be, ^{12}C and ^{16}O decays are observed to be well within the measurable range and therefore, they are predicted to be the possible decay modes in neutron-deficient Re isotopes. Cluster emissions are observed to slow down with the rise in the neutron number and hence no exotic decay is spotted for neutron-rich Re isotopes. It has been observed that the evaluated half-lives of proton decay and alpha decay are in good agreement with the available experimental data. The calculated half-lives of the respective decays lie close to those predicted using UDL model. It is found that proton decay from ^{159}Re isotope is the most probable decay mode in Re isotopes. Also, ^{12}C emission from ^{163}Re isotope is found to be the most probable cluster decay mode in Re isotopes. For ^{8}Be and ^{12}C cluster decays, the decay probability is found to be high if the daughter nucleus has nearly spherical shape. The plots of Q versus N_d and $\log_{10}T_{1/2}$ versus N_d for alpha, ^{8}Be, ^{12}C and ^{16}O decays almost appear as mirror reflected images. Proton decay is an exception in this case. It is observed that the probability of cluster emissions decreases with the increase in neutron number of daughter. The profiles for ^{8}Be, ^{12}C and ^{16}O emissions indicate the shell closure at $N_d = 82$, which points out the significance of neutron magicity in cluster decay.

Within the measurable range, the admissible decay modes in neutron-deficient Ir isotopes are found to be proton and alpha decays and some cluster decays like ^{8}Be, ^{12}C, ^{14}N, ^{16}O, ^{20}Ne and ^{24}Mg decays. Both proton and alpha decays and cluster emissions are observed to slow down with the increase in mass number of parent nucleus and as a result, these decays are not observed for neutron-rich isotopes of iridium. The estimated half-lives of alpha decay are observed to agree well with the available experimental data. The evaluated half-lives of the probable decay modes are observed to lie close to the UDL values. It is found that proton decay from ^{164}Ir isotope is the most probable decay mode in Ir isotopes. Also, ^{12}C emission from ^{165}Ir isotope is found to be the most probable cluster decay mode in Ir isotopes. For ^{12}C and ^{14}N cluster decays, the decay probability is found to be high if the daughter nucleus has nearly spherical or spherical shape. The profiles of $\log_{10}T_{1/2}$ versus N_d and Q versus N_d for alpha, ^{8}Be, ^{12}C, ^{16}O, ^{20}Ne and ^{24}Mg decays appear almost as mirror reflections. In this case, the plots for proton decay and ^{14}N decay are exceptions. It is observed that the probability of cluster emissions decreases with the increase in neutron number of daughter. In the plots for ^{12}C, ^{14}N, ^{16}O, ^{20}Ne and ^{24}Mg decays, shell closures are observed at or near $N_d = 82$, which points to the relevance of neutron magicity in cluster emissions. In the plot for ^{14}N decay, a large number of minima are observed, which indicates the possibility of a large number of emissions of ^{14}N cluster from Ir isotopes. The observation of the emission of ^{14}N cluster is a rare one since odd-odd cluster emissions have not been experimentally observed until now.

For Pt isotopes, the half-lives for alpha, ^{8}Be, ^{12}C, ^{16}O, ^{20}Ne and ^{24}Mg decays are perceived to be well within the measurable range and they are predicted to be the possible decay modes in proton-rich Pt isotopes. Cluster emissions are found to diminish with the rise in the number of neutrons and therefore, no cluster radioactivity is noted in the case of neutron-rich Pt isotopes. It has been noticed that the evaluated half-lives of alpha decay are in

remarkable agreement with the experimental data. The evaluated half-lives for alpha decay and ^{8}Be, ^{12}C, ^{16}O, ^{20}Ne and ^{24}Mg cluster decays are seen to be very near the range of those predicted using UDL model. It is found that alpha decay from ^{166}Pt isotope is the most probable decay mode in Pt isotopes. Also, ^{12}C emission from ^{166}Pt isotope is found to be the most probable cluster decay mode in Pt isotopes. For ^{12}C and ^{16}O cluster decays, the decay probability is found to be high if the daughter nucleus has nearly spherical or spherical shape. The profiles of $\log_{10}T_{1/2}$ versus N_d and Q versus N_d for alpha, ^{8}Be, ^{12}C, ^{16}O, ^{20}Ne and ^{24}Mg decays appear almost like mirror reflected images. It is observed that the probability of cluster emissions decreases with the increase in neutron number of daughter. The profiles for ^{12}C, ^{16}O, ^{20}Ne and ^{24}Mg emissions point to the shell closure at N_d = 82. Minimum value of half-life increases the probability of cluster decays. This sets forth the importance of neutron magicity in cluster radioactivity.

Geiger-Nuttall plots are drawn for the probable decay modes in W, Re, Ir and Pt isotopes and all of them show linear behaviour. This emphasizes the fact that the inclusion of surface potential in the interaction potential does not cause any variation to the linear nature that is usually observed in G-N plots for the system under pure Coulomb potential. Apparent shifts in the slopes and intercepts of G-N plots are due to the shell effects and surface potential included in the interaction barrier. From the slopes and intercepts of G-N plots and atomic number of the corresponding emitted cluster, we have derived the equations for logarithmic half-lives corresponding to all probable clusters emitted from W, Re, Ir and Pt isotopes.

Calculations using effective liquid drop potential in the mass range $150 < A < 200$ clearly indicate the possibility of having cluster emissions with decay half-lives in the measurable range. All the proton-rich or neutron-deficient isotopes of W, Re, Ir and Pt display the same characteristics

regarding probable cluster decay modes and shell closure property of daughter. The agreement between the predicted and experimental half-lives of proton and alpha decays reiterates the efficiency of the model used. The evaluations of half-lives for W, Re, Ir and Pt isotopes support the shell effects in cluster radioactivity, which were observed previously [1 – 6]. It is found that ^{12}C decay is the most probable cluster decay among others in these nuclei. Deformation effects are taken into account in the evaluations of mass defect. In all the systems we have studied, a change of shape is evident from the β_2 deformation values of both parent and daughter nuclei. Also, the probability of cluster decay is found to be high if the daughter nucleus is spherical or nearly spherical. It is evident that the shape of the daughter nucleus influences the cluster decay half-lives more than that of the parent nucleus. It is in conformity with the results obtained by Shi and Swiatecki [7]. A common observation in the case of neutron-rich isotopes of W, Re, Ir and Pt nuclei is that the decay rate of the most probable cluster decays reduces with the increase in neutron number. This property was also observed by Santhosh [8,9] in his previous studies. The study also points out the presence of neutron magicity in cluster radioactivity, which indicates the possibility of exotic decay around singly magic daughter nuclei. The role of neutron magicity in cluster radioactivity has also been studied earlier [6]. The observation of an odd-odd cluster emission in the case of Ir isotopes is also quite interesting. The observed proton radioactivity in the case of odd-Z rhenium and iridium isotopes are in conformity with the predictions made by Anu Radha [10] based on one-proton separation energy. When compared to other emissions, half-lives of alpha emission are found to be minimum for a large range of N_p (neutron number of parent) values, favoring high probability of alpha particle emission from the nuclei under study. For cluster emissions, it is found that the minimum value of half-life shifts towards the higher N_p values. A close similarity in the decay characteristics is observed between ^{12}C

and ^{16}O cluster decays and also between ^{20}Ne and ^{24}Mg cluster emissions. It is found that decay characteristics for proton decay and ^{14}N decay are much different from those of other decays. Also, for these decays, the probability of decay is found to be high for daughter having even number of neutrons. In our study, Geiger-Nuttall plots for all probable decays are found to be linear. Linearity in G-N plots has also been observed in the cluster decay studies of Xe and Ce isotopes [8,11]. In a recent work, a microscopic analysis has been done for alpha and cluster decay half-lives in tungsten isotopes [12]. In an earlier study, nuclear structure and decay properties of even-even nuclei have been analysed in Z = 70 – 80 drip line region [13]. In a study, alpha decay of tungsten isotopes with mass number above 180 is studied and results are reported [14]. In our study, calculations have been done for nuclei with mass number below 180.

From this study, it is clear that ELDM model is good enough to predict the existence of alpha-like clusters, since Q value is found to be positive for decays involving these clusters. Hence ELDM model can be considered as a cluster model capable of predicting the existence of nuclear clusters. So far, no experimental information of cluster radioactivity has been attempted in the mass range of nuclei we have studied. Under these circumstances, our findings will definitely be useful as a guide to the experimentalists and hence we presume that we have succeeded in meeting the objectives of the study.

8.2 Future plan

The present study is based on the unified fission model. The same estimations could be attempted in the preformed cluster model also. It is interesting to make a comparison of the two approaches.

In India, we are not having dedicated experimental facilities for cluster radioactivity research. Deeper understanding of this phenomenon could be obtained by associating with experimental groups active in labs outside India.

Another approach we can follow in cluster radioactivity is based on the cluster-phonon model. Though a bit cumbersome in terms of computation, it can shed more light on the role of nuclear structure effects in this rare decay mode.

References

1. D. N. Poenaru, M. Ivascu, A. Sandulescu and W. Greiner, *Phys. Rev. C* **32**, 572 (1985).
2. S. S. Malik and R. K. Gupta, *Phys. Rev. C* **39**, 1992 (1989).
3. Satish Kumar, Dharam Bir and R. K. Gupta, *Phys. Rev. C* **51**, 1762 (1995).
4. Sham K. Arun and R. K. Gupta, *Phys. Rev. C* **80**, 034317 (2009).
5. H. F. Zhang, J. M. Dong, G. Royer, W. Zuo and J. Q. Li, *Phys. Rev. C* **80**, 037307 (2009).
6. K. K. Girija and A. Joseph, *Turk. J. Phys.* **37**, 172 (2013).
7. Shi Yi-Jin and W. J. Swiatecki, *Nucl. Phys. A* **464**, 205 (1987).
8. K. P. Santhosh and A. Joseph, *Pramana J. Phys.* **62**, 957 (2004).
9. K. P. Santhosh, *Phys. Scr.* **81**, 015203 (2010).
10. C. Anu Radha, Ph.D Thesis, VIT university (2011).
11. K. P. Santhosh and A. Joseph, *Pramana J. Phys.* **58**, 611 (2002).
12. N. Ashok and A. Joseph, *Nucl. Phys. A* **977**, 101 (2018).
13. S. Mahapatro, C. Lahiri, Bharat Kumar, R. N. Mishra and S. K. Patra, *Int. J. Mod. Phys. E* **25**, 1650062 (2016).
14. F. A. Danevich, A. Sh. Georgadze, V. V. Kobychev, S. S. Nagorny, A. S. Nikolaiko, O. A. Ponkratenko, V. I. Tretyak, S. Yu. Zdesenko, Yu. G. Zdesenko, P. G. Bizzeti, T. F. Fazzini and P. R. Maurenzig, *Phys. Rev. C* **67**, 014310 (2003).